COMPARATIVE STUDY OF ATF FOR A CANDU LATTICE

COMPARATIVE STUDY OF ACCIDENT-TOLERANT FUEL FOR A CANDU LATTICE

By SIMON YOUNAN, B.Eng.

A Thesis Submitted to the School of Graduate Studies in Partial Fulfilment of the Requirements for the Degree Master of Applied Sciences

Descriptive Note

McMaster University MASTER OF APPLIED SCIENCES (2017) Hamilton, Ontario (Engineering Physics)

TITLE: Comparative study of accident-tolerant fuel for a CANDU lattice AUTHOR: Simon Younan, B.Eng. (McMaster University) SUPERVISOR: Dr. David Novog NUMBER OF PAGES: xiii, 120

Lay Abstract

Since the Fukushima accident in 2011, there have been an increasing number of studies on the use of accident-tolerant fuel in nuclear reactors to mitigate the consequences of a future severe accident, reducing the likelihood and severity of a radiation release. Canadian reactors are of the CANDU design, which differs greatly from the reactors most recent studies have focused on. The goal of this study is to determine the feasibility of using accident-tolerant fuel in CANDU reactors, studying different types.

In general, the goal of accident-tolerant fuels in CANDU reactors would be to reduce fuel temperatures and improve fission product retention, reducing the likelihood/magnitude of radioactive releases in a severe accident. However, nearly all types of accident-tolerant fuel would also require the uranium to be slightly enriched as opposed to the current fuel which is based on naturally-occurring uranium. This study outlines the results obtained by computer modelling of accident-tolerant fuel in a CANDU reactor, including the enrichment requirements, changes to important reactivity feedbacks, and impacts on accident performance.

Abstract

Since the Fukushima accident in 2011, there have been an increasing number of studies on the use of accident-tolerant fuel (ATF) in light water reactors to mitigate the consequences of a future severe accident, by better retaining fission products and/or providing operators more time to implement emergency measures.

However, few studies exist for CANDU reactors in this regard. The goal of this study is to determine how different types of ATF are expected to behave in a CANDU lattice when compared to the current UO_2 fuels. In particular, this study focuses on neutronic parameters calculated using the Serpent 2 code, but also models heat transfer and stylized accident scenarios. The ATF concepts tested include UO_2-SiC composites, UN and UN-based composites, U-9Mo, and fully ceramic microencapsulated (FCM) fuel, along with SiC and SS-coated cladding. Four general conclusions can be drawn:

1. Fuel temperature are lower for ATF as compared to traditional fuels. UO_2-SiC composite fuel exhibits a moderate temperature reduction compared to UO_2, particularly for fresh fuel. Other ATF fuel materials exhibit a substantial decrease in fuel temperature compared to UO_2. The lower fuel temperatures are also accompanied by lower melting temperatures for some fuels, hence each design requires specific assessments on safety.
2. As most ATF have a poorer neutron economy compared to standard fuel designs, enrichment is required to use ATF in a CANDU, particularly for UN and FCM fuel compositions. Coolant void reactivity (CVR) is lowest with FCM fuel and highest with U-9Mo fuel. Fuel temperature coefficient (FTC) is most negative for fuel containing UN or U-9Mo.
3. Changing the cladding material from zircaloy to SiC slightly improves neutron economy, while a FeCrAl surface layer impairs neutron economy. The impact of many ATF sheath materials is to greatly reduce or eliminate hydrogen production in some severe accidents. A specific assessment on hydrogen production was not performed in this study.
4. In stylized accident scenarios, all fuels exhibit only a small temperature spike due to the reactivity insertion of the LOCA as the reactor shutdown limits the power excursion. For cases where Emergency Core Cooling functions as designed, fuel and channel failures are precluded for both traditional fuels and ATF. For cases with impairment of ECC, most ATF fuels show lower fuel temperatures than UO2 fuels and adequate heat removal to the pressure-calandria tube fuel channel. The exception would be Mo-based fuels that reach the melting point prior to establishing an adequately high sheath temperature to sustain radiative heat removal to the PT-CT assembly.

Acknowledgements

I would like to thank my supervisor, Dr. David Novog, for reviewing this thesis and for supporting me throughout the research process. Through him I learned a great deal about the use and application of various reactor physics codes which I may potentially apply to future research.

I would also like to thank the other professors at McMaster University's Department of Engineering Physics, particularly Dr. Adriaan Buijs, Dr. John Luxat, and Dr. Ben Rouben, for being a major part of my academic journey, as without them I would have never reached this point in my academic career. I would also like to thank Nihan Onder in particular for providing the idea of carrying out this study.

I would also like to thank the VTT Technical Research Centre of Finland for developing and providing the Serpent Monte Carlo reactor physics code, which formed a core part of my research. In addition I would like to thank PDE Solutions Inc. for providing the FlexPDE code free of charge to students. Finally I would like to thank the developers of both the Python and GNU Octave programming languages, as they have provided me with a substantial improvement in efficiently preparing my computations and collecting results.

I would finally like to thank SHARCNET for making their computational resources available to my research and the research of many other students throughout Canada. Without these computational resources I would not have been able to obtain the necessary results to write this thesis.

Table of Contents

List of Figures

List of Tables

Notation and abbreviations

ATF	Accident-Tolerant Fuel
BCC	Body-Centred Cubic
BDBA	Beyond Design Basis Accident
BISO	Bistructural-Isotropic (Fuel)
BWR	Boiling Water Reactor
CANDU	CANada Deuterium Uranium
CVI	Chemical Vapour Infiltration
CVR	Coolant Void Reactivity
DBA	Design Basis Accident
DBRC	Doppler Broadening Rejection Correction
DNBR	Departure from Nucleate Boiling Ratio
ECCS	Emergency Core Cooling System
FCM	Fully Ceramic Microencapsulated (Fuel)
FPD	Full-Power Days
FTC	Fuel Temperature Coefficient
HTGR	High Temperature Gas-cooled Reactor
HTS	Heat Transport System
INES	International Nuclear and radiological Event Scale
k_{eff}	Effective Neutron Multiplication Factor
LEU	Lightly Enriched Uranium
LOCA	Loss Of Coolant Accident
LWR	Light Water Reactor
MTC	Moderator Temperature Coefficient
NU	Natural Uranium
pcm	Per Cent Mille (1 pcm = 10 ppm = 0.001%)
PRA	Probabilistic Risk Assessment
PWR	Pressurized Water Reactor
PyC	Pyrolytic Carbon
RIA	Reactivity-Initiated Accident
SBO	Station Blackout
SEU	Slightly Enriched Uranium
SiC	Silicon Carbide
SS	Stainless Steel
SWU	Separative Work Unit
TRISO	Tristructural-Isotropic (Fuel)
TRU	Transuranics
UN	Uranium Nitride
UO_2	Uranium Dioxide
wt%	Weight Percentage

Declaration of Academic Achievement

The basis of this research is a collaboration between myself, my supervisor Dr. Novog, and the fuel development branch at Canadian Nuclear Laboratories, and it was through this collaboration that a case table was built to determine which ATF concepts to test, and under which parameters, including desired exit burnup.

My supervisor provided guidance on how to conduct my research, such as choosing to use the Serpent code for reactor physics, to use FlexPDE to model heat transfer in a simplified manner, and to model some sort of transient. CANDU lattice properties (Table 3.2) were selected through a combination of literature review as well as through the selection of values used and accepted by other students within my research group for modelling the CANDU lattice. Other parameters were selected through a combination of literature review, calculation, and personal judgement.

However, the research conducted to obtain the results is original research, including the preparation of input files for Serpent and FlexPDE, along with interpreting and plotting the results. The stylized accident modelling was entirely my own development, with some input parameters based on literature.

The first draft of this dissertation was prepared by myself. Review and revision was performed by my supervisor, along with myself.

1 Introduction

Nuclear fuel made with uranium dioxide pellets and zirconium-based cladding has been successfully used for generations in nuclear power reactors. Uranium dioxide is very stable and has a very high melting point [1], while the cladding protects the ceramic fuel and acts as a barrier to radioactive release. However, the Fukushima Daiichi disaster revealed the potential weaknesses of this fuel to beyond design-basis accidents. In particular, zirconium-based sheath materials oxidize rapidly in high-temperature steam, producing additional heat and hydrogen gas [2]. Since 2011, a great deal of focus has gone towards emergency response planning/drilling in the event of a severe accident coupled with potential design changes to fuel and sheaths to improve the fuels robustness during these events [3].

One option that is being studied extensively is to use novel fuel designs that can better withstand accident conditions. Studies have been done not only on changing the cladding to make it more resistant to oxidation, but also on changing the fuel material itself, to reduce operating temperatures and/or to add additional barriers to fission product release [4]. The goal is to design fuel that is not only safer, but also as economical as or more economical than current fuel designs [5] [6].

While there is a plethora of literature on accident-tolerant fuel designs for LWRs, very little exists for the CANDU design. This dissertation serves as a comparative overview on how different accident-tolerant fuel designs will behave compared to the standard fuel currently in use.

2 Literature Review

Nearly all power reactors, including water-cooled reactors such as LWRs and CANDU reactors, contain uranium fuel in the ceramic oxide form UO_2. Compared to uranium metal, UO_2 is much more stable, and has a much higher melting point. While uranium metal melts at only roughly 1135°C [7], uranium dioxide doesn't melt until it reaches roughly 2850°C [1]. On the other hand, UO_2 has a rather low thermal conductivity, particularly at elevated temperatures and for irradiated fuel [1], leading to significant temperature gradients within the ceramic pellets, resulting in thermal stress and potential cracking.

The fuel is designed to provide multiple barriers to fission product release [8] as the pellets themselves contain most of the fission products. In addition, the fuel is surrounded by a zirconium alloy cladding, which supports and contains the fuel pellets, as well as containing fission products, including volatile elements such as iodine and xenon which tend to diffuse out of the pellets. However, if the fuel cladding fails, then fission products and fuel pellet fragments can escape into the heat transport system.

Zirconium alloys are used in reactor design due to the very low neutron capture cross-section of zirconium compared to other metals. However, zirconium is vulnerable to oxidation in steam at elevated temperatures, where an energetic exothermic, hydrogen-producing reaction can occur. Fuel cladding oxidization can lead to early cladding failure and an elevated risk of a hydrogen explosion should hydrogen mitigation measures fail. Under normal conditions, this is not an issue since water will readily convect heat from the fuel cladding and keep it well below the temperatures at which oxidation can occur. However, under accident conditions where cooling is lost, the cladding temperature can become elevated and potentially lead to rapid oxidation.

2.1 Overview of Severe Accident Progression in Water-Cooled Power Reactors

Since the Fukushima disaster, analysis of BDBAs and severe accidents has increased significantly, so as to incorporate lessons learned and improve accident responses. The initial event triggering the disaster was a magnitude 9.0 earthquake, which was detected and resulted in all reactors tripping [2]. However, the earthquake resulted in loss of external AC power, and the subsequent tsunami flooded the site and resulted in loss of all power, including backup AC and DC power [2]. Coolant boiled away over a period of time resulting in some fuel being uncovered. With fuel rods partially exposed to steam, they overheated and cladding oxidized released hydrogen, which eventually leaked into the reactor building. The damaged fuel also released fission products which were either leaked and/or were vented out of containment. In addition, the hydrogen accumulated

outside of containment but within the reactor building and exploded, resulting in additional damage and dispersion of fission products [2]. The accident was rated 7 (the highest level) on the INES [2].

While reactors with normal UO_2/zircaloy fuel are designed to survive design-basis accidents, such as an RIA or a LOCA with ECCS operational, the response of the fuel materials in unmitigated BDBAs was not fully studied [3]. The new target for nuclear reactor safety is to mitigate the effect of BDBA using a combination of enhanced design features and accident response such that the releases to the environment are small or zero [5], should an unlikely event occur.

Accident-tolerant fuels would provide additional levels of safety in the event of a DBA and BDBA and could either greatly extend the response time during an accident or eliminate releases altogether. The U.S. Department of Energy has established a goal to design and manufacture a rod or assembly and test it in a commercial reactor by 2022 [6]. No such design targets or goals exist yet for CANDU reactors.

For CANDU reactors, the progression of such an accident would be different. For example, in the event of a LOCA with ECCS failure, or a prolonged SBO, low coolant flow will result in fuel heating up. However, this heat will be transported to the pressure tubes through conduction or radiation, at which point the heated pressure tubes will either balloon (at high pressure) or sag (at 850°C) to contact the calandria tubes, allowing efficient conduction to the moderator, which acts as a very large heat sink [9]. Therefore additional water make-up to the low pressure calandria would effectively terminate the accident sequence. In the event that emergency measures could not supply water the calandria vessel in a timely fashion, the shield tank would still act as an additional heat sink after some core disassembly, thus acting to contain a release of fission products for an even longer time [9].

The objectives of ATF would thus differ somewhat in the case of a CANDU reactor as compared to LWR technologies. Mitigating the steam oxidation of fuel cladding would still be beneficial. However, in a CANDU the pressure tube will deform and make contact with the calandria tube before significant fuel melting and sheath oxidization can occur [9]. This is achievable with UO_2 due to its high melting point. However, certain alternate fuels considered for ATF, particularly uranium-molybdenum alloy fuels, have very low melting points and could conceivably melt and result in fuel failure before the pressure tube can deform, likely precluding their use as ATF in CANDU. An ideal fuel material would provide better fission product retention, more robust behaviour under DBA and BDBA events, and lower fuel temperatures while still avoiding early fuel melting.

2.2 Overview of Accident-Tolerant Fuel

The simplest change to the fuel material that can be done is the addition of another material to the UO_2 pellets to form a mixture with enhanced thermal conductivity. The additive material considered for this in LWR research is typically silicon carbide. The very high thermal conductivity of SiC results in a significant improvement for the mixture over standard fuel, as a 10% SiC addition by volume can improve thermal conductivity by 62% [10]. The silicon carbide itself would have little effect on the neutronics, but since some uranium is displaced, the fuel enrichment would have to be increased somewhat to achieve comparable fuel performance. However, the improvement in heat transfer would significantly reduce fuel temperature for a given power, improving the margin of safety for fuel melting as well as slowing the release of fission gas egress from the fuel [10]. The centreline temperature could decrease by 20% [10]. The proposed manufacturing method by Permar *et al.* [10] is spark plasma sintering, which would dramatically reduce processing costs and produce fully dense pellets much more quickly than conventional methods for generating Si-U mixture fuels [10].

Another choice of additive is diamond [11]. By sintering a mixture of UO_2 and diamond powder with 10 µm particle size for the diamond, thermal diffusivity can be improved in a similar manner to the addition of SiC [11]. An additional choice is beryllium oxide [12], which acts similarly to increase the thermal conductivity of the fuel pellets, although use of beryllium may be precluded for other environmental reasons due to its toxicity.

Several alternate uranium compounds have been considered to replace uranium dioxide altogether. One major example is uranium nitride. It has a greater density and superior thermal conductivity compared to UO_2, but lacks UO_2's stability in an oxidizing environment, as UN can potentially react with water [13], which is conceivable in an accident scenario. Another compound which exists is uranium silicide, which is less dense than UN and with lower thermal conductivity, but still better than UO_2, while being less susceptible to oxidation than UN.

Another potential alternative is to use uranium-molybdenum alloys. Pure uranium metal possesses a good thermal conductivity and the highest possible uranium density. However, it possesses several undesirable properties, including material instability and a low melting point. Molybdenum improves uranium's material properties by stabilizing the γ-phase and raising the melting temperature [7], while still maintaining a high uranium density and minimal parasitic neutron capture.

Another option is to replace the standard fuel with fully ceramic microencapsulated (FCM) fuel, where TRISO particles are encapsulated within an inert matrix, such as silicon carbide. The primary advantage of such fuel is that it provides additional barriers to

prevent fission products from being dispersed into the environment [4]. Silicon carbide within the TRISO-like particles and of the matrix itself acts as a barrier to fission product escape, so that fission product gas cannot escape into the fuel-clad gap such that even if the clad fails, fission products can still be contained. As well, the high thermal conductivity of silicon carbide brings down fuel temperatures greatly, improving safety margins while reducing thermal stresses. Silicon carbide is also quite stable under irradiation [4]. The primary downside is that most of the fuel volume would consist of inert material, thus requiring a high level of enrichment to bring the fissile content to a similar level as standard fuel [4].

A similar concept that exists is microcell fuel. In this fuel style, UO_2 is formed into microscopic cells, forming a regular lattice, with a metallic or ceramic cell wall. The cell wall is continuous and thus contains the fuel, and the wall material improves the pellet's properties. A metallic cell wall would have a very high thermal conductivity and thus significantly improve the thermal conductivity of the pellet as a whole, while ceramic materials could be chosen to improve fission product retention [14]. For example, microcell fuel with a metallic wall could increase thermal conductivity by up to a factor of 2 at elevated temperatures [14]. However, a metallic cell wall could be vulnerable to oxidation, while ceramic material would resist oxidation [14]. As well, metallic cell walls would reduce the fuel cycle length significantly, requiring increased enrichment to compensate, while ceramic cell walls could be made thinner and have very little effect on cycle lengths [14].

According to [15] the objective of accident-tolerant fuel designs is to:

- Increase the length of time between loss of active cooling and onset of fuel damage and fission product release, giving operators more time to restore cooling, to enhance fission product retention, and to avoid or reduce the potential for rapid oxidization.
- The fuel should also have comparable or improved performance versus standard fuel under normal conditions, and be compatible with existing reactor systems.
- All operational, control, and safety parameters should be maintained or improved.

Important properties for nuclear fuel include uranium density, thermal conductivity, melting point, as well as mechanical properties. A higher uranium density improves the cycle length of the fuel, while greater thermal conductivity reduces fuel temperatures, lowering thermal stresses and providing a greater margin to avoid melting. Mechanical

properties can predict whether pellets may crack during operation, or how large a fuel-clad gap must be to accommodate thermal expansion.

Table 2.1: Uranium Density Comparison for UO_2 and ATF Fuel

Fuel Material	Uranium Density (g/cm^3)	Ref.
UO_2 (Fully Dense)	9.66	[13]
UO_2 (5% Porosity)	9.18	
UN (Fully Dense)	13.55	[13]
U_3Si_2 (Fully Dense)	11.31	[13]
U-8Mo (Fully Dense)	16.1	[7]
FCM UO_2/SiC (55\% TRISO Packing)	1.84	[4]
FCM UN/SiC (55\% TRISO Packing)	2.72	[4]

Table 2.2: Melting Points for UO_2 and ATF Fuel Materials

Fuel Material	Melting Point (°C)	Ref.
UO_2	2847	[16]
UN	2680	[17]
U_3Si_2	1665	[16] [17]
U-8Mo	1135	[7]
SiC	2457	[4]

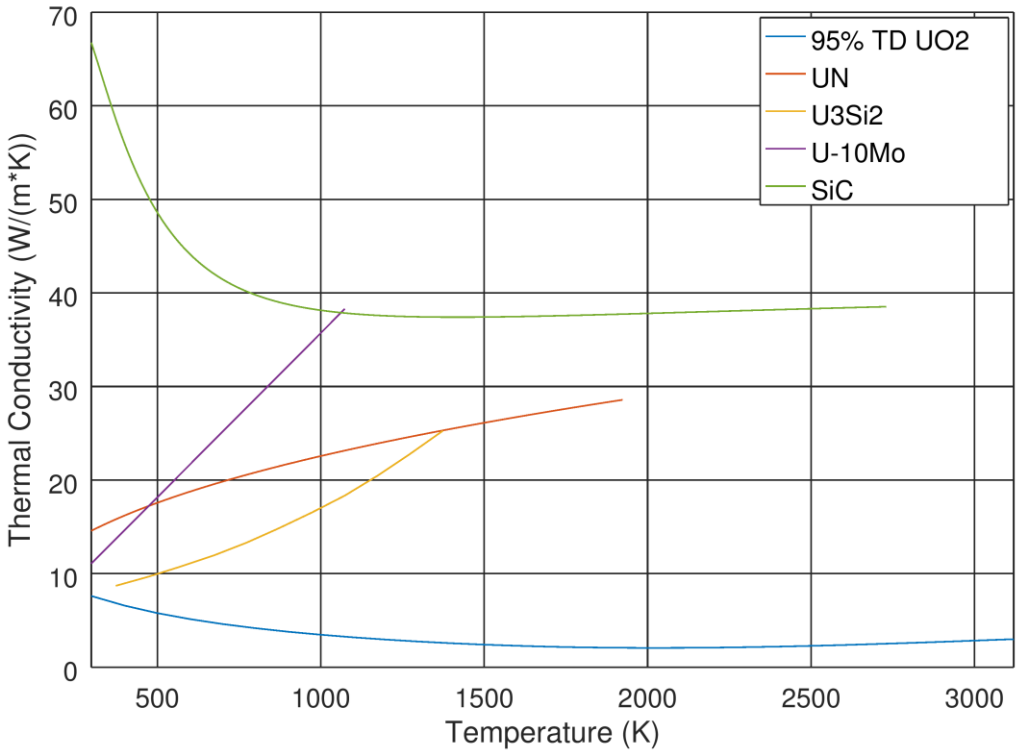

Figure 2.1: Comparison of thermal conductivity of UO_2 and ATF materials [1] [4] [13] [18]

2.3 Uranium Nitride Fuel

Uranium nitride possesses much greater density and thermal conductivity than UO_2. Uranium nitride can be used as whole pellets or as kernels in FCM fuel [19]. One method of manufacturing high-purity uranium nitride involves hydriding the metal, followed by nitriding and spark plasma sintering, resulting in UN with typical carbon and oxygen impurity levels of around 0.12% and 0.30% by weight, respectively [20], with the potential for further improvement, and up to 99.5% theoretical density.

For porosity P up to 0.2, and for T between 298 K and 1923 K, the thermal conductivity of uranium nitride can be given by [4]:

$$k = 1.864\, e^{-2.14P} T^{0.361} \tag{2.1}$$

This is a large improvement over uranium dioxide, which can be seen in Figure 2.1. At room temperature, the thermal conductivity exceeds that of UO_2 by a significant margin. At reactor operating temperatures, the difference becomes a factor of 5 or more. As a result, fuel centreline temperatures for UN fuel can be much lower than for UO_2 fuel, with temperature gradients of less than 300 K in the fuel, compared to over 1000 K for UO_2,

especially in the hottest pins where UO_2's decreasing thermal conductivity at high temperatures contrasts with the increasing thermal conductivity of uranium nitride.

One issue identified with uranium nitride, however, is that it can react with water [13], which is important during an accident scenario where the cladding fails, allowing contact between fuel and water. Other materials, such as uranium silicide and uranium dioxide, are less susceptible to these reactions.

It is possible to combine the advantages of both by manufacturing composite fuel. It has been proposed that uranium nitride particles be embedded in a continuous matrix of uranium silicide. Such a composite material would possess the stability of uranium silicide but additionally gain some of the advantage of uranium nitride's greater density and thermal conductivity. Uranium silicide itself has a much better thermal conductivity than UO_2, and follows a similar trend to uranium nitride of better thermal conductivity at high temperatures [13].

One method of producing a high-quality hybrid mixture involves milling the U_3Si_2 into very fine particles (about 1 μm diameter) before mixing with the coarser UN particles and sintering, in order to produce a composite with high density and few impurity phases [17]. Another method involves liquid phase sintering, where the temperatures used are high enough to melt the U_3Si_2 phase [21].

A similar concept is a UO_2-UN composite fuel. When UN particles are embedded in a UO_2 matrix, the latter would act as a protective barrier for oxidation, while still benefitting from the increased density and thermal conductivity of UN [14]. Once uranium nitride is produced, it would be mixed with uranium dioxide and sintered at high temperature in an inert environment to produce a composite pellet [22].

Another issue is that nitrogen-14 is a strong neutron absorber, and becomes carbon-14, which is a mobile fission product [23]. Therefore, enriching to nitrogen-15 can significantly improve the neutron economy of reactors using this fuel, perhaps reducing uranium requirements by 25%, but would require new infrastructure to be developed [23]. Enrichment of nitrogen would also reduce carbon-14 production, but most likely it would still be significantly higher than for UO_2 fuel, thus requiring additional controls [23].

In addition to the considerations discussed above, increasing the amount of heavy metal in the reactor (relative to hydrogen) tends to harden the neutron spectrum all other things being equal, so moderator temperature coefficients could improve, but boron and control rod worths may decrease, thus the impact on safety would need to be evaluated [23].

2.4 Uranium Silicide Fuel

A similar option to using UN fuel is to use uranium silicide fuel. Similarly to UN, it has a higher density and thermal conductivity than UO_2, although not as high as that of uranium nitride [13]. The best uranium densities come from U_3Si_2 and U_3Si. However, U_3Si has high irradiation-induced swelling and disassociates above 900°C [24], thus U_3Si_2 is the preferred compound for nuclear applications. High-purity uranium silicide can be produced by putting a pressed mixture of uranium and silicon powders into an arc melter [24]. Ingots must then be made into powder to then be pressed and sintered into pellets [24]. Optimizing the process allows the production of pellets with greater than 94% theoretical density. A further step to test this fuel material will be to perform irradiation tests on test rods containing U_3Si_2 fuel [16].

2.5 Uranium-Molybdenum Fuel

Molybdenum can be added to uranium metal to make reactor fuel, as uranium metal would otherwise be unsuitable due to mechanical instability, among other undesirable material properties. This allows the advantages of metallic fuel to be realized – high thermal conductivity along with a very high density (higher than UN).

Uranium metal normally exists in the orthorhombic "α-phase" below 668°C (941 K) [7]. This phase is unstable, can corrode easily, and is weak [7]. The BCC "γ-phase" is isotropic and has superior properties, but can only exist at elevated temperatures for pure uranium. Certain metals, particularly molybdenum, make the desired γ-phase a metastable state. This state can be retained indefinitely at room temperature, but can decompose at elevated temperatures, unless the temperature exceeds the eutectoid temperature of about 565°C (838 K), above which the γ-phase is stable [7]. This can present concerns with reactor operation using such fuels. However, it is believed that the energy of nuclear fission induces a local recrystallization which would compete with the decomposition effect and potentially maintain the metastable phase [7].

The fuel still corrodes if directly exposed to water, so diffusing a surface layer of a corrosion-resistant metal such as aluminum, chromium, or niobium can be performed as an additional corrosion barrier [23].

Table 2.3: Density of uranium-molybdenum alloys [25]

Molybdenum Concentration (wt%)	Density (g/cm^3)	U-Density (g/cm^3)
8	17.5	16.1
12	16.9	14.9

Table 2.4: Thermal conductivity of U-10Mo [18]

Temperature (°C)	Thermal Conductivity (W/(m·K))
20	11.3 ± 1.4
100	13.2 ± 1.3
200	17.1 ± 2.4
300	20.3 ± 2.7
400	23.7 ± 2.3
500	27.6 ± 2.5
600	31.9 ± 3.1
700	35.4 ± 2.1
800	37.5 ± 0.2

Alloys with different molybdenum concentrations have similar values for thermal conductivity [7].

The reactivity of this fuel could be improved by depleting the molybdenum of the ^{95}Mo isotope responsible for most of the neutron absorption [23]. This would save roughly 10% uranium consumption, which may or may not justify the cost of depleting the molybdenum.

In addition, like with uranium nitride, increasing the amount of heavy metal in the reactor (relative to hydrogen) tends to harden the neutron spectrum, so moderator temperature coefficients could improve, but boron and control rod worths may decrease, thus the impact on safety would need to be evaluated [23].

Finally, the reduction of the fuel melting temperature may subtly impact the accident progression in CANDUs [26]. For example the combined effects of higher conductivity and lower fuel melting temperatures in some fuel designs may result in cases where the fuel fails prior to PT-CT contact, which would be undesirable from an accident progression standpoint.

2.6 Fully Ceramic Microencapsulated (FCM) Fuel

There is an existing research initiative evaluating the feasibility of replacing standard UO_2 fuel in LWRs with FCM fuel, composed of TRISO particles embedded in a silicon carbide matrix [4]. This would provide an additional barrier to fission product release and improve thermal safety margins. The plenum region in LWR assemblies could be reduced as there would be no fission gas buildup with irradiation, and the fuel-clad gap could be made smaller and thus improve heat conduction [4]. However, since FCM fuel contains much less uranium than solid UO_2 fuel, the enrichment level needs to be raised

significantly in order to get a similar cycle life, well above the 5% that enrichment facilities are currently licensed for, requiring up to 19.9% enrichment, which is the limit for LEU [23]. Even at this enrichment, UO_2 FCM fuel would have a limited batch fuel cycle length in existing LWR designs [23].

The TRISO kernels are not limited to using UO_2. A much-considered option is to use UN instead, owing to its higher uranium density, which will offset some of the uranium displaced by switching to FCM. However, one concern with UN is the production of nitrogen gas, which can react with silicon carbide and reduce its capability to contain fission products [4]. Another consideration is to modify the geometry of the assemblies to increase the volume of FCM material in each assembly. Since the FCM material has superior heat conduction properties, the pin diameter and/or pin power can be increased while still maintaining a low fuel centre-line temperature. Either the pin diameter is increased while maintaining the same number of fuel pins, or assemblies with fewer pins are used in order to obtain an even wider pin diameter and potentially greater fuel volume. Using larger diameter fuel pins also improves neutronic efficiency by improved self-shielding thereby allowing cycle length to be re-optimized [4]. However, there are thermalhydraulic considerations as well. Increasing the pin diameter, while increasing the surface area for heat transfer (increasing DNBR), reduces the hydraulic diameter for coolant flow (reducing DNBR). Decreasing the number of pins but maintaining the same volume of fuel decreases the surface area for heat transfer (reducing DNBR). The OPR-1000 reactor uses 16x16 UO_2 assemblies [4]. The proposed assemblies are either 16x16 with slightly wider pins, or 12x12 assemblies with even wider pins [4].

The zirconium alloy cladding can be replaced by either stainless steel or silicon carbide. Both of these oxidize much more slowly and thus do not pose the same hydrogen production hazard. Additionally, silicon carbide has a much higher melting point than the metallic clad options. However, silicon carbide cladding must be made thicker than the typical metallic cladding options, which would reduce the fuel volume for a given pin diameter [4]. Using a stainless steel cladding maximizes the fuel volume, but the SS cladding also has greater parasitic absorption.

Of course, neither using high-density fuel kernels nor changing the geometry can fully compensate for switching to FCM ATF, thus a higher fuel enrichment is required to maintain a similar fissile mass as standard fuel (typically 4.5%). The enrichment can potentially be increased up to 20%, limited by non-proliferation concerns [4]. The OPR-1000 reactor would require roughly 20% enrichment for 16x16 assemblies, or 15% for 12x12 assemblies [4]. Guide tubes and structural materials would be made from stainless steel to eliminate zirconium alloy completely [4]. In the case of the Westinghouse reactor, 17x17 UO_2 assemblies would be replaced by 13x13 ATF assemblies [4].

Several designs were considered for FCM ATF fuel, with different assembly geometries and different clad materials (either SiC or SS). Another potential option available for manufacturing FCM fuel is to form monolithic pins. In this case, the entire pin is made of solid silicon carbide with the TRISO particles embedded within. There is no clad, as the monolithic silicon carbide matrix plays the role of containing fission products. However, this design was not explored in detail. [4]

Table 2.5: Candidate FCM replacement fuel designs for OPR-1000 [4]

Parameter	Unit	16x16 Solid	12x12 FCM	12x12 FCM	16x16 FCM	16x16 FCM
Fissile Material		UO_2	UN	UN	UN	UN
Cladding		Zircaloy	SS	SiC	SS	SiC
Enrichment	wt%	4.5/4.0	15.12	14.54	19.42	19.90
Fuel Density	g/cm^3	10.176	14.32	14.32	14.32	14.32
Pellet Radius	cm	0.4095	0.6725	0.6315	0.4325	0.3915
Clad Thickness	cm	0.057	0.059	0.100	0.059	0.100
Gap Between Rods	cm	0.335	0.235	0.235	0.285	0.285
HM Loading Ratio	%	100.0	42.8	37.8	33.7	27.6

A typical TRISO particle has a radius of 490 µm, with a fissile fuel kernel radius of 350 µm [4]. Thus, only about 36.4% of a TRISO particle by volume actually contains fissile material. Combined with a maximum feasible packing fraction of 55%, which was used in Table 2.5, the FCM fuel only contains 20% uranium compounds by volume, the rest being inert. To improve this figure to a more practical value, two changes were made. The first is the change from UO_2 to the denser UN, which improves this figure to about 30%. The second is the change in geometry, which increases the total fuel volume by making the pins larger, up to around 40% when using 12x12 assemblies instead of 16x16 assemblies to maximize pin diameter. This allows for enrichments around 15% with similar cycle length to the reference UO_2 fuel.

Compared to UO_2 fuel, FCM ATF can attain similar k_{eff} values. However, the FTC and MTC tend to become less negative compared to reference fuel [4]. In addition, gadolinium-based burnable absorber tends to burn off too quickly, resulting in reactivity rising significantly during the first portion of the fuel cycle [4]. Using the weaker absorber erbium instead would prevent this from occurring [4].

For the Westinghouse reactor, a 17x17 UO_2 assembly with 4% enrichment would be replaced by a 13x13 FCM assembly with 40% packing fraction and 13.11% enrichment to get the same amount of fissile material, assuming no clad change. However, as there is significantly less ^{238}U in the FCM core, it breeds significantly less plutonium and thus

would have a shorter cycle length at this enrichment – a higher enrichment would be needed to obtain the same cycle length [4].

Other changes to explore would be to develop TRISO particles with larger kernel diameters, or switch to BISO particles to increase the size of the kernel relative to the entire particle [23].

In addition, the fast neutron fluence in a PWR is several times higher than the HTGR that TRISO particles were developed for, thus TRISO particles may potentially fail at high pin burnups, as experiments of their performance for these conditions are not available [23]. An FCM-fuelled PWR would also require somewhat more mined NU and significantly more SWU to produce the same amount of energy compared to a UO_2 PWR [23]. Fuel assembly costs would also be greater [23].

On the back end of the cycle, FCM assemblies would contain a similar amount of fission products, but have the advantage of containing less heavy metal, less TRU, and be less reactive than spent UO_2 assemblies, along with having greater proliferation resistance [23]. The carbon and silicon in the fuel become additional waste [23].

2.7 Accident Tolerant Cladding

The cladding may also be replaced as part of a holistic view of safety improvements, as the oxidation of zirconium with release of steam is a major issue in a BDBA. Proposed accident-tolerant claddings include other metals such as stainless steel and molybdenum [5], ceramics such as silicon carbide, as well as multi-layer claddings where a thin surface layer protects the zirconium alloy from oxidation.

Along with evaluating the mechanical and thermal properties of candidate cladding materials, compatibility with existing structural materials must be considered. In LWRs, grid-to-rod fretting is a common fuel failure mode [27]. Replacement of the relatively soft zirconium alloy cladding material with a harder ATF material could potentially increase wear on the zirconium alloy spacer grids and other related structural materials, requiring replacement with either a harder zirconium-based alloy, or replacement with the same ATF material being used as cladding [27]. Similar issues of end-plate stability, pressure tube interactions, fuel handling, etc., must also be considered.

Another consideration is that cladding thicknesses may need adjustment due to differing mechanical properties. For example, a FeCrAl cladding could be made thinner, while a SiC cladding would probably need to be thicker than a normal zircaloy cladding. If the assembly geometry is to be kept the same, making the cladding thinner allows for larger fuel pellets and thus more fuel which may perhaps offset some of the fuel displaced

in some ATF designs. In an LWR, adding more fuel compared to moderator hardens the neutron spectrum [28]. This affects properties such as MTC and control rod worths, as mentioned before [23], but also affects the progression of an RIA as a harder spectrum shortens the mean generation time [28]. For a prompt-supercritical insertion, the power pulse for a thinner clad is higher but narrower, while the opposite occurs for a thicker clad [28]. The energy deposition is similar in all cases – slightly higher energy deposition for thicker clads [28].

2.7.1 Non-Zirconium-Based Metallic Cladding

One option is to use another metal, such as stainless steel or FeCrAl [6], which retains high strength but has more favorable oxidization characteristics as compared to Zr-based sheaths. Another option is molybdenum [5], or molybdenum-based alloys, which are stronger at higher temperatures than stainless steels (which tend to weaken beyond 1000°C [29]). Stainless steel also melts at a lower temperature than zircaloy – 1450°C versus 1850°C [23], while molybdenum has a very high melting point of 2620°C [23]. The disadvantage is that these metals have a greater neutron absorption cross-section, thus taking neutrons away from the chain reaction and shortening the cycle length and/or requiring enrichment. Such impacts on the neutron economy can be partially mitigated by taking advantage of the strength and oxidation resistance of stainless steel and reducing the cladding thickness [23]. Overall, increasing the melting point and reducing oxidization-driven heat loads could potentially provide additional time for operator actions, however, the dominant impact would be a reduction in the hydrogen generated during an accident.

Another concern with metallic cladding is the plastic deformation and potential bursting at elevated temperatures. When several FeCrAl alloys and other steels were tested, softer alloys failed below 800°C, while harder alloys maintained geometry at higher temperatures, which would help limit geometrical deformations during extreme events [30].

Multilayer metallic cladding can also be considered. The study by Cheng *et al.* [29] looks at molybdenum cladding, with coatings of either FeCrAl or a Zr-based alloy for corrosion and oxidation resistance under both normal and accident conditions. While it may seem counterintuitive to use a Zr surface layer, the amount of hydrogen generated is reduced compared to standard Zr-based cladding, with the ZrO_2 surface layer which forms acting to protect the underlying Mo from corrosion [29], as molybdenum corrodes quickly in at high temperatures in water [23]. Other coatings on top of a Zr-based cladding may be superior in this regard as discussed in subsequent sections.

Refractory alloys can also be considered, such as TZM, which is primarily molybdenum with a small amount of titanium and zirconium that provides high strength [31]. Molybdenum has a smaller neutron absorption cross-section than other refractory alloys which use tungsten or tantalum [31]. Again, a coating is required for corrosion protection.

2.7.2 Silicon Carbide Cladding

Silicon carbide can potentially withstand temperatures in the 1700°C to 2000°C range [5]. Depending on the type of accident, this could provide a substantial increase in the amount of time for operators to react to an accident, potentially with SiC cladding remaining intact long after other alternatives would have failed completely and the core destroyed [32]. It is stable, resists irradiation damage, and has a high melting point. In addition, it does not have the neutron absorption penalty of stainless steel, and in fact has even less parasitic neutron absorption than zircaloy [14], thus potentially providing a slight *benefit* to fuel cycle length [5]. However, a thicker cladding may be required to provide the necessary strength [4], and manufacturing is more difficult compared to metallic cladding [14] [23]. As well, SiC has a lower thermal conductivity than zircaloy, particularly when irradiated, thus fuel centre-line temperatures may increase somewhat [23].

Similar to SiC are composite claddings, such as SiC/SiC [33] and SiC/SiC_6 [14], which can further improve the properties of the cladding [14]. Low fracture toughness would preclude use of monolithic SiC as a reactor fuel cladding, as cladding rupture is to be avoided [33]. A composite cladding would consist of SiC fibres embedded in a matrix of SiC. The fibres would reinforce the material and improve fracture toughness and ductility [33]. However, using CVI to produce SiC composite of the necessary purity produces a material with significant porosity (5%), which would allow fission gas to permeate through the cladding [33]. Thus a combination of impermeable monolithic SiC with the tougher composite material would produce a fully accident-tolerant cladding using only SiC [33]. However, even the composite SiC proposed by Deck *et al.* [33] is not as ductile as metallic cladding and microscopic cracks can form under even low strain levels potentially allowing fission product leakage.

In a LWR, stresses would initially be compressive, or primarily compressive, due to coolant pressure, with a gradient dependent on the temperature gradient, with tension on the outer wall and compression inside [34]. Irradiation-induced swelling inverts this stress distribution, putting compression on the outer wall and tension on the inner wall [34], with fission gas pressure adding tension. Once the reactor is put in cold shutdown, the temperature gradient and coolant pressure compression effects disappear, resulting in high tensile stresses, particularly near the inner wall, with enough stress for the pseudo-

plastic deformation to occur [34]. Thus, a good choice would be for an inner composite layer with an outer monolithic layer, as the outer layer will always be in compression, and thus remain intact as a fission product barrier [34]. If the composite layer were outside the monolithic layer, tensile stresses would likely fracture the monolithic layer at the end of cycle when the reactor is shut down [34]. A layered structure with an inner monolith is much more likely to fail than one with an outer monolith, while a composite-only clad would certainly "fail" by allowing fission product to escape, despite remaining geometrically intact [34].

However, CANDU cladding is designed to be collapsible, in contrast to LWR cladding, thus conclusions based on conditions in an LWR are not applicable to CANDU, and thus separate studies would be needed to determine an ideal configuration for SiC cladding in the CANDU system.

Silicon carbide is a weaker absorber of neutrons than zirconium. However, it is also a scatterer of neutrons, and thus its scattering properties need to be accurately modelled as well. SiC can moderate neutrons somewhat, adding reactivity to under-moderated reactor designs [35]. A comparison of MCNP simulations with critical experiments on solid columnar SiC found significant discrepancies with harder neutron spectra, suggesting that data for Σ_a for SiC is accurate, but that scattering data could be improved [35].

Manufacture of SiC cladding is more difficult than for zircaloy. One particular issue identified is the joining of end caps to the cladding tube, since it is necessary for these joints to be radiation tolerant and meet the mechanical and thermal requirements while maintaining a hermetic seal [36]. One solution that was investigated was a "multiphase braze alloy interlayer consisting of silicon and aluminum with a two-phase joined microstructure" [36].

2.7.3 Multilayer Cladding

Another option is to keep the zircaloy cladding, but coat it with a thin layer of another material which is more resistant to oxidation. Examples include plating with metals such as chromium [14] [37], or dispersion of ceramics such as yttria [14] or silicon carbide [38]. Using a thin layer would minimize the penalty to reactivity that comes from using materials with significant neutron capture.

It is also possible to dope the surface of the zirconium with another material to form an alloy which is more resistant to oxidization than regular zirconium. One such option is aluminum, forming an Al_3Zr layer [39].

An alternative coating material is a class of materials called "MAX phase materials" [40]. These have the high oxidation resistance of ceramics along with the high thermal

conductivity of metals. One such material is Ti_2AlC. This coating has a slight impact on neutronics, with a reactivity loss of roughly 25 pcm per micron of coating thickness [40]. Other options include Ti_3AlC_2, Nb_2AlC, and TiAlN [41]. Comparing these options, for a given thickness, Nb_2AlC has a smaller cycle length penalty than the titanium-containing options [41] [42], while TiAlN has a significantly lower thermal conductivity than the others [41]. Still, these penalties are very small compared to the penalty of replacing the entire cladding with FeCrAl [41], stainless steel, or molybdenum alloys [42].

2.8 Summary of Literature

While a wide variety of literature relevant to LWR accident tolerant fuels and sheaths is available, relatively little exists for CANDU. Many of the LWR candidates are not well suited for CANDU since their impact on CANDU-specific accident sequences may not be desirable and/or may provide little benefit. Nevertheless, we examine a wide range of options to establish their impact on physics and thermalhydraulics such as to provide better recommendations for CANDU specific work in the future.

3 Methodology

In collaboration with Canadian Nuclear Laboratories [43], the following ATF concepts were selected for analysis as potential ATFs in standard CANDU reactors:

- UO_2/SiC composite fuel.
- Uranium Nitride fuel.
- UN/U_3Si_2 composite fuel.
- UN/ZrN composite fuel.
- U-9Mo fuel.
- FCM with UO_2 and UN in SiC, assuming bare kernels embedded in the matrix to maximize fuel loading, thus acting more like a microcell fuel.
- FCM with UN TRISO particles in SiC.
- Silicon Carbide cladding.
- Two-layer cladding using zircaloy with a 20% thickness FeCrAl layer.

Only material substitutions are investigated in this dissertation. The same 37-element CANDU bundle geometry was used for all test cases in order to isolate the effect of changing the material on the neutronics.

It was initially decided to investigate all cases with an equal exit burnup of 200 MWh/kgU, along with a subset of cases at a higher 600 MWh/kgU (by increasing the enrichment). However, different fuel materials with different uranium densities will have differing residence times for a fixed exit burnup. Therefore, at 200 MWh/kgU, the high-density fuels (uranium nitride and U-9Mo) will have a longer residence time in the core, i.e. fewer fuelling operations per day. However, some ATF fuel will have a substantially shorter residence time at a fixed burn-up level. Most likely, if ATF fuel were adopted, a constant fuelling machine load would be targeted, rather than a fixed exit burnup. Therefore, it was decided to collect an additional set of data on ATF fuel enriched to achieve the same residence time as standard UO_2 bundles.

Table 3.1: ATF Case Table Analyzed

Case	Fuel	Cladding	Target BU (MWh/kgU)
0	Uranium Dioxide	Zircaloy-4	200 (NU)
1	Uranium Dioxide	Zircaloy-4	600
2	UO_2 + 3% SiC by volume	Zircaloy-4	NU, 200, 600
3	UO_2 + 3% SiC by volume	SiC	200
4	UO_2 + 3% SiC by volume	Zr/FeCrAl	200
5	UO_2 + 6% SiC by volume	Zircaloy-4	200
6	UO_2 + 10% SiC by volume	Zircaloy-4	200
7	Uranium Nitride	Zircaloy-4	NU, 200, 600
8	UN + 3% U_3Si_2 by volume	Zircaloy-4	NU, 200, 600
9	UN + 6% U_3Si_2 by volume	Zircaloy-4	200
10	UN + 10% U_3Si_2 by volume	Zircaloy-4	200
11	UN + 3% ZrN by volume	Zircaloy-4	200
12	U-9Mo	Zircaloy-4	200
13	FCM, UO_2 Kernels in SiC, 40% packing, 700 µm diameter	Zircaloy-4	NU, 200, 600, *
14	FCM, UO_2 Kernels in SiC, 45% packing, 700 µm diameter	Zircaloy-4	200, *
15	FCM, UO_2 Kernels in SiC, 35% packing, 700 µm diameter	Zircaloy-4	200, *
16	FCM, UO_2 Kernels in SiC, 40% packing, 650 µm diameter	Zircaloy-4	200, *
17	FCM, UO_2 Kernels in SiC, 40% packing, 750 µm diameter	Zircaloy-4	200, *
18	FCM, UO_2 Kernels in SiC, 50% packing, 700 µm diameter	Zircaloy-4	200, *
19	FCM, UO_2 Kernels in SiC, 55% packing, 700 µm diameter	Zircaloy-4	200, *
20	FCM, UN Kernels in SiC, 40% packing, 700 µm diameter	Zircaloy-4	200, *
21	FCM, UN Kernels in SiC, 45% packing, 700 µm diameter	Zircaloy-4	200, *
22	FCM, UN Kernels in SiC, 35% packing, 700 µm diameter	Zircaloy-4	200, *
23	FCM, UN Kernels in SiC, 50% packing, 700 µm diameter	Zircaloy-4	200, *
24	FCM, UN Kernels in SiC, 55% packing, 700 µm diameter	Zircaloy-4	200, *
25	FCM, UN TRISO in SiC, 55% packing, 700 µm diam. kernels	Zircaloy-4	*

* Indicates additional cases performed with burnup calculated to give equivalent fuel residency (i.e., fuelling rate) to standard UO_2 bundles.

3.1 Overview of Codes Used

For reactor physics analysis, the Serpent code has been selected for this project. Serpent [44], and its development version, Serpent 2 [45], are Monte Carlo neutron transport and burnup codes, similar to MCNP [46], but utilizing the Woodcock delta-tracking method [47] to propagate neutrons more efficiently in lattice physics applications [47] than using only ray-tracing. In particular, Serpent permits the explicit modelling of dispersed fuels such as FCM fuel, which contains hundreds of thousands of tiny particles and would be untenable to accurately model using a conventional ray-tracing method. However, the delta-tracking method is incompatible with track-length estimation, and it has issues when small, heavily absorbing regions exist [47]. Thus, Serpent uses a hybrid method where it switches to surface tracking when the sampling efficiency of collisions is low [47].

For this dissertation, the CANDU core was modelled as a 2-dimensional infinite lattice of fuel channels. However, the inherent 3-d nature of FCM fuel cannot be modelled directly in 2-d. Therefore, for FCM fuel, where the fuel particles are dispersed in a 3-d matrix, the 2-d model was extruded by one bundle length to create a simplified 3-d model. The fuel particles could then be dispersed within the cylindrical matrix of each pin.

For calculating the expected temperatures of the fuel, the general-purpose finite-element code FlexPDE [48] was used. The steady radial heat equation was solved with the following characteristics:

- Fission power distribution as determined in Serpent.
- Temperature dependent fuel thermal conductivity, density and specific heat.
- Temperature dependent cladding thermomechanical properties.
- Contact thermal resistance based on existing CANDU collapsible sheath concepts.
- The coolant is not explicitly modelled, rather a convective boundary condition is used assuming the same local coolant properties and convection coefficients as typically occurs in a CANDU high power channel.

From this, the one-dimensional cylindrical heat equation can be solved to determine the temperature distribution for a fuel pin and cladding, along with average and peak fuel and cladding temperatures. For the stylized transients the time dependent heat equation is solved in FlexPDE using time dependent power as determine by the kinetics calculations and time dependent coolant boundary conditions for the stylized scenario.

3.2 Calculation Methodology

First, the required enrichment was computed for each case by altering the appropriate sheath and fuel material compositions and properties. Other parameters, such as the fuel and cladding temperature, were fixed at their reference values at this stage such that the enrichment could be easily estimated. Once the enrichment was obtained the burnup calculations were performed, saving the isotopic concentrations at each burnup step so that physics parameters such as CVR and FTC could be calculated for fresh and for irradiated fuel.

However, an important consideration for ATF is that fuel temperatures are typically lower than UO_2 fuel, thus it would be inappropriate to leave out the effect of temperature differences which are primarily due to improvements in thermal conductivity. Thus, the power profiles were calculated for fresh fuel and used to calculate the average fuel and clad temperatures for an average pin. The enrichment could then be adjusted and the burnup and physics parameter calculations repeated with a more suitable fuel temperature.

In addition, temperature profiles were also calculated for a "hot" pin, so that the maximum fuel centerline temperature could be predicted. Such calculations are based on a typical maximum bundle power in a CANDU core.

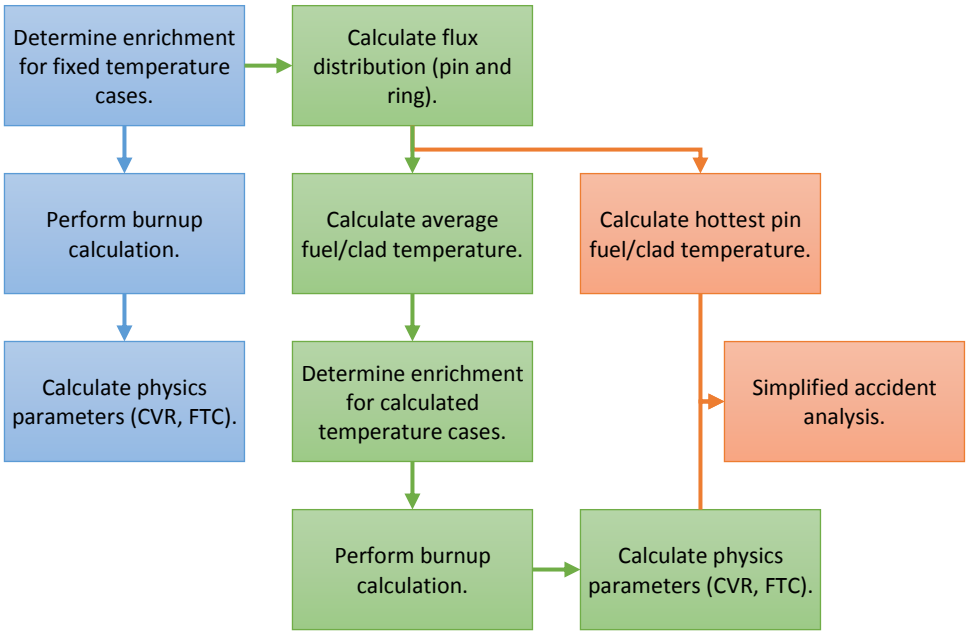

Figure 3.1: Methodology process.

The following properties were used:

Table 3.2: CANDU Lattice Properties

Element	Property	Units	Value				Comment
Fuel	Temperature	K	941.29				
	Diameter	cm	1.2244				
Cladding	Temperature	K	560.66				
	OD	cm	1.308				
Fuel Bundle	Type		37-element				
	No. of Pins		1	6	12	18	
	Ring Radii	cm	0	1.5	2.9	4.35	
	Ring Pitches	°	0	0	15	0	
Coolant	Composition		D_2O				99.2% purity
	Density	g/cm^3	0.81212				
	Temperature	K	560.66				
Pressure Tube	Composition		Zr-Nb Alloy				97.5 wt% Zr 2.5 wt% Nb
	Density	g/cm^3	6.57				
	Temperature	K	560.66				
	ID	cm	10.3378				
	OD	cm	11.2064				
Gas Gap	Composition		CO_2				
	Density	g/cm^3	0.002297				
	Temperature	K	345.66				
Calandria Tube	Composition		Zr Alloy				97.24 wt% Zr 1.6 wt% Fe 1.1 wt% Cr 0.06 wt% Ni
	Density	g/cm^3	6.44				
	Temperature	K	345.66				
	ID	cm	12.8956				
	OD	cm	13.1750				
Moderator	Composition		D_2O				99.91% purity
	Density	g/cm^3	1.082885				
	Temperature	K	345.66				
Lattice Pitch		cm	28.575				

3.2.1 Determination of Enrichment

To determine the required enrichment for each fuel type from the lattice calculation, it is assumed that all burnups from zero to the exit burnup contribute equally to the reactivity of the core. The reactivity as a function of burnup is integrated from zero to the exit burnup using the trapezoidal method, then divided by the exit burnup to get the

average. Since the lattice calculation does not include leakage or reactivity devices, this reactivity should be positive.

While the actual reactivity loss due to leakage and reactivity devices cannot be calculated directly from the lattice calculations, it can be estimated by taking a configuration that should be critical and calculating the excess reactivity of an infinite lattice. In this case, the standard UO_2 fuel using natural uranium is used as the baseline. All other cases have their enrichment adjusted until the amount of excess reactivity is similar to the base case. This also assumes that leakage and reactivity device worths do not change with the fuel configuration. These are primarily influenced by the neutron spectrum – a harder spectrum will result in adjuster rods becoming less "opaque" and thus potentially reducing their worth [23]. In LWRs, this can arise when the ratio of heavy metal to hydrogen in the core is increased, such as by switching to uranium nitride [23]. However, CANDU's neutron spectrum is over-moderated compared to that of an LWR [49], thus changes to the fuel configuration should have a lesser effect on the neutron spectrum and in turn on leakage and rod worths. Therefore, it is reasonable to assume that the excess reactivity of the infinite lattice may be similar as a first-order approximation. Future work could determine the actual enrichments, leakages and rod worths based on 3D diffusion calculations.

An iterative method is required to obtain the correct enrichment. Initially, the excess reactivity as a function of enrichment was found for the standard UO_2 case. For other cases, after running on natural uranium, the excess reactivity would be different from the UO_2 case. It was then assumed that this difference in reactivity was independent of the enrichment:

$$\bar{\rho}_{case,e} = \bar{\rho}_{UO2,e} + \Delta\rho \tag{3.1}$$

$\Delta\rho$ is calculated for natural uranium ($e = 0.711\%$). Then, $\bar{\rho}_{case,e}$ is set equal to $\bar{\rho}_{UO2,nat}$ and the corresponding value of $\bar{\rho}_{UO2,e}$ determined. The corresponding enrichment e to get $\bar{\rho}_{UO2,e}$ can then be determined, and the case simulated at that enrichment. However, it was found that this provided an imperfect approximation, and $\bar{\rho}_{case,e}$ would still differ from $\bar{\rho}_{UO2,nat}$ significantly enough to require another iteration. In this case, an interpolation (or extrapolation) would be performed based on the first two guesses:

$$\bar{\rho}_{UO2,nat} = (1 - x)\bar{\rho}_{case,e1} + x\bar{\rho}_{case,e2} \tag{3.2}$$

After the interpolation variable x has been determined, the corresponding UO_2 reactivity can be determined:

$$\bar{\rho}_{UO2,e3} = (1-x)\bar{\rho}_{UO2,e1} + x\bar{\rho}_{UO2,e2} \tag{3.3}$$

This assumes that $\Delta\rho$ is a linear function of enrichment over the incremental range of reactivities being examined. The enrichment e_3 is then looked up for $\bar{\rho}_{UO2,e3}$ and used as the next guess for the ATF case enrichment.

Based on the issues related in determining enrichment discussed above it was decided that the assumptions on $\Delta\rho$ were not sufficiently robust. Therefore, in subsequent calculations, a general observation that a change of enrichment of 0.01 wt% produced a reactivity change of roughly 2 mk was used to produce a second guess. For subsequent guesses, either direct linear interpolation and/or manual adjustment were used to achieve comparable excess reactivity as UO_2 fuel. For this linear interpolation, equation (3.2) was used, but equation (3.3) was replaced by the simpler equation:

$$e_3 = (1-x)e_1 + xe_2 \tag{3.4}$$

Iteration of enrichment was continued until the resulting excess reactivity was within 1-2 mk of the base case, corresponding to an enrichment uncertainty of roughly 0.01 wt% ^{235}U.

Uranium also contains a third isotope, ^{234}U. To estimate the approximate weight percentage of ^{234}U for a given weight percentage of ^{235}U, the following equation is used [50]:

$$e_{234} = 0.0015 + 0.0058e_{235} + 0.000054e_{235}^2 \tag{3.5}$$

The quantities e_{235} and e_{234} in the equation above are given as percentages, i.e. $e_{235} = 0.711$ for natural uranium.

3.2.2 Burnup Calculation

For burnup calculations, four depletion regions were specified – one for each ring (centre pin plus inner, intermediate, and outer rings). ENDF/B-VII.0 libraries provided with Serpent were used for cross-sections, decay, and fission product yields. DBRC was enabled for ^{238}U for energies between 0.4 eV and 210 eV.

Table 3.3: Serpent Burnup Calculation Parameters

Parameter	Value
fpcut	10^{-9}
stabcut	10^{-12}
ttacut	10^{-18}
xsfcut	10^{-6}

The predictor-corrector method was enabled in the linear-interpolation linear-extrapolation mode in Serpent 2. It is normally assumed that the flux profile (in space and energy), and thus transmutation cross-sections, are constant in time during each burnup step. The predictor-corrector method estimates the average values for each step, in contrast to the Euler method which uses the values from the beginning of the step. Other settings were as default. Serpent does not use unresolved resonance probability tables by default – the effect of this is considered to be insignificant for thermal reactors, and was tested to be on the order of 15 pcm for a CANDU lattice, but requires a significant amount of additional computer memory.

Table 3.4: Serpent Burnup Calculation Steps

Step	Burnup (MWd/kg(U))	Step	Burnup (MWd/kg(U))	Step	Burnup (MWd/kg(U))
0	0	11	0.60	21	3.50
1	0.03	…	…	…	…
2	0.06	15	1.20	26	6.00
…	…	16	1.50	27	7.00
7	0.21	17	1.80	28	8.00
8	0.25	18	2.10	29	9.00
9	0.30	19	2.50	30	10.00
10	0.45	20	3.00	…	…
11	0.60	21	3.50	50	30.00

The burnup calculation was performed either to 10 MWd/kg(U) or 30 MWd/kg(U) depending on the target exit burnup. The bundle power was assumed to be at a typical value of 700 kW.

Each half-step was run with 20 inactive generations and 500 active generations of 5000 neutrons each. For the cases where the temperature was calculated for each case, the number of neutrons per generation was increased to 16000.

For this analysis, the temperature was assumed not to change during the burnup. In reality, the temperature could be expected to increase due to degradation of heat transport capability of the fuel and cladding materials when irradiated. In the reactor environment, this would be offset by a reduction in fission power compared to nearby bundles with fresher fuel and greater fissile density. Nevertheless, the operating history effect on burn-up was not included in this analysis.

3.2.3 Calculation of CVR and FTC

For each case, the coolant void reactivity and fuel temperature coefficient were calculated. This was done both for fresh fuel (zero burnup) and for fuel irradiated to 4 MWd/kg(U), or roughly mid-burnup for fuel with a target exit burnup of 8.33 MWd/kg(U). For fuel irradiated to higher burnups, an additional burnup step was selected closest to half of exit burnup.

For the CVR calculation, the reactivity between the reference branch (no perturbation) and a branch where the coolant material is replaced with void was determined. Each branch was run with 20 inactive generations and 500 active generations of 50000 neutrons each.

For the FTC calculation, the reactivity was determined for two branches with the fuel temperature perturbed by 100 K in each direction. The slope then determines the FTC. Each branch was run with 20 inactive generations and 500 active generations of 256000 neutrons each.

3.2.4 Calculation of Fission Distribution and Temperatures

The power generation within each fuel pin is needed for thermal calculations and hence flux calculations from Serpent are used as outlined below. Since fissions are not uniformly distributed within a CANDU bundle the power density is slightly depressed in the centre of each pin. On a larger scale, the outer rings of pins shield the inner rings from thermal flux, significantly reducing the power density of the inner rings compared to the outer ring. To calculate the distribution of flux, 20 inactive generations and 500 active generations with 10000 neutrons per generation were run for each case for fresh fuel, using the reference temperatures for a CANDU lattice. Each pin was split into either five or twenty bins, equally spaced by radius, depending on whether the fuel was modelled as homogeneous (all cases except FCM) or dispersed (FCM). For calculating the average flux distribution within a pin, all pins are summed to get an average for each bin in a given ring.

For non-FCM fuel, the power distribution within an average pin can be approximated with the following equation [51]:

$$Q(r) = Q_0 I_0(\kappa r) \tag{3.6}$$

The function I_0 is the modified Bessel function of the first kind, while κ is the fitting parameter and Q_0 is the normalization parameter so that the average pin power is fixed at $^1/_{37}$ of 700 kW. Therefore, κ and Q_0 are dependent on one another and thus κ is set so that the weighted sum of squared errors is minimized.

The sum of squared errors is calculated by integrating equation for each bin (3.6) for the *area* of the bin, subtracting the actual power for that bin, then dividing by the standard deviation for that bin, and squaring. The errors are then summed to get the overall error. A numerical method was used to determine the value of κ that minimized this error.

$$e_i^2 = \left(\frac{\left(\int_{r_{0i}}^{r_{1i}} Q(r) 2\pi r \, dr \right) - \mu_i}{\sigma_i} \right)^2 \tag{3.7}$$

$$E = \sum_i e_i^2 \tag{3.8}$$

The function is then used as input to FlexPDE for the power density to solve for the local fuel and sheath temperatures.

For FCM fuel, the approximation from equation (3.6) is not appropriate due to the heterogeneity of the fuel. Therefore, twenty bins were used instead of five in the flux calculation. To get an "average" element power in a bundle, the bins were still summed over and divided by 37 as before. The binned data would then be used directly in the FlexPDE calculation, without a fitting function.

To calculate the maximum fuel temperatures for a limiting location in the core, the bundle power was assumed to increase to 880 kW, and an outer ring pin was considered. The distribution of heat within the "hot" pin was assumed to be the same as for an "average" pin, except for the magnitude:

$$Q_{hot}(r) = Q(r) * \frac{880 \text{ kW}}{700 \text{ kW}} * \frac{\overline{Q_{outer}}}{\overline{Q_{pin}}} \tag{3.9}$$

In the above equation, $\overline{Q_{pin}}$ is the average pin power for the entire bundle and $\overline{Q_{outer}}$ is the average pin power amongst the *outer ring pins only*, as they "burn" the hottest.

To calculate the temperatures, a one-dimensional heat transfer model was implemented in FlexPDE, using thermal conductivity data for different fuel configurations. Thermal conductivity for multi-phase fuel mixtures was estimated using relations found in literature [52]. Relations for fresh fuel were used. It was assumed that the coolant temperature was 560.66 K, the heat transfer coefficient to the coolant was 45000 W/(m^{2}K), and the contact conductance between pellet and clad was 80000 W/(m^{2}K).

For UO_2, thermal conductivity data from the IAEA [1] for 0% and 5% porosity was used, and linearly interpolated or extrapolated to the appropriate porosity. A spline fit was used between the temperature data points.

For UN, equation (2.1) was used [4]. For U_3Si_2, the collected data is shown in Figure 2.1 [13].

For U-9Mo, the following correlation was used [18], with T in °C, assuming that U-9Mo will have a similar thermal conductivity to U-10Mo:

$$k = 10.2 + 0.0351T \tag{3.10}$$

For SiC, the following correlation was used [4], with T in Kelvin:

$$k = 42.58 - (1.5564 * 10^4)T^{-1} + (1.2977 * 10^7)T^{-2} - (1.8458 * 10^9)T^{-3} \tag{3.11}$$

For FeCrAl, the following table was used [53]:

Table 3.5: Thermal conductivity for Kanthal APMT

Temperature (°C)	Thermal Conductivity (W m^{-1} K^{-1})
50	11
600	21
800	23
1000	27
1200	29

For the mixed fuels, the following model is used to estimate the thermal conductivity [52]:

$$R_e = \frac{2\tan^{-1}\left(\frac{B}{2}\sqrt{\frac{-C'(k_d - k_c)}{k_c + B(k_d - k_c)}}\right)}{\sqrt{-C'(k_d - k_c)\left(k_c + B(k_d - k_c)\right)}} + \frac{1 - B}{k_c}, \qquad k_d < k_c \tag{3.12}$$

$$R_e = \frac{\ln\dfrac{\sqrt{k_c + B(k_d - k_c)} + \frac{B}{2}\sqrt{C'(k_d - k_c)}}{\sqrt{k_c + B(k_d - k_c)} - \frac{B}{2}\sqrt{C'(k_d - k_c)}}}{\sqrt{C'(k_d - k_c)\left(k_c + B(k_d - k_c)\right)}} + \frac{1 - B}{k_c}, \qquad k_d > k_c \tag{3.13}$$

$$k_e = 1/R_e \tag{3.14}$$

$$C = -4\sqrt{\frac{2}{3}P_d}, \qquad C' = -C, \qquad B = -\frac{4}{C} \tag{3.15}$$

The volume fraction of the discontinuous phase is given by P_d, while k_c and k_d give the thermal conductivities of the continuous and discontinuous phase, respectively. The continuous phase is assumed to be UO_2 or UN for non-FCM fuel, and SiC for FCM fuel.

For the TRISO fuel, the discontinuous phase actually consists of several materials, thus a volume-average thermal resistance was calculated for the particle and used for k_d:

Table 3.6: Composition of TRISO particle [4]

Layer	Material	Outer Radius (μm)	Vol. Frac. (%)	Thermal Conductivity (W m^{-1} K^{-1})
Kernel	UN	350	36.4	Temperature Dependent
Buffer	Low-density PyC	400	18.0	0.5
Inner PyC	High-density PyC	435	15.6	4
SiC Coating	SiC	470	18.3	Temperature Dependent
Outer PyC	High-density PyC	490	11.8	4

3.2.5 Transient Analysis

A simplified transient was modelled in FlexPDE to determine the approximate impact of the ATF and cladding during stylized accident conditions. The same pin model was subjected to stylized conditions indicative of a large break LOCA without ECC. The initial conditions were based on the steady-state temperatures discussed above. While the conditions of this analysis were very simple and do not predict the true progression of the accident, the simplified model allows for a comparative study of the different fuel types under transient conditions, so that it can be determined which ought to be studied in more detail in future research. Inferences can also be made by looking at how ATF fuel behaves differently from UO_2 and by comparing to previous studies that used more thorough models.

Several pieces of literature were consulted in order to obtain the stylized transients considered here. The system pressure in each core-pass for each loop was modelled based on transient data presented by AECL [54]. A relationship between pressure and coolant temperature and void fraction was established using heavy water steam tables from Wolfram|Alpha [55], which also uses REFPROP as a principal source [56]. Isenthalpic expansion was assumed, which could be expected to be a reasonable approximation for the first few seconds where neutronic effects dominate. For the bundle in the broken loop, the heat transfer coefficient to the coolant was assumed not to change until the

pressure dropped to 5 MPa, after which h was reduced linearly from 45000 W/m^{2}K to 150 W/m^{2}K with respect to pressure until the pressure dropped to 1 MPa. Afterwards it was assumed that h was proportional to pressure, dropping to 15 W/m^{2}K at atmospheric pressure, roughly corresponding to convection to nearly stagnant steam at low pressure, since the flow rate will be low after the blowdown period. The heat transfer coefficient was then multiplied by a coefficient that reduced linearly from 1 to 0.2 between 40 s and 120 s to account for the fact that the low coolant temperatures predicted by isenthalpic expansion are likely inaccurate post-blowdown, so that the ultimate heat transfer coefficient was 3 W/m^{2}K. For calculating the transient in fission power, heat transfer by radiation was ignored since the time period and temperatures being examined here precludes significant radiation heat transfer until the fission power drops to virtually zero.

The transient is initiated such that voiding starts at $t = 0$ s while significant voiding starts at $t = 0.5$ s. The neutronics are modelled using point kinetics with one delayed group for simplicity. The reactivity insertion due to voiding follows:

$$\rho_{cv}(t) = CVR\big(0.25\alpha_1(t) + 0.25\alpha_2(t) + 0.5\alpha_3(t)\big) \tag{3.16}$$

Where α_1 and α_2 are the void fractions in the two passes of the broken loop, while α_3 is the void fraction for the intact loop. The latter has little effect on the transient since the intact loop experiences a relatively slow exponential decline in pressure, and the reactor will be shut down before voiding begins here.

The core reactivity is then modelled as:

$$\rho(t) = FTC(\bar{T}(t) - \bar{T}_{ss}) + \rho_{cv}(t) + \rho_{SDS1}(t) \tag{3.17}$$

The steady-state average temperature $\bar{T}_{ss}$ is the temperature calculated in the steady-state model, so that the transient model can approach the same steady state prior to the transient. The shutdown reactivity term ρ_{SDS1} is zero up to $t = 1$ s and is linearly ramped to -50 mk over a period of 1 second.

The point kinetics equations are then:

$$\frac{dN(t)}{dt} = \frac{\rho - \beta}{\Lambda} N(t) + \lambda C(t) \tag{3.18}$$

$$\frac{dC(t)}{dt} = \frac{\beta}{\Lambda} N(t) - \lambda C(t) \tag{3.19}$$

Both the neutron flux $N(t)$ and delayed precursor concentration $C(t)$ are normalized so that the steady-state $N(t)$ is equal to fission power as a fraction of full power. This will be roughly 0.94 since roughly 6% of the total thermal power is "decay heat".

The delayed group parameters β and λ, along with the prompt generation time Λ, are obtained from the Serpent output for each fuel type, using best estimate values.

Decay heat follows the equation [57]:

$$D(t) = 0.1((t_s + 10)^{-0.2} - (t_s + \tau + 10)^{-0.2} + 0.87(t_s + \tau + 2 * 10^7)^{-0.2} - 0.87(t_s + 2 * 10^7)^{-0.2}) \quad (3.20)$$

Where t_s is the time from shutdown, and τ the time of operation since startup. τ is assumed to be 365 days for this purpose, while $t_s = t - 1.25$ s, i.e. the shutdown time is assumed to be at $t = 1.25$ s for the decay heat calculation.

The total reactor power is the sum of prompt power $N(t)$ and decay power $D(t)$, both of which are normalized to full power. The prompt and delayed power are the only two sources of heat in this model. Heat from cladding oxidation is not modelled since the time period of this analysis precludes significant oxidization.

The problem is solved in two stages. For the first stage, the nominal power is that for the "average" pin. This calculation is used to calculate the transient for $N(t)$. The second stage removes the point kinetics calculations and instead uses the calculated $N(t)$ from the first stage, and uses the peak bundle power, along with modelling a pin from each of the four rings. In addition, for this calculation the effects of radiation were added to the model, with the pressure tube's temperature also modelled.

The analysis was performed on UO_2, on the three UO_2-3%SiC cases with different cladding, the UO_2-10%SiC case, UN, U-9Mo, and the FCM cases with the same in-core residence time as UO_2 bundles.

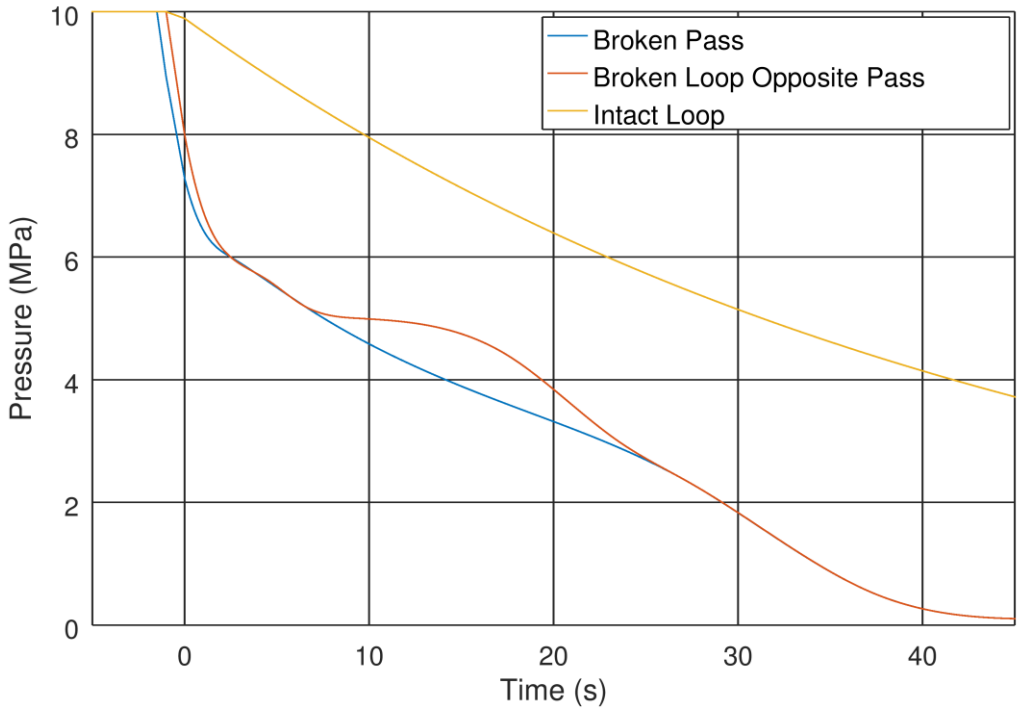

Figure 3.2: Stylized pressure transient

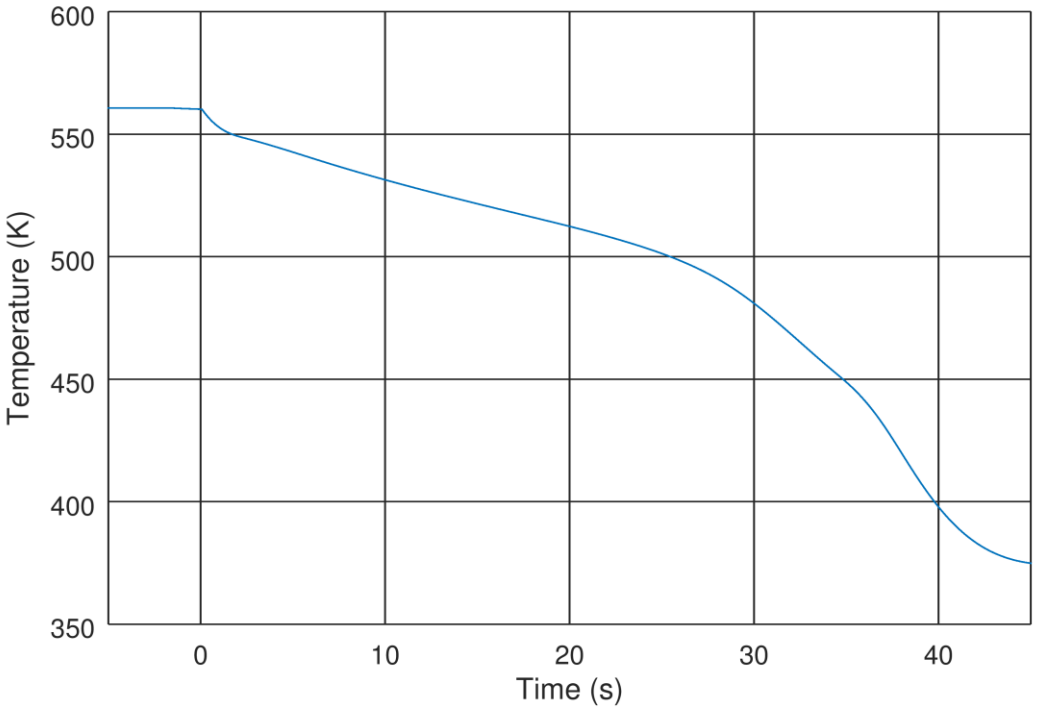

Figure 3.3: Coolant temperature for stylized transient using isenthalpic expansion

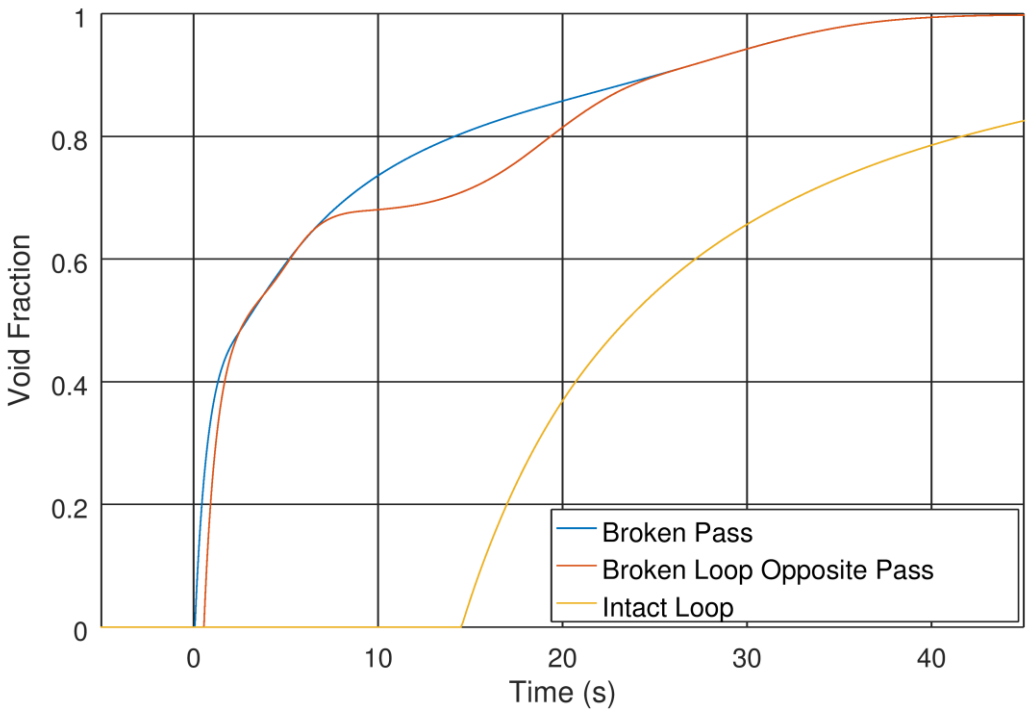

Figure 3.4: Coolant voiding for stylized transient using isenthalpic expansion

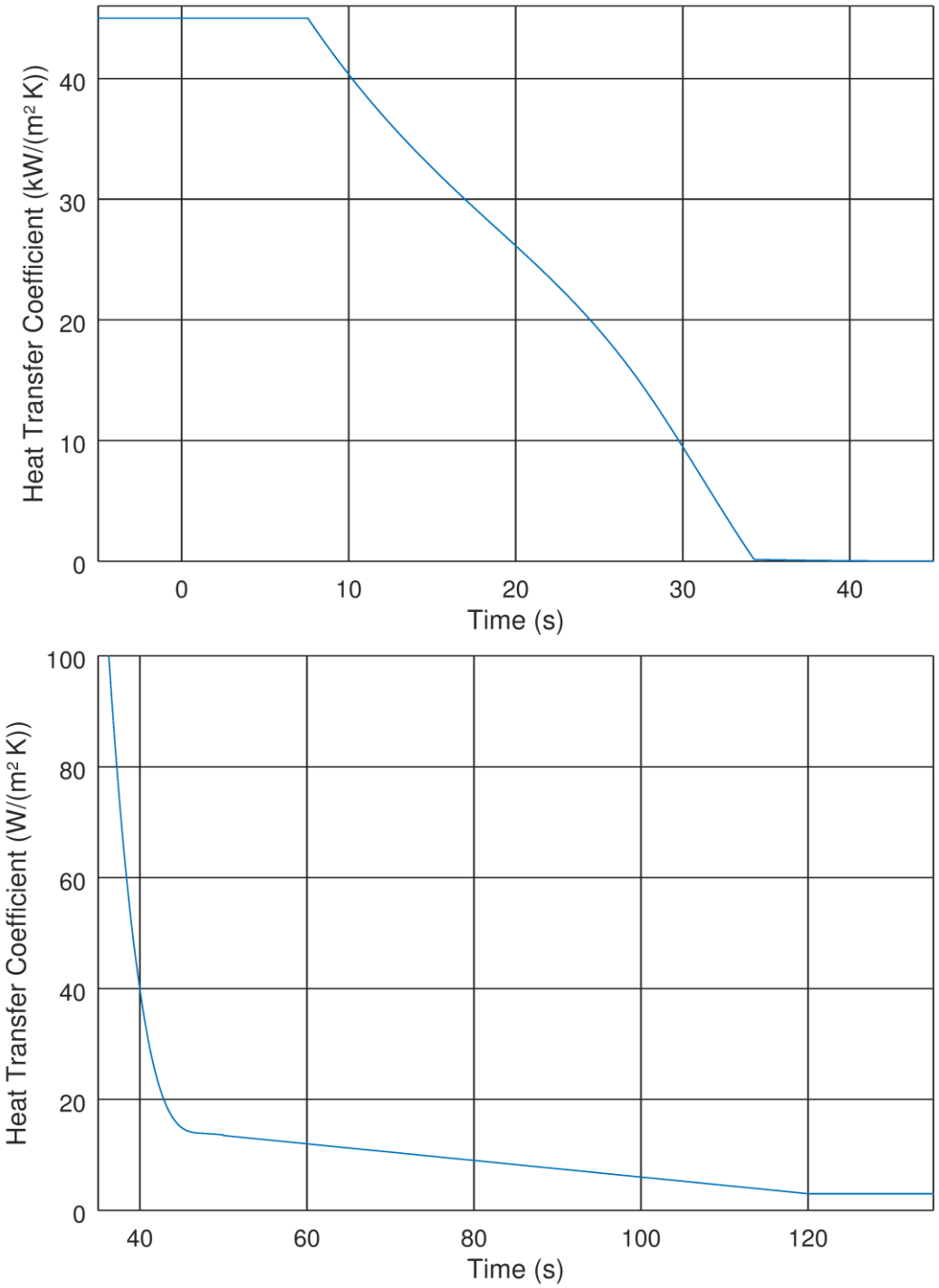

Figure 3.5: Stylized heat transfer degradation

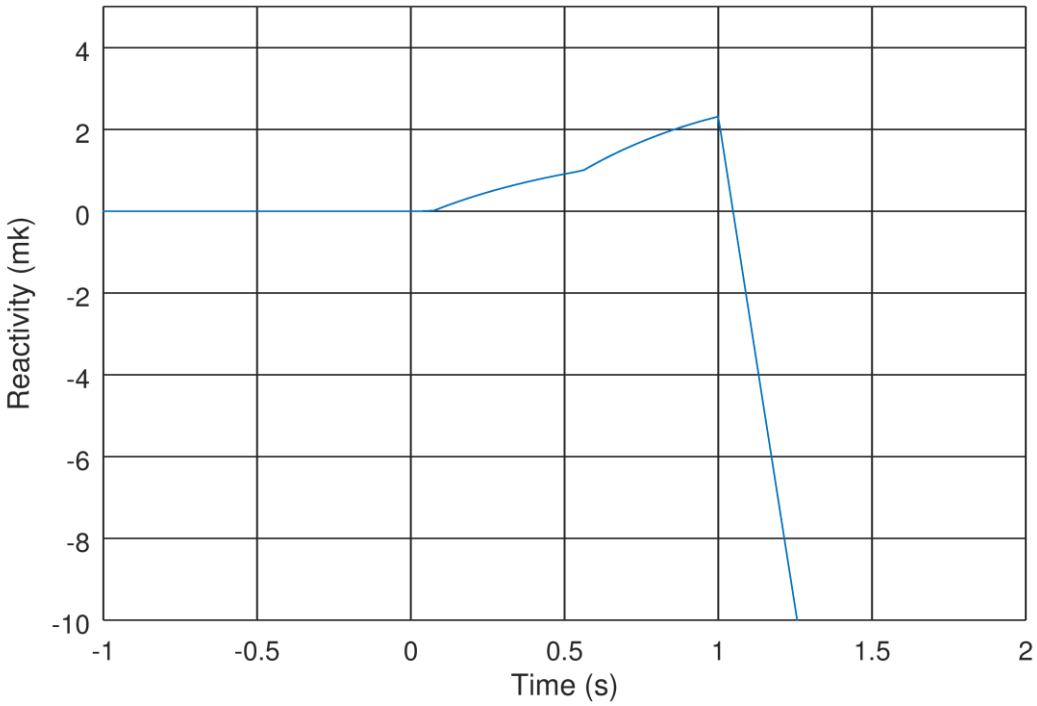

Figure 3.6: Stylized reactivity transient (UO_2 case)

Instead of modelling a single pin as was done for the power transient, the temperature transient modelled the temperature in each ring separately, along with a space-independent pressure tube temperature. Radiation is modelled in this case assuming no geometric deformation, while heat produced from oxidation remains neglected.

The emissivity of zircaloy is initially 0.20 [58], and this value is also used for other metals. When oxidized, the emissivity increases to 0.82 [58]. For FeCrAl, the emissivity of fully oxidized material is 0.70 [53], while 0.90 was used for SiC [59]. All materials were assumed to be gray. The view factor matrix for the four rings and pressure tube was computed using a Monte Carlo algorithm using 360000 emissions per ring, for each cladding type and for unoxidized and oxidized states, with the oxidized state assuming oxidation of the cladding but not the pressure tube as the pressure tube temperature is lower. This can be considered conservative as a lower emissivity for the pressure tube corresponds to a reduced ability to capture radiation from the fuel. In the model, emissivities and view factors begin at their unoxidized values and are linearly interpolated to the oxidized values between $t = 300$ s and $t = 360$ s, except for SiC cladding where there is only one set of values.

The pressure tube is modelled in a space-independent manner, which is the stored energy per unit length calculated as a product of the specific heat, density, and cross-sectional area of the Zircaloy pressure tube. Heat transfer from the pressure tube is due

to convection to the coolant along with radiation to and from the fuel pins. In addition, it is assumed that once the pressure tube temperature reaches 1200 K, an additional heatsink is added at a temperature of 700 K and a linear heat transfer coefficient of 200 W/K, to model pressure tube deformation and contact with the calandria tube and heat transfer to the moderator. The temperature is set to 700 K rather than the roughly 350 K of the moderator to account for the average temperature of the PT at contact, similar to results from literature [26].

4 Results

Prior to the research on ATF, a number of Serpent calculations were performed to verify consistency with other codes and benchmarks. In particular, Serpent results for k_{inf} and nuclide concentrations were consistent with results from TRITON [60] for PWR and BWR pin benchmarks, as well as for a CANDU lattice. Additionally, values of CVR and FTC predicted at different burnups were consistent between Serpent and TRITON within a reasonable uncertainty.

4.1 UO_2-SiC Composite Fuel

The introduction of SiC to UO_2 fuel reduces the fuel's uranium density, requiring a slight enrichment to achieve a similar exit burnup. Increasing the enrichment to 1.3% allows for the exit burnup to be tripled.

The addition of SiC improves the thermal conductivity of the composite fuel over normal UO_2 fuel reducing the average and maximum pin temperatures significantly. Adding 10% SiC by volume reduces the maximum temperature from 2070 K to 1464 K, which is roughly a 30% decrease in centre-line temperature. However the thermal conductivity of SiC degrades with irradiation and hence improvement will be less than noted above. For SiC, irradiation defects saturate due to competition with thermal recovery [38] so that under 4 MWd/kg(U) burnup the peak temperature is 2306 K for UO_2 and 1881 K with the 10% SiC additive.

The coolant void reactivity is decreased slightly for UO_2-SiC composite fuel compared to standard fuel. The overall effect on FTC is not significant, as there appears to be a slight positive contribution, offset by a slight negative contribution from the temperature reduction.

Table 4.1: Required Enrichment for UO_2-SiC composite fuel

Fuel	Exit Burnup (MWh/kg(U))	Enrichment (wt% ^{235}U)	
		Fixed T	Calculated T
UO_2	200	0.711%	0.711%
	600	1.30%	1.30%
UO_2 + 3% SiC	200	0.72%	0.72%
	600	1.32%	1.32%
UO_2 + 6% SiC	200	0.72%	0.72%
UO_2 + 10% SiC	200	0.73%	0.73%

Table 4.2: Average pin temperatures for UO_2-SiC composite fuel

Description	Enrichment (wt% ^{235}U)	Fuel CL Temp. (K)	Fuel Avg. Temp. (K)	Clad Avg. Temp. (K)
UO_2	0.711%	1437.0	981.6	593.9
	1.300%	1429.1	979.4	593.9
UO_2 + 3% SiC	0.711%	1269.9	913.5	593.9
	0.720%	1269.7	913.5	593.9
	1.320%	1264.0	911.8	593.9
UO_2 + 6% SiC	0.720%	1190.9	880.6	593.9
UO_2 + 10% SiC	0.730%	1115.5	848.5	593.9

Table 4.3: Maximum pin power for UO_2-SiC composite fuel

Description	Enrichment (wt% ^{235}U)	Outer Ring Power Factor	Linear Element Rating (W/m^2)
UO_2	0.711%	1.14236	54855
	1.300%	1.19599	57430
UO_2 + 3% SiC	0.711%	1.13925	54706
	0.720%	1.13958	54722
	1.320%	1.19267	57271
UO_2 + 6% SiC	0.720%	1.13643	54570
UO_2 + 10% SiC	0.730%	1.13289	54400

Table 4.4: Hottest pin temperatures for UO_2-SiC composite fuel

Description	Enrichment (wt% ^{235}U)	Fuel CL Temp. (K)	Fuel Avg. Temp. (K)	Clad Avg. Temp. (K)
UO_2	0.711%	2069.6	1248.4	608.3
	1.300%	2159.0	1290.1	610.5
UO_2 + 3% SiC	0.711%	1760.1	1124.3	608.2
	0.720%	1760.3	1124.4	608.2
	1.320%	1835.4	1157.7	610.4
UO_2 + 6% SiC	0.720%	1607.6	1064.4	608.0
UO_2 + 10% SiC	0.730%	1463.7	1007.1	607.9

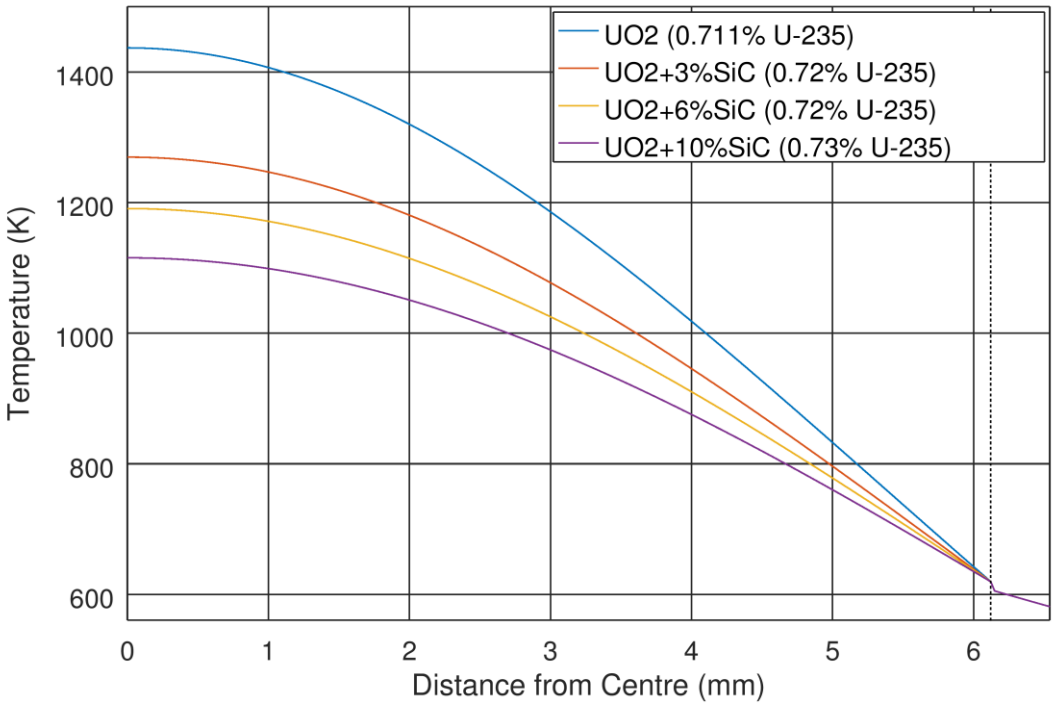

Figure 4.1: Average pin temperatures for UO_2-SiC fuels

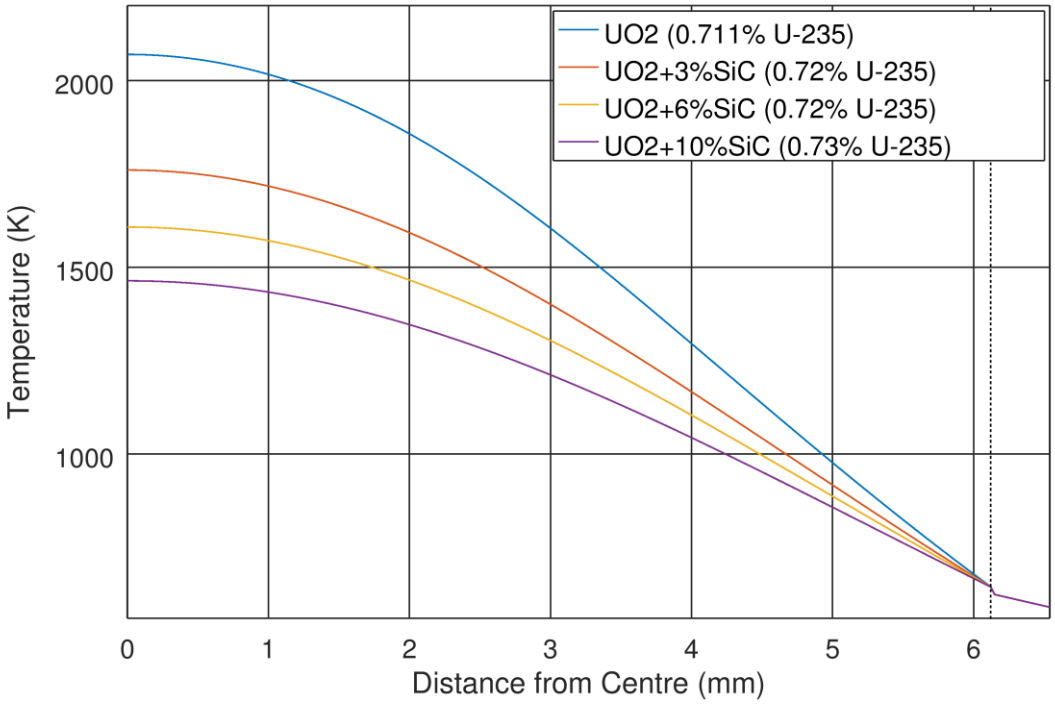

Figure 4.2: Hottest pin temperatures for UO_2-SiC fuels

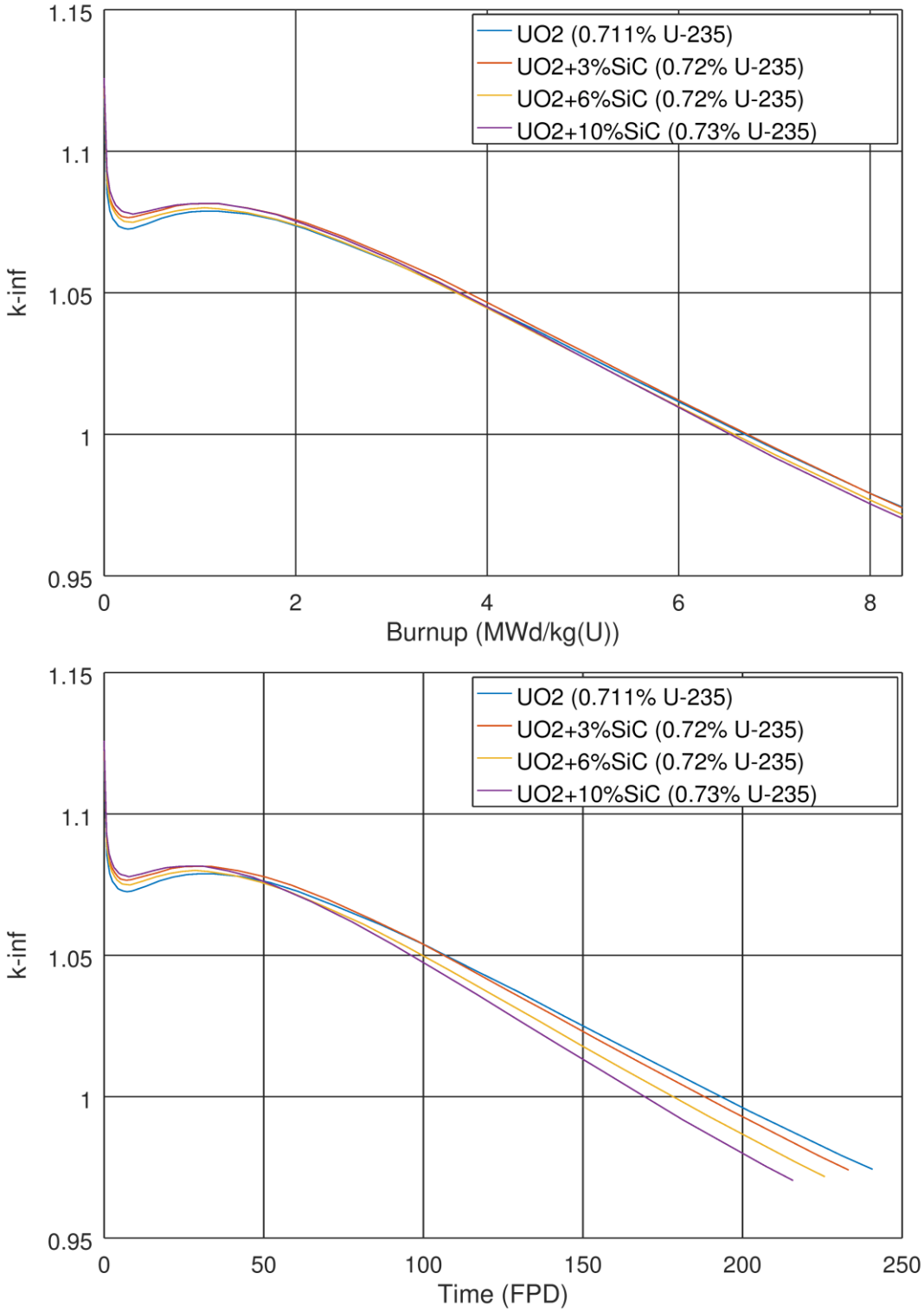

Figure 4.3: Reactivity of UO_2-SiC fuels – calculated temperature

Table 4.5: CVR and FTC calculations for UO_2-SiC composite fuel

Description	Enrichment (wt% ^{235}U)	Burnup (MWd/kg(U))	Calculated T			T = 941.29 K	
			k_∞	CVR (mk)	FTC (pcm/K)	CVR (mk)	FTC (pcm/K)
UO_2	0.711%	0	1.11850	16.79 ± 0.07	-1.22 ± 0.03	16.73 ± 0.07	-1.23 ± 0.03
		4	1.04513	14.59 ± 0.09	-0.12 ± 0.03	14.49 ± 0.09	-0.14 ± 0.03
	1.300%	0	1.35036	12.13 ± 0.06	-0.83 ± 0.02	12.24 ± 0.06	-0.85 ± 0.02
		4	1.21457	13.29 ± 0.07	-0.66 ± 0.03	13.42 ± 0.07	-0.70 ± 0.03
		12	1.04183	16.24 ± 0.10	-0.16 ± 0.04	16.06 ± 0.10	-0.16 ± 0.04
UO_2 + 3% SiC	0.711%	0	1.11792	16.60 ± 0.07	-1.26 ± 0.03	16.47 ± 0.08	-1.21 ± 0.03
		4	1.04358	14.33 ± 0.09	-0.16 ± 0.03	14.26 ± 0.09	-0.11 ± 0.03
	0.720%	0	1.12319	16.49 ± 0.07	-1.24 ± 0.03	16.41 ± 0.07	-1.23 ± 0.03
		4	1.04638	14.37 ± 0.09	-0.18 ± 0.03	14.32 ± 0.09	-0.17 ± 0.03
	1.320%	0	1.35597	11.97 ± 0.06	-0.88 ± 0.02	12.01 ± 0.06	-0.89 ± 0.02
		4	1.21929	13.19 ± 0.07	-0.72 ± 0.03	13.38 ± 0.07	-0.66 ± 0.03
		12	1.04463	15.82 ± 0.09	-0.17 ± 0.04	15.84 ± 0.10	-0.19 ± 0.04
UO_2 + 6% SiC	0.720%	0	1.12203	16.27 ± 0.07	-1.27 ± 0.03	16.47 ± 0.07	-1.23 ± 0.03
		4	1.04462	13.98 ± 0.09	-0.19 ± 0.03	14.10 ± 0.09	-0.08 ± 0.03
UO_2 + 10% SiC	0.730%	0	1.12577	16.05 ± 0.07	-1.33 ± 0.03	16.12 ± 0.07	-1.24 ± 0.03
		4	1.04509	13.70 ± 0.09	-0.16 ± 0.03	13.93 ± 0.09	-0.07 ± 0.03

In the case of a transient, the size of the power pulse is reduced slightly for composite fuel compared to standard fuel. After shutdown, there is no significant difference in the temperature behaviour of the fuel.

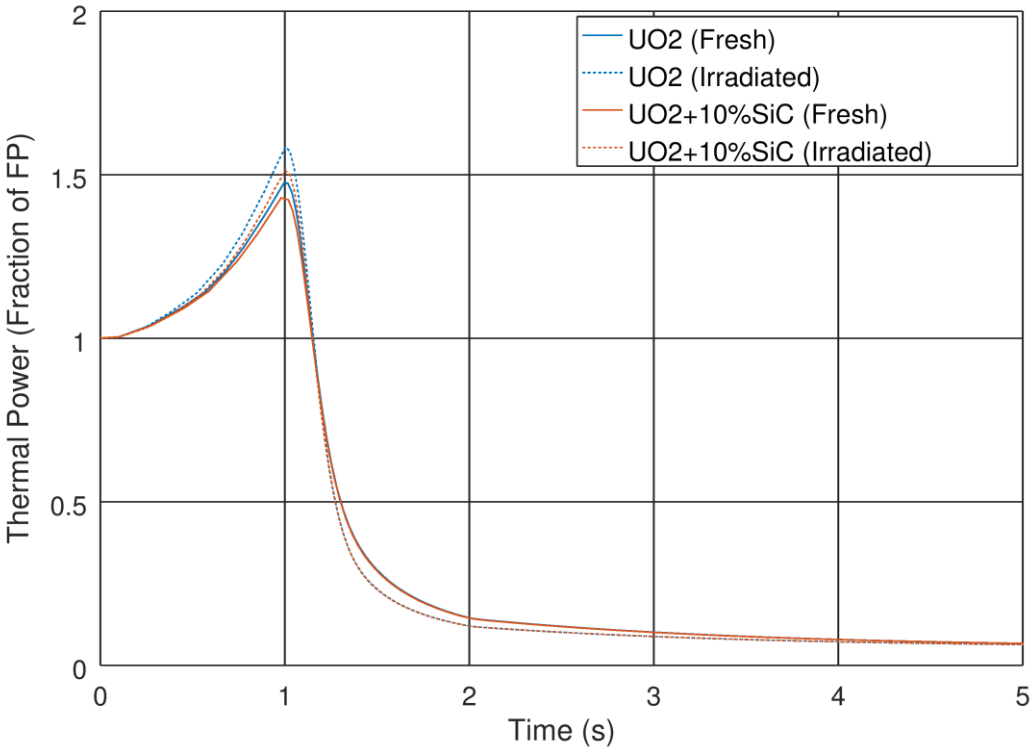

Figure 4.4: Reactor power transient for UO_2-SiC composite fuel

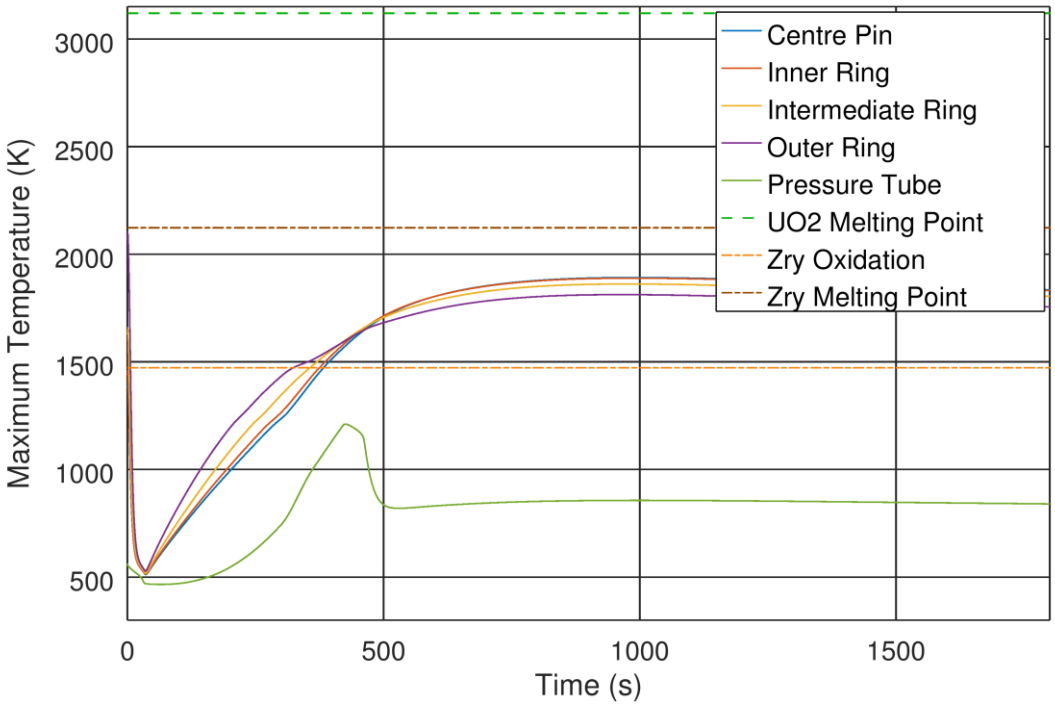

Figure 4.5: Fuel bundle temperature transient for fresh UO_2

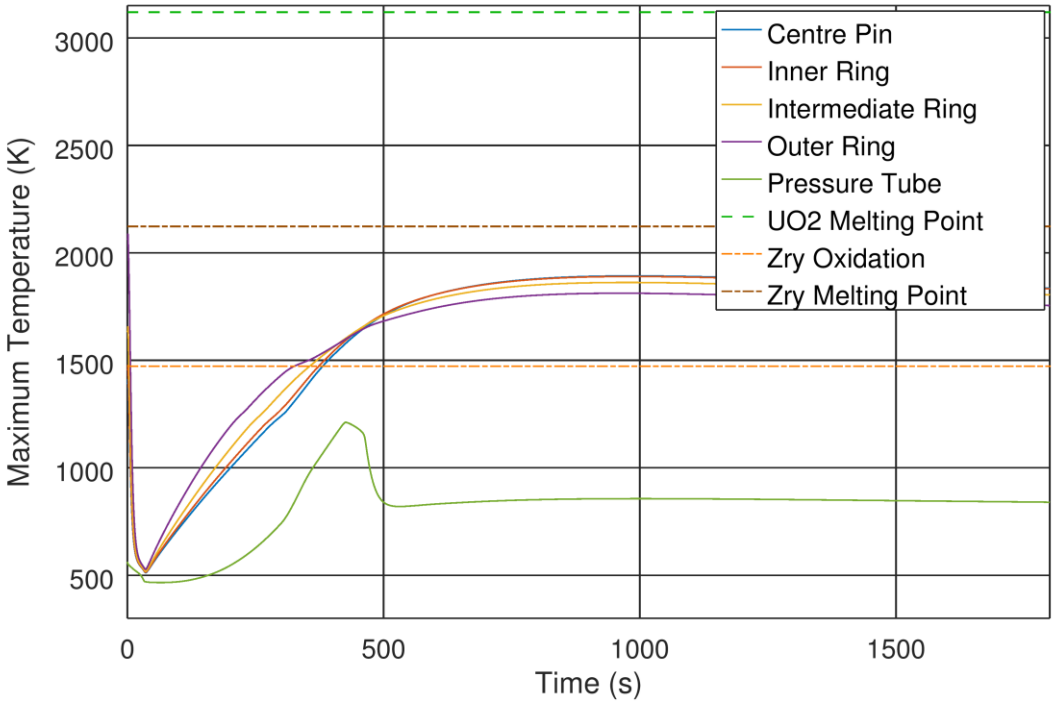

Figure 4.6: Fuel bundle temperature transient for irradiated UO_2

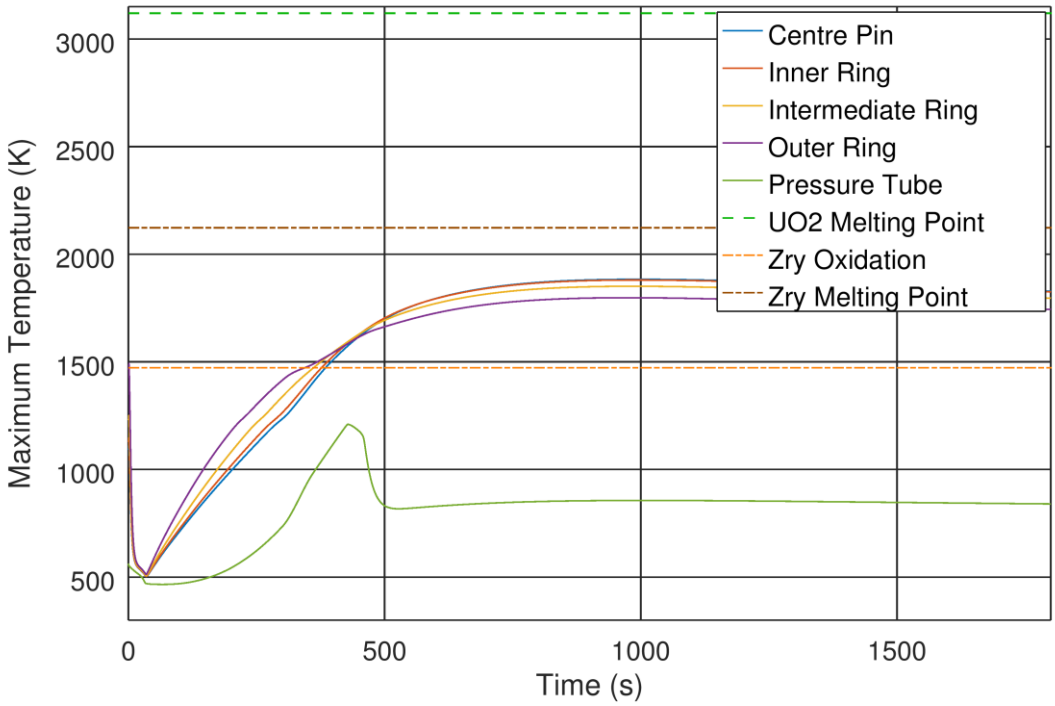

Figure 4.7: Fuel bundle temperature transient for fresh UO_2 + 10% SiC

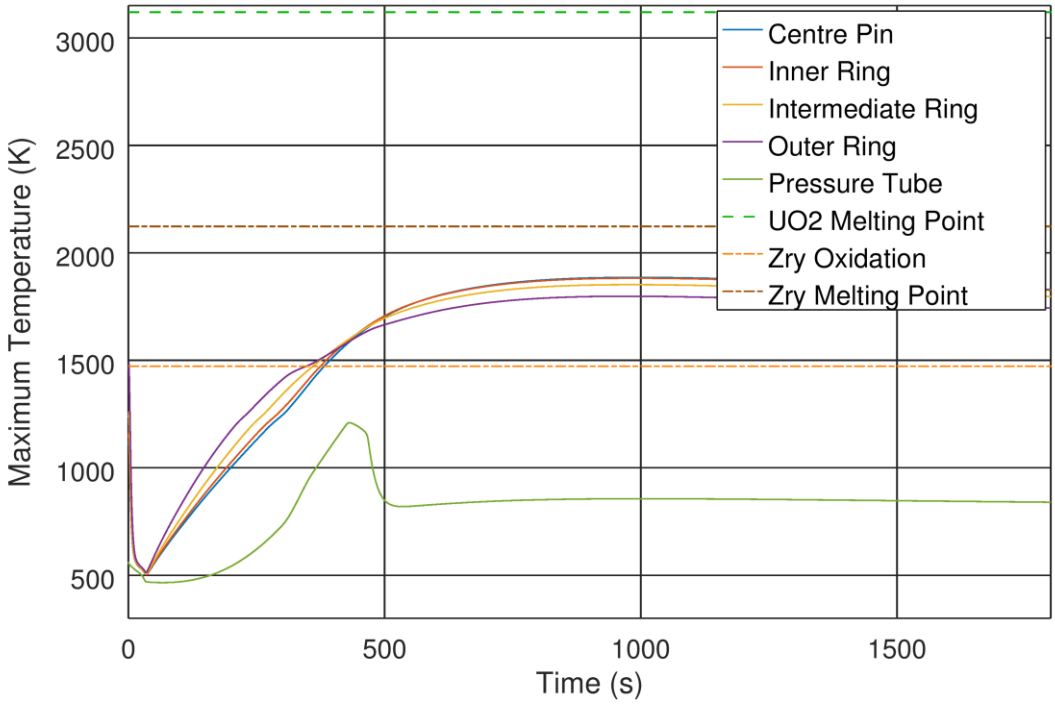

Figure 4.8: Fuel bundle temperature transient for irradiated UO_2 + 10% SiC

4.2 UN Fuel

As the nitrogen in uranium nitride fuel absorbs a significant proportion of neutrons, a significantly greater enrichment is required to achieve a similar exit burnup as standard fuel. However, since UN is denser than UO_2, fuelling machine utilization would be reduced given the same exit burnup.

Due to the higher enrichment, the "plutonium peak" in reactivity observed for UO_2 fuel is absent for UN fuel.

The improved thermal conductivity offered by UN results in very low fuel temperatures, with the maximum being 893 K for UN fuel. The addition of U_3Si_2, which has a somewhat lower thermal conductivity, increases the fuel temperature slightly, while the addition of ZrN decreases the fuel temperature slightly, though the difference is only a few degrees.

Compared to UO_2 fuel, UN fuel has a substantially more negative FTC, as there is not only a negative contribution due to the fuel temperature reduction, but also a negative contribution for irradiated fuel due to the material change itself. CVR is smaller for fresh UN fuel but larger for irradiated UN fuel, though the magnitude of the changes are only a small fraction of the total CVR.

Table 4.6: Required Enrichment for UN-based fuel

Fuel	Exit Burnup (MWh/kg(U))	Enrichment (wt% ^{235}U)	
		Fixed T	Calculated T
UN	200	1.28%	1.28%
	600	2.04%	2.04%
UN + 3% U_3Si_2	200	1.27%	1.26%
	600	2.02%	2.02%
UN + 6% U_3Si_2	200	1.25%	1.25%
UN + 10% U_3Si_2	200	1.23%	1.23%
UN + 3% ZrN	200	1.30%	1.30%

Table 4.7: Average pin temperatures for UN-based fuel

Description	Enrichment (wt% ^{235}U)	Fuel CL Temp. (K)	Fuel Avg. Temp. (K)	Clad Avg. Temp. (K)
UN	0.711%	771.1	696.9	593.9
	1.280%	769.6	696.4	593.9
	2.040%	767.7	695.7	593.9
UN + 3% U_3Si_2	0.711%	772.9	697.8	593.9
	1.270%	771.4	697.3	593.9
	2.020%	769.5	696.6	593.9
UN + 6% U_3Si_2	1.250%	773.3	698.3	593.9
UN + 10% U_3Si_2	1.230%	776.1	699.7	593.9
UN + 3% ZrN	1.300%	768.0	695.5	593.9

Table 4.8: Maximum pin power for UN-based fuel

Description	Enrichment (wt% ^{235}U)	Outer Ring Power Factor	Linear Element Rating (W/m^2)
UN	0.711%	1.23971	59530
	1.280%	1.30258	62548
	2.040%	1.36828	65704
UN + 3% U_3Si_2	0.711%	1.23697	59398
	1.270%	1.29860	62357
	2.020%	1.36372	65485
UN + 6% U_3Si_2	1.250%	1.29395	62134
UN + 10% U_3Si_2	1.230%	1.28902	61897
UN + 3% ZrN	1.300%	1.29579	62223

Table 4.9: Hottest pin temperatures for UN-based fuel

Description	Enrichment (wt% ^{235}U)	Fuel CL Temp. (K)	Fuel Avg. Temp. (K)	Clad Avg. Temp. (K)
UN	0.711%	880.2	768.9	612.3
	1.280%	892.9	778.1	614.9
	2.040%	905.2	787.4	617.6
UN + 3% U_3Si_2	0.711%	882.0	769.8	612.2
	1.270%	894.5	778.9	614.7
	2.020%	906.8	788.1	617.4
UN + 6% U_3Si_2	1.250%	896.0	779.6	614.5
UN + 10% U_3Si_2	1.230%	898.7	780.9	614.3
UN + 3% ZrN	1.300%	889.0	775.8	614.6

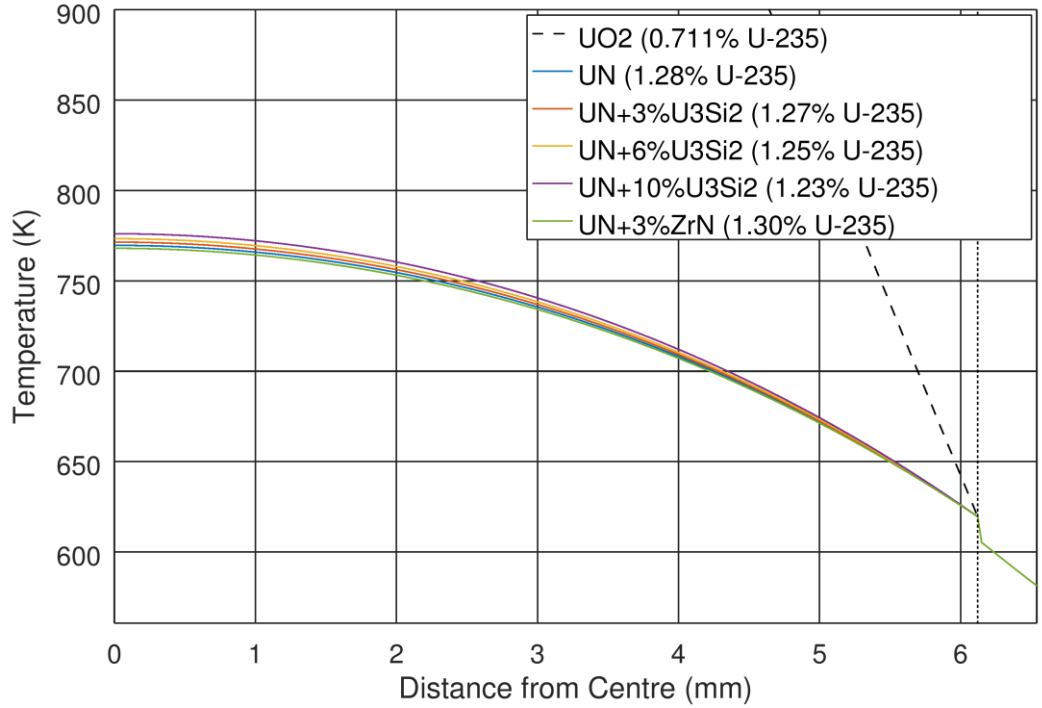

Figure 4.9: Average pin temperatures for UN fuels

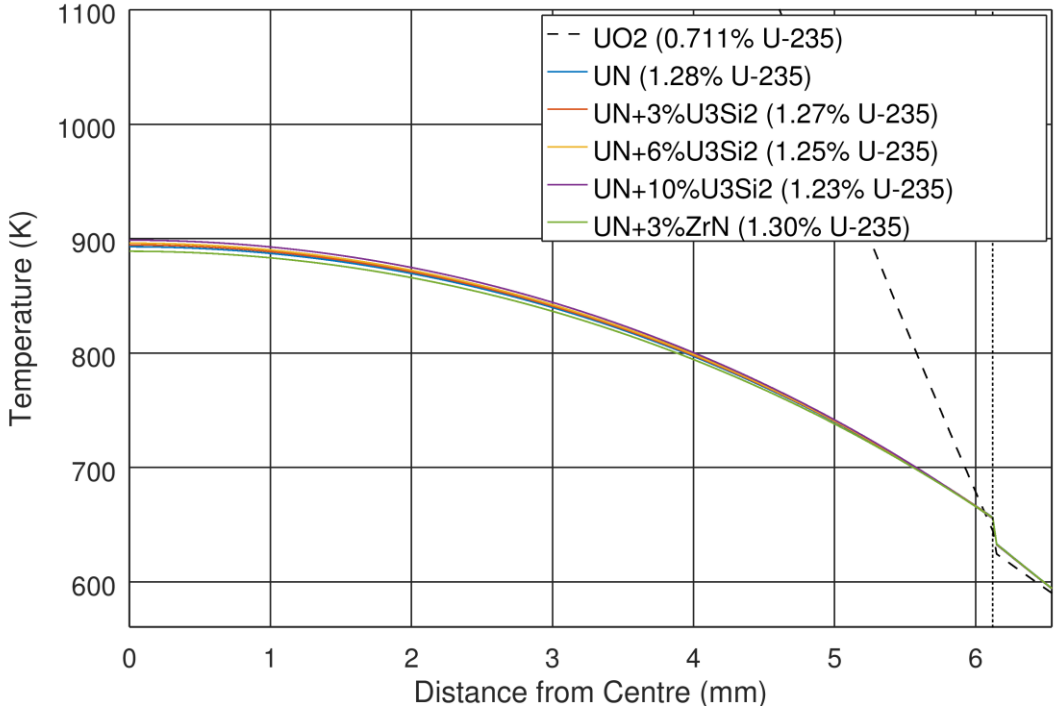

Figure 4.10: Hottest pin temperatures for UN fuels

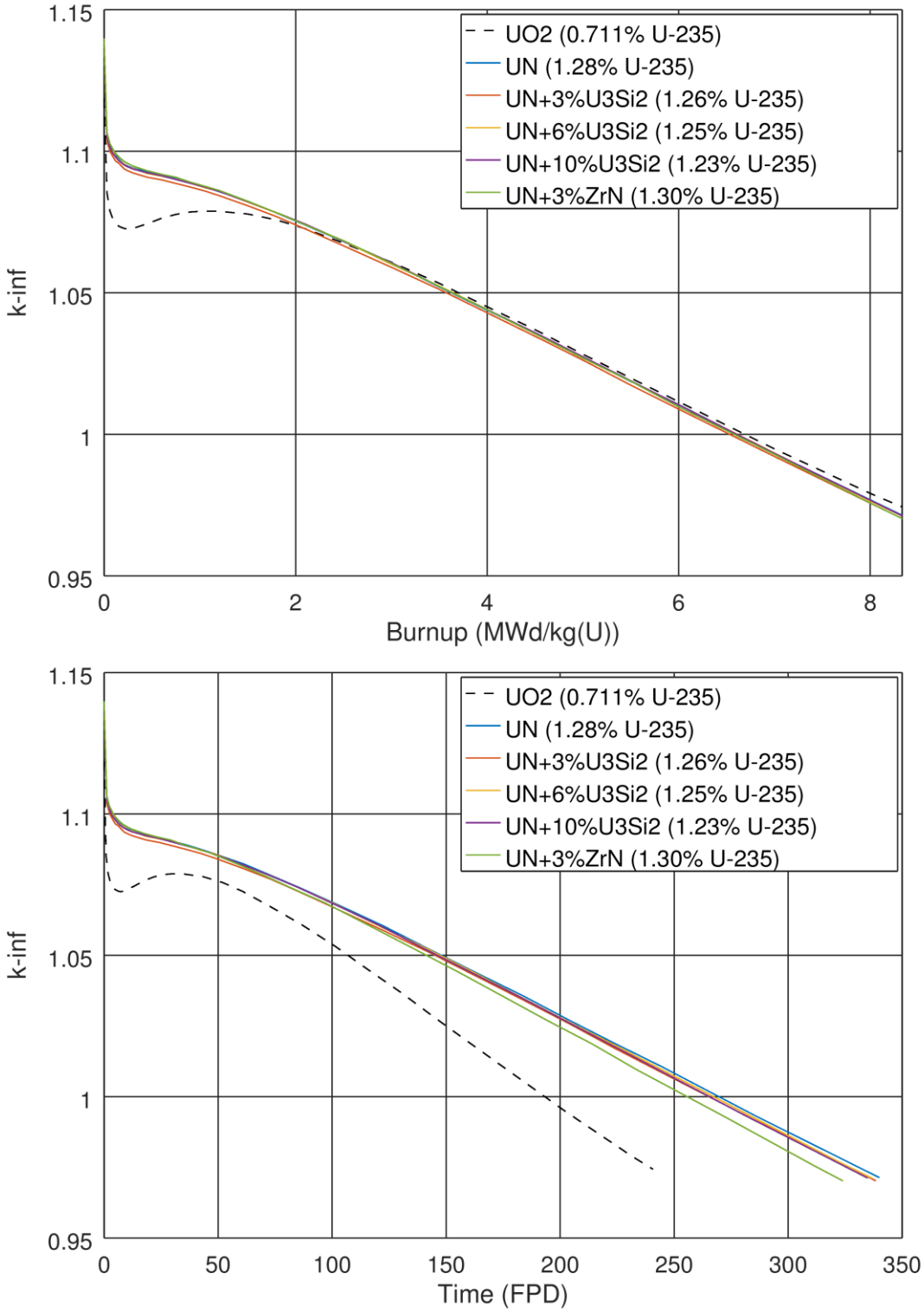

Figure 4.11: Reactivity of UN fuel – calculated temperature

Table 4.10: CVR and FTC calculations for UN fuel

Description	Enrichment (wt% ^{235}U)	Burnup (MWd/kg(U))	Calculated T			T = 941.29 K	
			k_∞	CVR (mk)	FTC (pcm/K)	CVR (mk)	FTC (pcm/K)
UN	0.711%	0	0.89689	21.11 ± 0.10	-2.07 ± 0.04	21.17 ± 0.11	-1.86 ± 0.04
		4	0.89177	17.09 ± 0.12	0.47 ± 0.05	17.52 ± 0.12	0.75 ± 0.05
	1.280%	0	1.13865	14.12 ± 0.08	-1.40 ± 0.03	14.48 ± 0.08	-1.24 ± 0.03
		4	1.04406	15.38 ± 0.09	-0.67 ± 0.03	15.56 ± 0.10	-0.51 ± 0.04
	2.040%	0	1.30916	11.03 ± 0.07	-1.08 ± 0.03	11.19 ± 0.07	-0.97 ± 0.03
		4	1.19431	12.85 ± 0.08	-0.97 ± 0.03	13.16 ± 0.08	-0.80 ± 0.03
		12	1.05159	17.97 ± 0.10	-0.69 ± 0.04	18.21 ± 0.10	-0.49 ± 0.04
UN + 3% U_3Si_2	0.711%	0	0.90153	20.86 ± 0.10	-2.06 ± 0.04	21.00 ± 0.10	-1.80 ± 0.04
		4	0.89502	16.93 ± 0.12	0.41 ± 0.04	17.24 ± 0.12	0.79 ± 0.05
	1.260%	0	1.13704	14.38 ± 0.08	-1.39 ± 0.03	14.44 ± 0.08	-1.27 ± 0.03
		4	1.04282	15.58 ± 0.09	-0.78 ± 0.04	15.70 ± 0.09	-0.50 ± 0.04
	2.020%	0	1.30997	11.12 ± 0.07	-1.07 ± 0.03	11.33 ± 0.07	-0.96 ± 0.03
		4	1.19473	12.77 ± 0.08	-0.97 ± 0.03	13.03 ± 0.08	-0.83 ± 0.03
		12	1.05165	17.71 ± 0.10	-0.71 ± 0.04	18.14 ± 0.10	-0.44 ± 0.04
UN + 6% U_3Si_2	1.250%	0	1.13883	14.12 ± 0.08	-1.40 ± 0.03	14.48 ± 0.08	-1.27 ± 0.03
		4	1.04412	15.37 ± 0.09	-0.72 ± 0.04	15.61 ± 0.10	-0.44 ± 0.04
UN + 10% U_3Si_2	1.230%	0	1.13868	14.26 ± 0.08	-1.39 ± 0.03	14.58 ± 0.08	-1.20 ± 0.03
		4	1.04420	15.41 ± 0.09	-0.67 ± 0.03	15.83 ± 0.10	-0.47 ± 0.04
UN + 3% ZrN	1.300%	0	1.13967	13.93 ± 0.08	-1.40 ± 0.03	14.02 ± 0.08	-1.29 ± 0.03
		4	1.04414	14.90 ± 0.09	-0.75 ± 0.03	15.30 ± 0.09	-0.48 ± 0.04

In the case of a transient, compared to UO_2, the power pulse is slightly smaller for fresh fuel and similar for irradiated fuel.

When the bundle is modelled with radiative heat transfer, the results are primarily affected by the distribution of power density in the bundle. Since the spatial self-shielding effect is stronger in UN, the temperature difference between outer and inner rings is more substantial compared to UO_2 fuel, for the early portion of the transient. The late portion of the transient, after pressure tube creep occurs, is very similar for UO_2 and UN fuels.

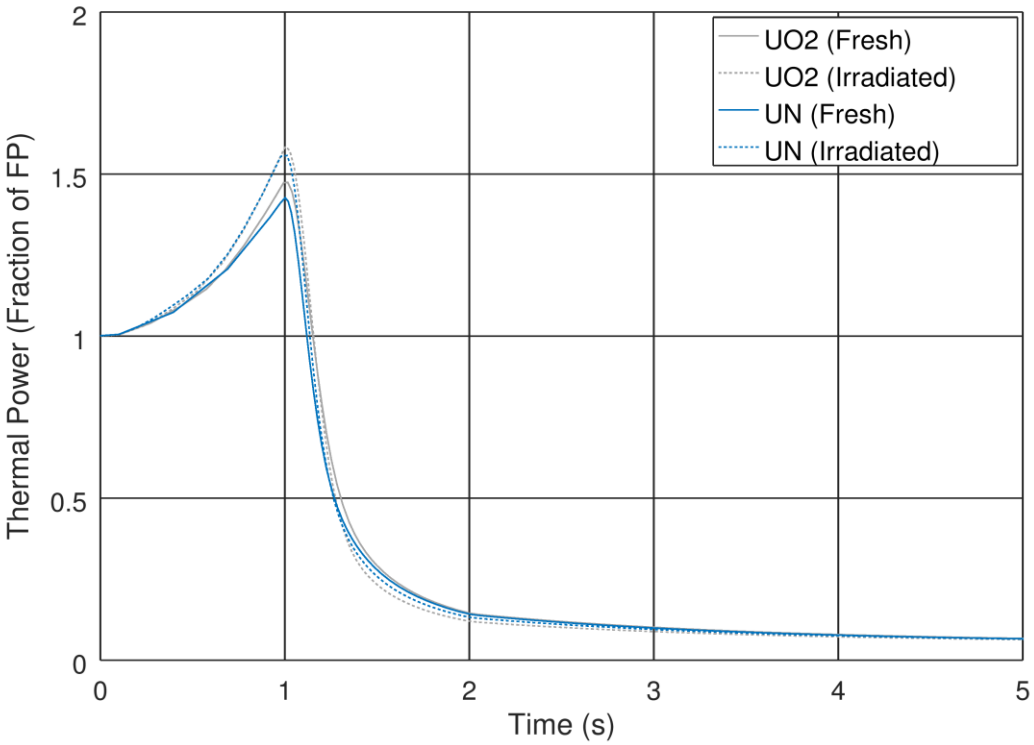

Figure 4.12: Reactor power transient for UN fuel

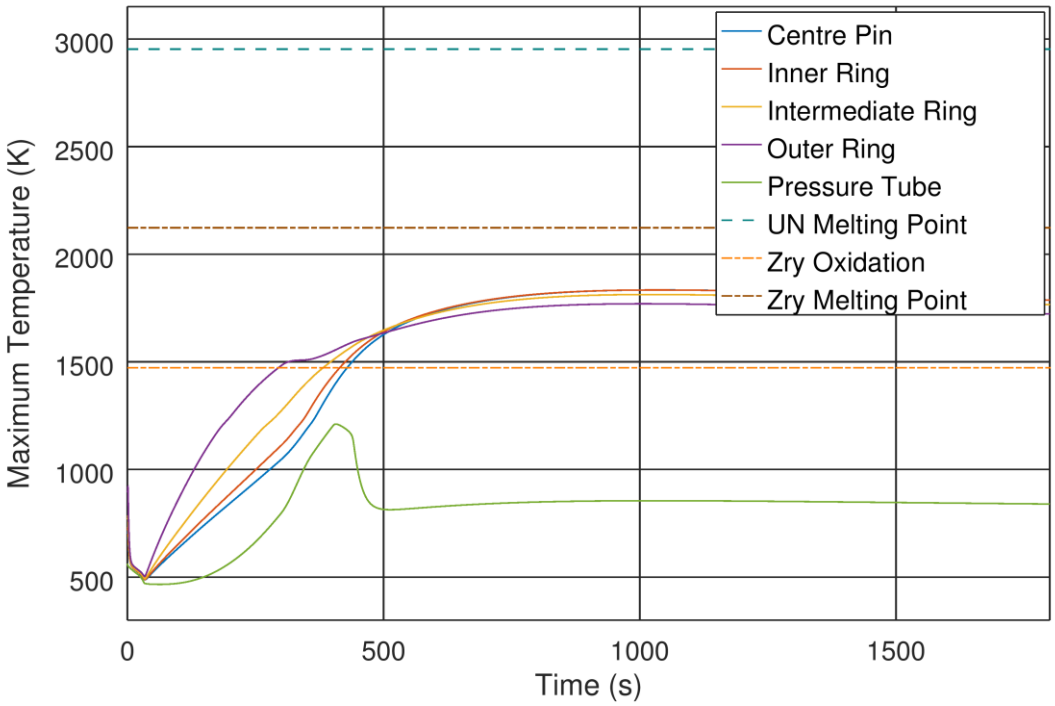

Figure 4.13: Fuel bundle temperature transient for fresh UN

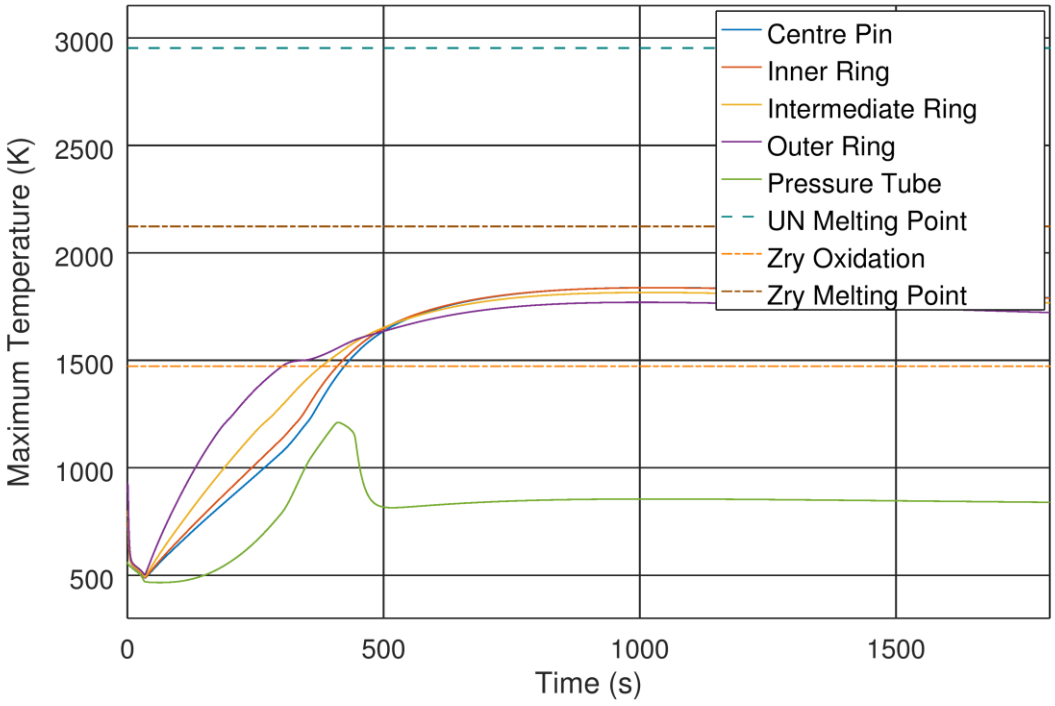

Figure 4.14: Fuel bundle temperature transient for irradiated UN

4.3 U-9Mo Fuel

As molybdenum absorbs some neutrons in the reactor, the uranium must be enriched to obtain a similar exit burnup to standard fuel. The required enrichment is less than that for UN. However, since U-9Mo is denser than UO_2, fuelling machine utilization would be reduced given the same exit burnup.

The improved thermal conductivity offered by U-9Mo results in very low fuel temperatures, with the maximum being 825 K.

Compared to UO_2 fuel, switching to U-9Mo fuel introduces a significant positive contribution to FTC for fresh fuel, but a substantial negative contribution to FTC for irradiated fuel, such that the FTC is very similar for fresh and irradiated fuel. An additional negative contribution to FTC is introduced due to the reduction in temperature. However, the CVR for U-9Mo fuel is substantially greater than for UO_2 fuel.

Table 4.11: Properties for U-9Mo fuel

Exit Burnup (MWh/kg(U))		200	
Enrichment (wt% ^{235}U)	Fixed T	0.94%	
	Calculated T	0.93%	
Outer Ring Power Factor		1.23517	
Maximum Linear Element Rating (W/m^2)		59312	
Fuel Temperature Average / Hottest	Fuel CL Temp. (K)	740.6	825.1
	Fuel Avg. Temp. (K)	682.3	742.3
	Clad Avg. Temp. (K)	593.9	612.1

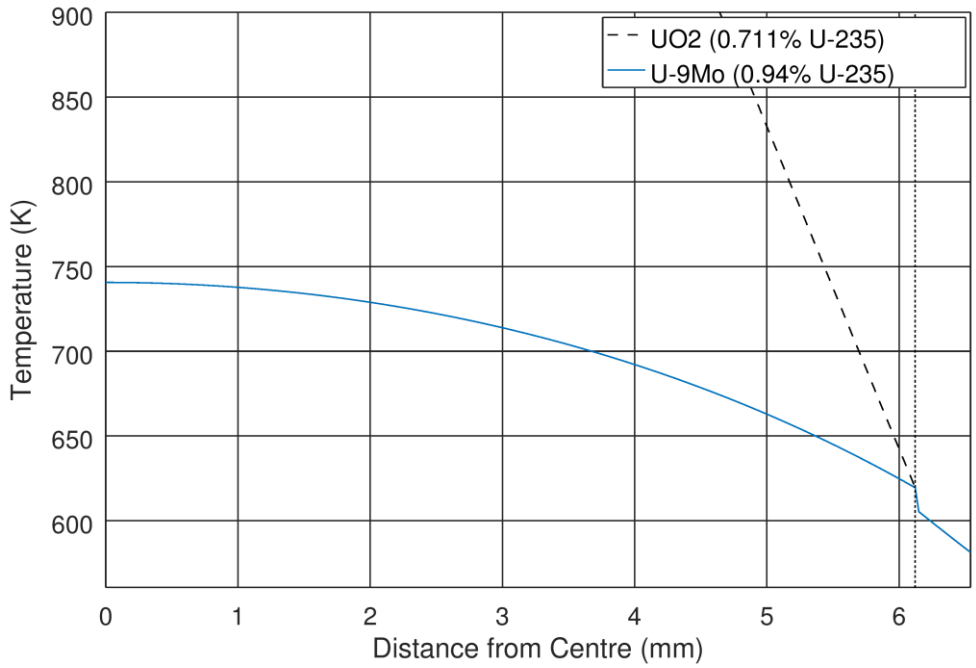

Figure 4.15: Average pin temperatures for U-9Mo fuel

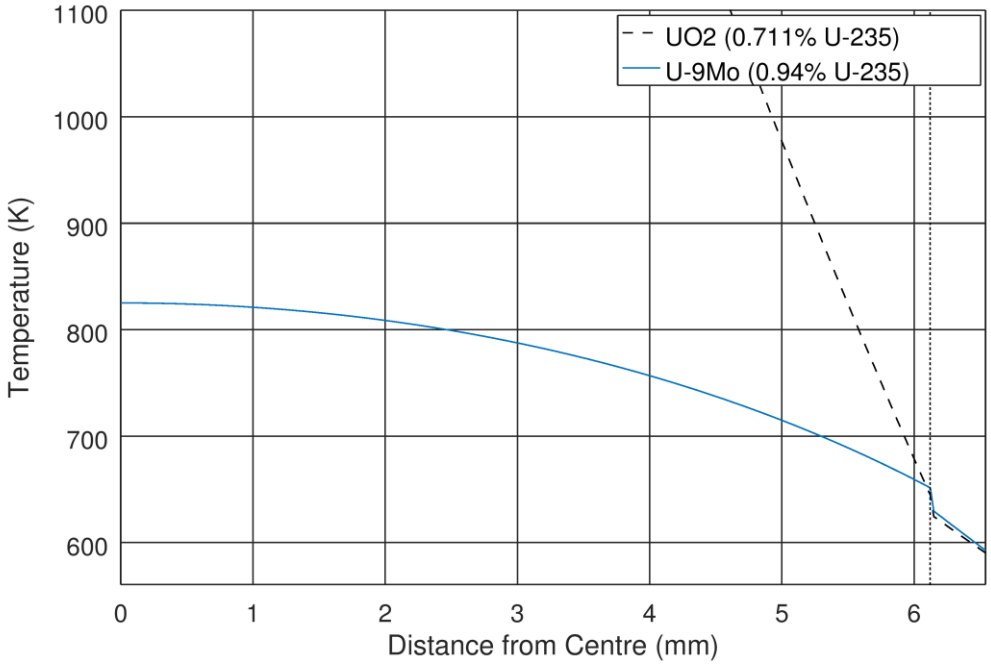

Figure 4.16: Hottest pin temperatures for U-9Mo fuel

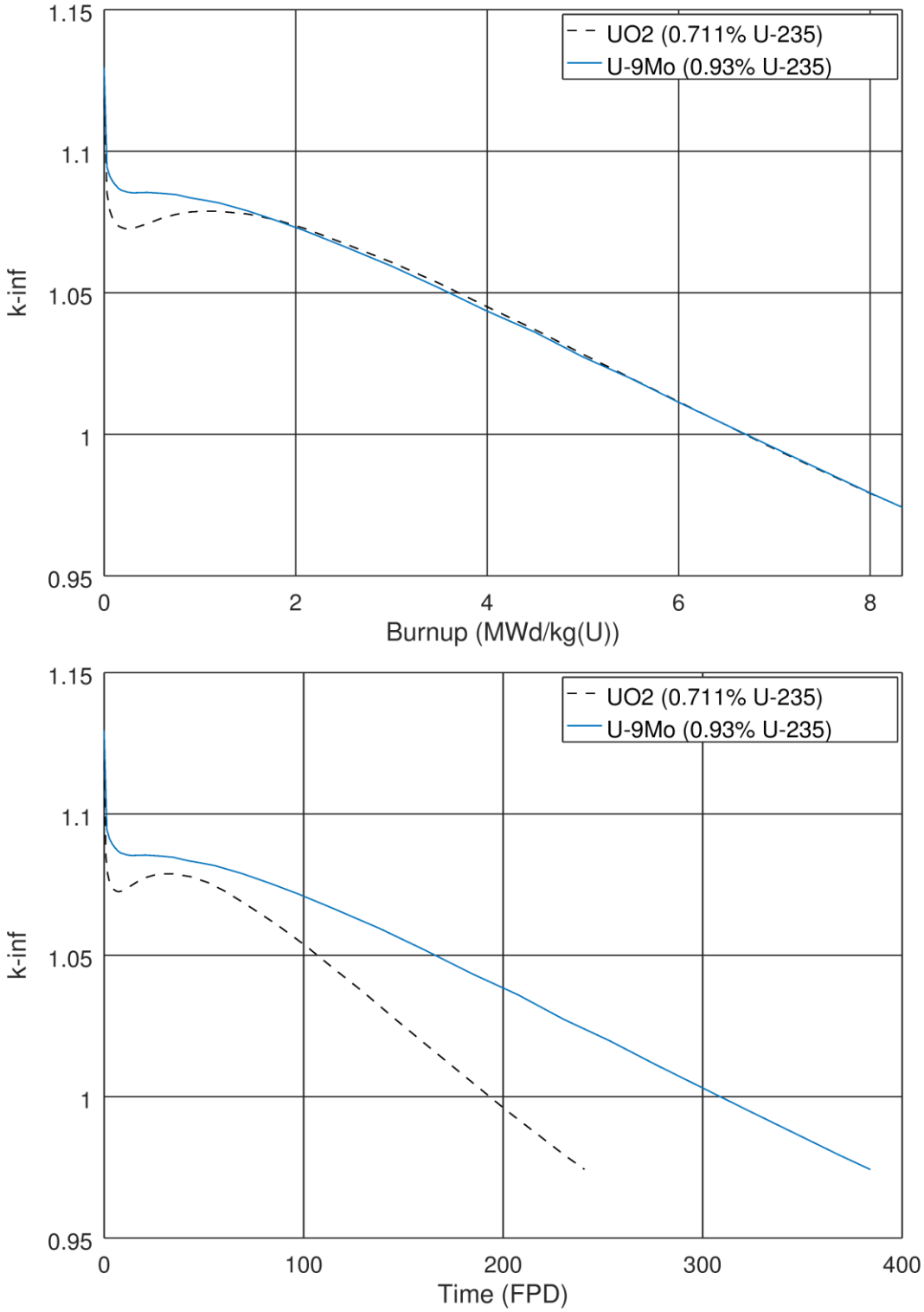

Figure 4.17: Reactivity of U-9Mo fuel – calculated temperature

Table 4.12: CVR and FTC calculations for U-9Mo fuel

Description	Enrichment (wt% ^{235}U)	Burnup (MWd/kg(U))	Calculated T			T = 941.29 K	
			k_∞	CVR (mk)	FTC (pcm/K)	CVR (mk)	FTC (pcm/K)
U-9Mo	0.930%	0	1.12952	19.15 ± 0.08	-1.01 ± 0.03	19.33 ± 0.09	-0.84 ± 0.03
		4	1.04379	20.02 ± 0.10	-1.05 ± 0.04	20.03 ± 0.10	-0.85 ± 0.04

In a transient, the greater CVR insertion results in a larger power pulse than for UO_2 fuel. However, the main issue with U-9Mo is its low melting point. Fuel can reach its melting point in five minutes or less, resulting in complete failure of the fuel before the moderator can be established as a heatsink for the decay heat of the fuel.

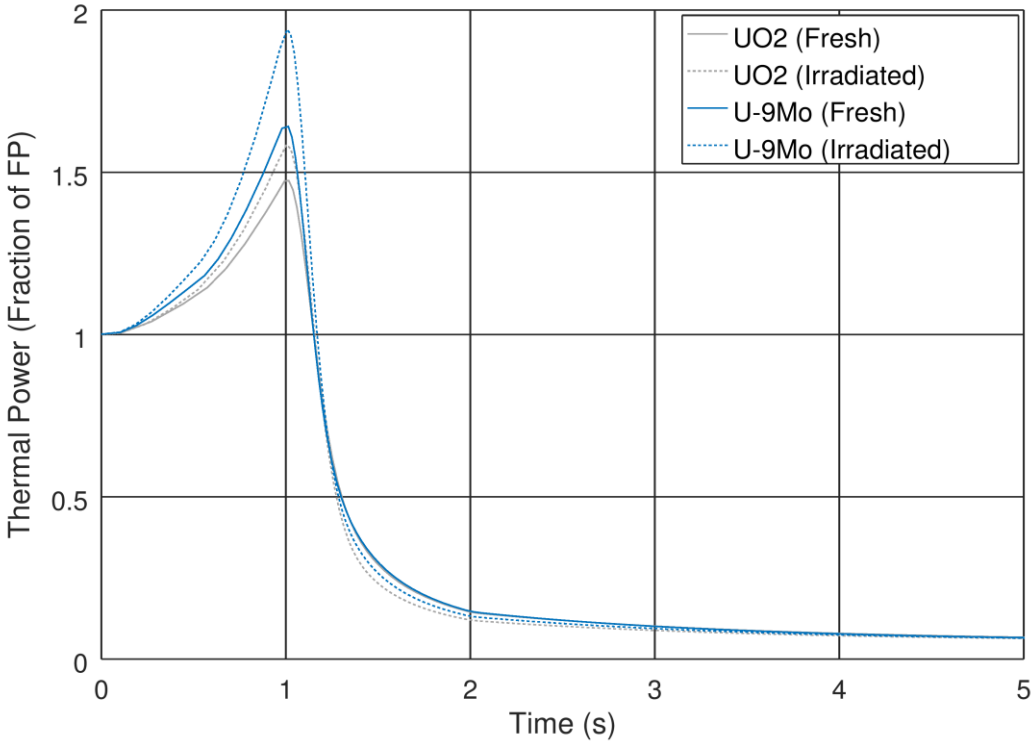

Figure 4.18: Reactor power transient for U-9Mo fuel

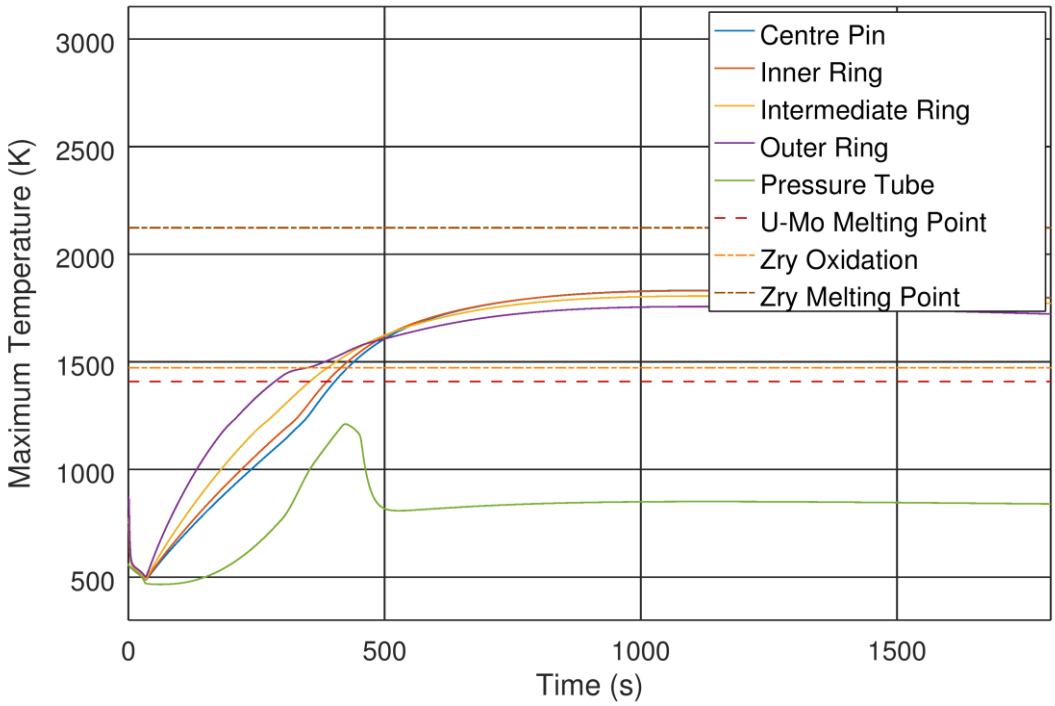

Figure 4.19: Fuel bundle temperature transient for fresh U-9Mo

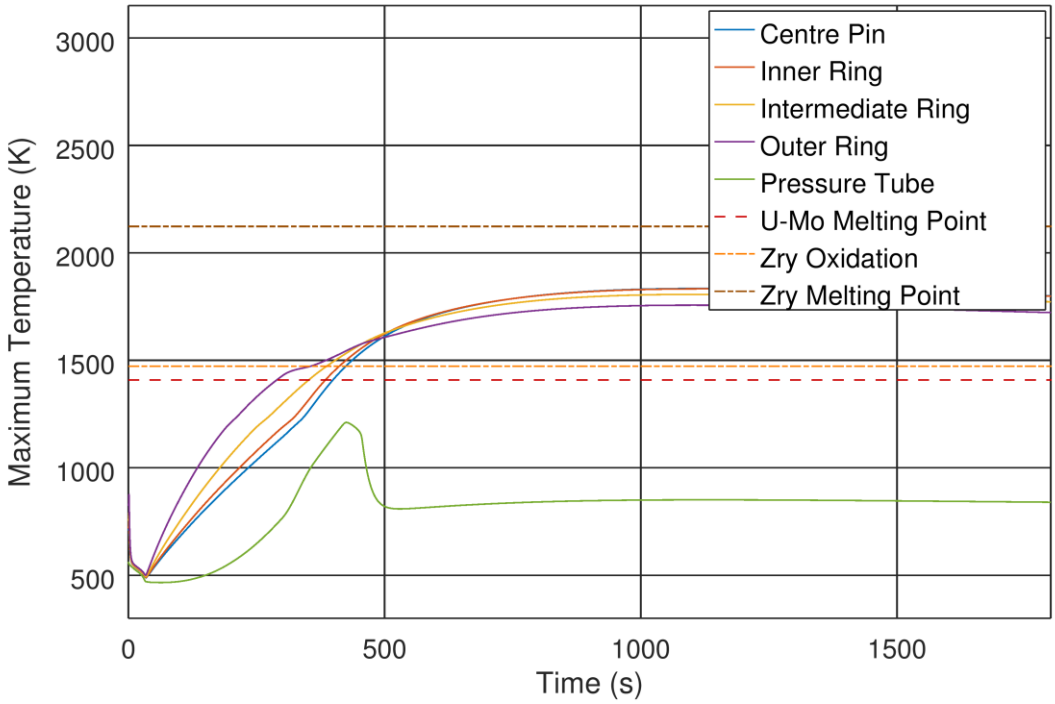

Figure 4.20: Fuel bundle temperature transient for irradiated U-9Mo

4.4 FCM Fuel

Replacing the fuel material with FCM fuel substantially reduces the amount of uranium in each fuel bundle. As a result, the fuel must be enriched to achieve a similar exit burnup to standard fuel. However, at such a burnup, the fuelling machine utilization would be substantially greater, as more bundles must be exchanged to exchange the same mass of uranium. Therefore, even higher enrichments are needed to achieve a similar level of fuelling machine utilization, particularly if the fuel packing fraction is low.

In particular, the higher density of UN is more advantageous when used as a kernel for FCM fuel, particularly for low packing fractions. To achieve the same fuelling machine load with a kernel packing fraction of 35%, UN fuel actually requires a lower enrichment than UO_2 fuel. For greater packing fractions, UN fuel requires a higher enrichment.

As the SiC matrix has a very high thermal conductivity, the fuel temperature is substantially reduced when compared to UO_2 fuel. Increasing the packing fraction results in an increase in fuel temperature.

For FCM fuel, the CVR and FTC may be compared to the solid fuel with the same material as the kernels. The CVR for FCM fuel is significantly less than for solid fuel, particularly for lower packing fractions. The FTC is more negative for fresh fuel but less negative for irradiated fuel, when the exit burnup is fixed. Increasing the enrichment to reduce fuelling machine utilization results in a positive contribution to FTC, resulting in an overall positive FTC for mid-burnup FCM fuel with UO_2 kernels. The FTC remains negative for FCM fuel with UN kernels. In addition, the reduction of fuel temperature provides an additional negative contribution to FTC, though FCM fuel with UO_2 kernels still shows a positive FTC at mid-burnup for higher packing fractions.

For the FCM fuel with complete TRISO particles with UN kernels embedded in the SiC matrix, the required enrichment is significantly higher. However, it provides the lowest CVR out of all the ATF options analyzed. The temperature is somewhat higher due to reduced thermal conductivity of some of the TRISO layers compared to the SiC matrix and UN kernel.

Table 4.13: Required Enrichment for FCM fuel

Fuel	Exit Burnup (MWh/kg(U))	Enrichment (wt% ^{235}U)	
		Fixed T	Calculated T
UO_2 FCM 35% packing	200	1.08%	1.07%
	597	1.90%	1.89%
UO_2 FCM 40% packing (Base case)	200	1.01%	1.01%
	522	1.63%	1.62%
	600	1.82%	1.80%
UO_2 FCM 45% packing	200	0.96%	0.95%
	464	1.44%	1.43%
UO_2 FCM 50% packing	200	0.92%	0.91%
	418	1.29%	1.28%
UO_2 FCM 55% packing	200	0.88%	0.88%
	380	1.17%	1.16%
UO_2 FCM 40% packing 650 µm diameter	200	1.01%	1.01%
	522	1.63%	1.62%
	600	1.82%	1.80%
UO_2 FCM 40% packing 750 µm diameter	200	1.01%	1.01%
	522	1.63%	1.62%
	600	1.82%	1.80%
UN FCM 35% packing	200	1.42%	1.41%
	405	1.82%	1.81%
UN FCM 40% packing	200	1.38%	1.37%
	354	1.67%	1.66%
UN FCM 45% packing	200	1.36%	1.35%
	315	1.56%	1.55%
UN FCM 50% packing	200	1.34%	1.33%
	283	1.48%	1.47%
UN FCM 55% packing	200	1.32%	1.32%
	257	1.42%	1.41%
UN TRISO 55% packing	707	2.78%	2.77%

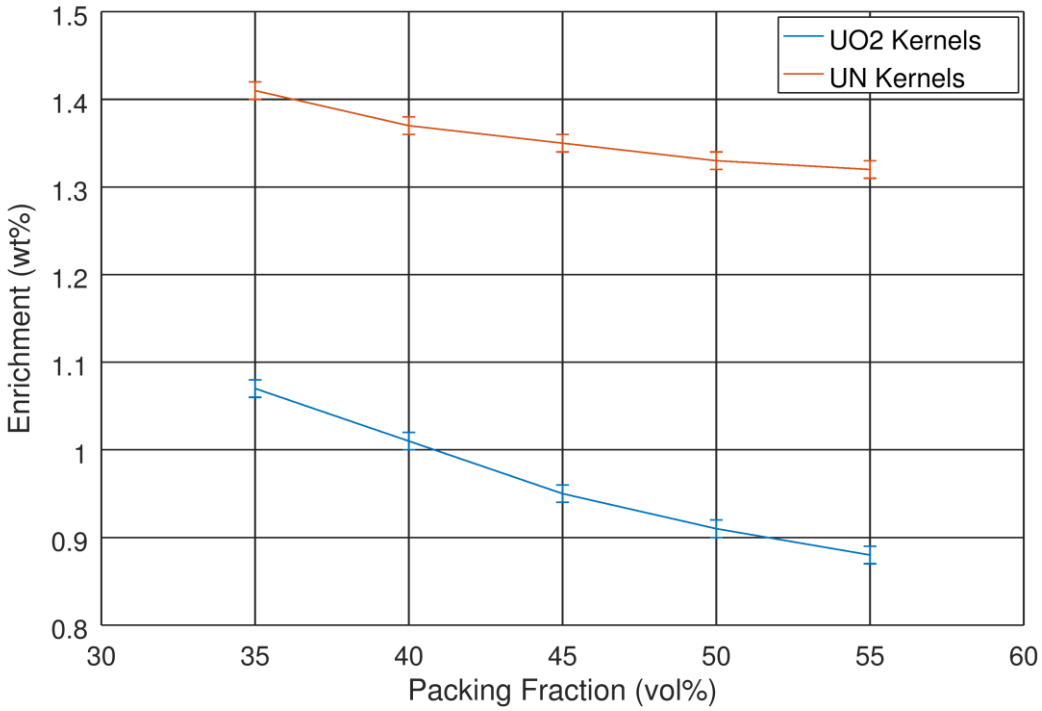

Figure 4.21: Enrichment requirements for FCM fuel for 200 MWh/kg(U) exit burnup

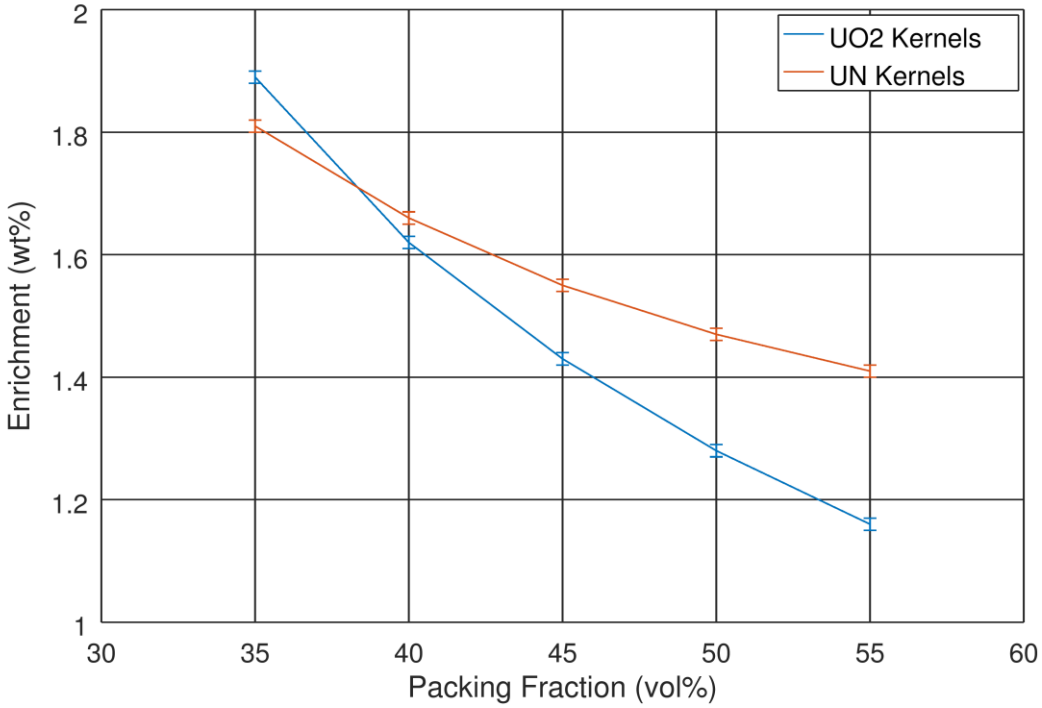

Figure 4.22: Enrichment requirements for FCM fuel for fixed fuelling machine load

Table 4.14: Average pin temperatures for FCM fuel

Description	Enrichment (wt% ^{235}U)	Fuel CL Temp. (K)	Fuel Avg. Temp. (K)	Clad Avg. Temp. (K)
UO_2 FCM in SiC 35% Packing Fraction 700 µm Diameter	1.080%	744.2	681.5	593.9
	1.900%	743.9	681.4	593.9
UO_2 FCM in SiC 40% Packing Fraction 700 µm Diameter	0.711%	758.7	688.4	593.9
	1.010%	758.5	688.4	593.9
	1.630%	758.1	688.3	593.9
	1.820%	758.0	688.2	593.9
UO_2 FCM in SiC 45% Packing Fraction 700 µm Diameter	0.960%	775.8	696.6	593.9
	1.440%	775.4	696.5	593.9
UO_2 FCM in SiC 50% Packing Fraction 700 µm Diameter	0.920%	796.7	706.6	593.9
	1.290%	796.3	706.5	593.9
UO_2 FCM in SiC 55% Packing Fraction 700 µm Diameter	0.880%	822.7	719.1	593.9
	1.170%	822.3	719.0	593.9
UO_2 FCM in SiC 40% Packing Fraction 650 µm Diameter	1.010%	758.0	688.1	593.9
	1.630%	757.7	688.0	593.9
UO_2 FCM in SiC 40% Packing Fraction 750 µm Diameter	1.010%	758.9	688.6	593.9
	1.630%	758.7	688.5	593.9
UN FCM in SiC 35% Packing Fraction 700 µm Diameter	1.420%	712.5	666.2	593.9
	1.820%	712.3	666.2	593.9
UN FCM in SiC 40% Packing Fraction 700 µm Diameter	1.380%	716.5	668.2	593.9
	1.670%	716.3	668.1	593.9
UN FCM in SiC 45% Packing Fraction 700 µm Diameter	1.360%	720.6	670.2	593.9
	1.560%	720.4	670.1	593.9
UN FCM in SiC 50% Packing Fraction 700 µm Diameter	1.340%	724.5	672.2	593.9
	1.480%	724.4	672.1	593.9
UN FCM in SiC 55% Packing Fraction 700 µm Diameter	1.320%	728.3	674.1	593.9
	1.420%	728.2	674.1	593.9
UN FCM in SiC 55% TRISO Packing Fraction 700 µm Kernel Diameter	2.780%	860.9	739.3	593.9

Table 4.15: Maximum pin power for FCM fuel

Description	Enrichment (wt% ^{235}U)	Outer Ring Power Factor	Linear Element Rating (W/m^2)
UO_2 FCM in SiC 35% Packing Fraction 700 µm Diameter	1.080%	1.08453	52078
	1.900%	1.11342	53465
UO_2 FCM in SiC 40% Packing Fraction 700 µm Diameter	0.711%	1.07632	51684
	1.010%	1.08833	52261
	1.630%	1.11345	53467
	1.820%	1.11948	53756
UO_2 FCM in SiC 45% Packing Fraction 700 µm Diameter	0.960%	1.09262	52466
	1.440%	1.11428	53507
UO_2 FCM in SiC 50% Packing Fraction 700 µm Diameter	0.920%	1.09717	52685
	1.290%	1.11539	53560
UO_2 FCM in SiC 55% Packing Fraction 700 µm Diameter	0.880%	1.10113	52875
	1.170%	1.11724	53649
UO_2 FCM in SiC 40% Packing Fraction 650 µm Diameter	1.010%	1.08902	52294
	1.630%	1.11366	53477
UO_2 FCM in SiC 40% Packing Fraction 750 µm Diameter	1.010%	1.08837	52263
	1.630%	1.11349	53468
UN FCM in SiC 35% Packing Fraction 700 µm Diameter	1.420%	1.14652	55055
	1.820%	1.16527	55955
UN FCM in SiC 40% Packing Fraction 700 µm Diameter	1.380%	1.15910	55659
	1.670%	1.17402	56375
UN FCM in SiC 45% Packing Fraction 700 µm Diameter	1.360%	1.17286	56320
	1.560%	1.18427	56868
UN FCM in SiC 50% Packing Fraction 700 µm Diameter	1.340%	1.18570	56936
	1.480%	1.19394	57332
UN FCM in SiC 55% Packing Fraction 700 µm Diameter	1.320%	1.19811	57532
	1.420%	1.20443	57836
UN FCM in SiC 55% TRISO Packing Fraction 700 µm Kernel Diameter	2.780%	1.13819	54655

Table 4.16: Hottest pin temperatures for FCM fuel

Description	Enrichment (wt% ^{235}U)	Fuel CL Temp. (K)	Fuel Avg. Temp. (K)	Clad Avg. Temp. (K)
UO_2 FCM in SiC 35% Packing Fraction 700 µm Diameter	1.080%	814.8	727.0	605.9
	1.900%	821.5	731.5	607.1
UO_2 FCM in SiC 40% Packing Fraction 700 µm Diameter	0.711%	833.1	735.4	605.6
	1.010%	836.0	737.3	606.1
	1.630%	842.3	741.4	607.1
	1.820%	843.7	742.4	607.3
UO_2 FCM in SiC 45% Packing Fraction 700 µm Diameter	0.960%	862.1	749.8	606.2
	1.440%	867.9	753.5	607.1
UO_2 FCM in SiC 50% Packing Fraction 700 µm Diameter	0.920%	893.7	765.0	606.4
	1.290%	899.2	768.4	607.2
UO_2 FCM in SiC 55% Packing Fraction 700 µm Diameter	0.880%	933.4	784.0	606.6
	1.170%	938.7	787.3	607.3
UO_2 FCM in SiC 40% Packing Fraction 650 µm Diameter	1.010%	835.6	737.1	606.1
	1.630%	841.7	741.1	607.1
UO_2 FCM in SiC 40% Packing Fraction 750 µm Diameter	1.010%	836.7	737.6	606.1
	1.630%	843.1	741.8	607.1
UN FCM in SiC 35% Packing Fraction 700 µm Diameter	1.420%	780.6	713.2	608.5
	1.820%	783.9	715.6	609.2
UN FCM in SiC 40% Packing Fraction 700 µm Diameter	1.380%	788.5	717.5	609.0
	1.670%	791.2	719.5	609.6
UN FCM in SiC 45% Packing Fraction 700 µm Diameter	1.360%	797.0	722.2	609.5
	1.560%	798.9	723.7	610.0
UN FCM in SiC 50% Packing Fraction 700 µm Diameter	1.340%	804.9	726.7	610.1
	1.480%	806.5	727.8	610.4
UN FCM in SiC 55% Packing Fraction 700 µm Diameter	1.320%	812.6	731.2	610.6
	1.420%	813.8	732.0	610.8
UN FCM in SiC 55% TRISO Packing Fraction 700 µm Kernel Diameter	2.780%	997.1	819.3	608.1

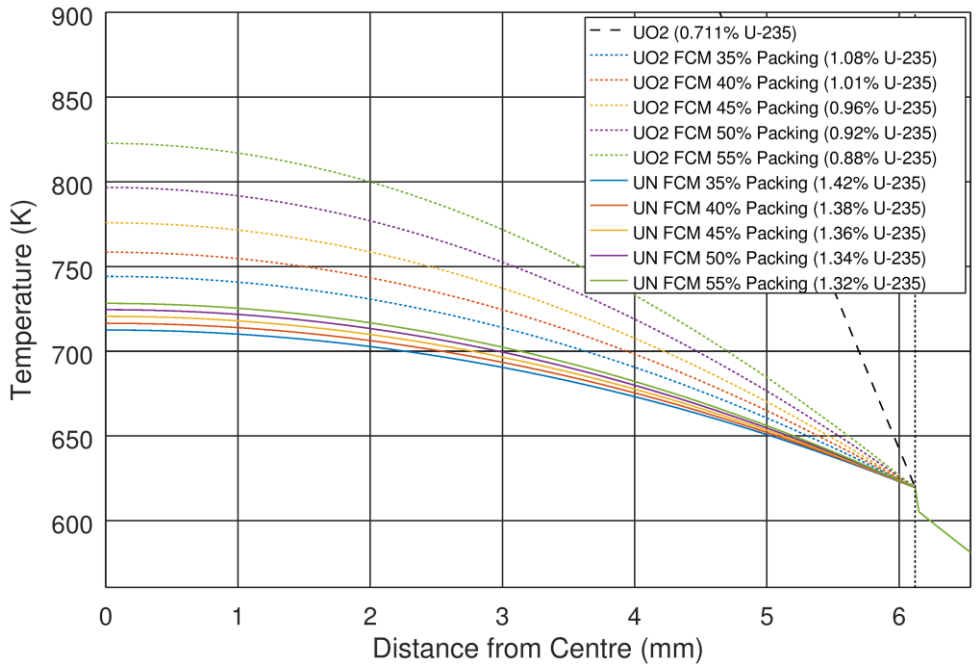

Figure 4.23: Average pin temperatures for FCM fuel

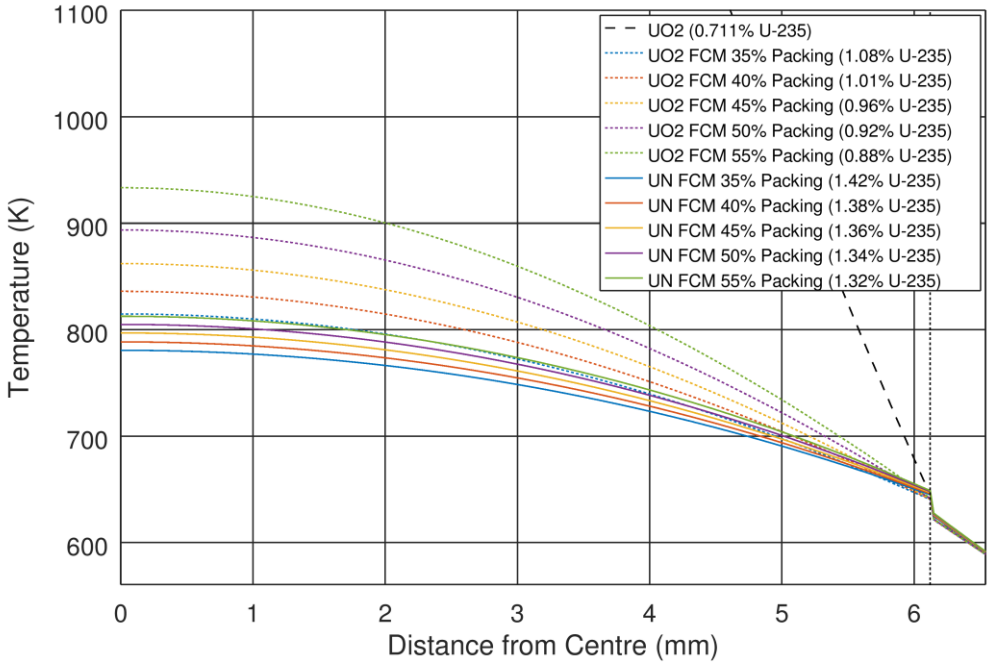

Figure 4.24: Hottest pin temperatures for FCM fuel

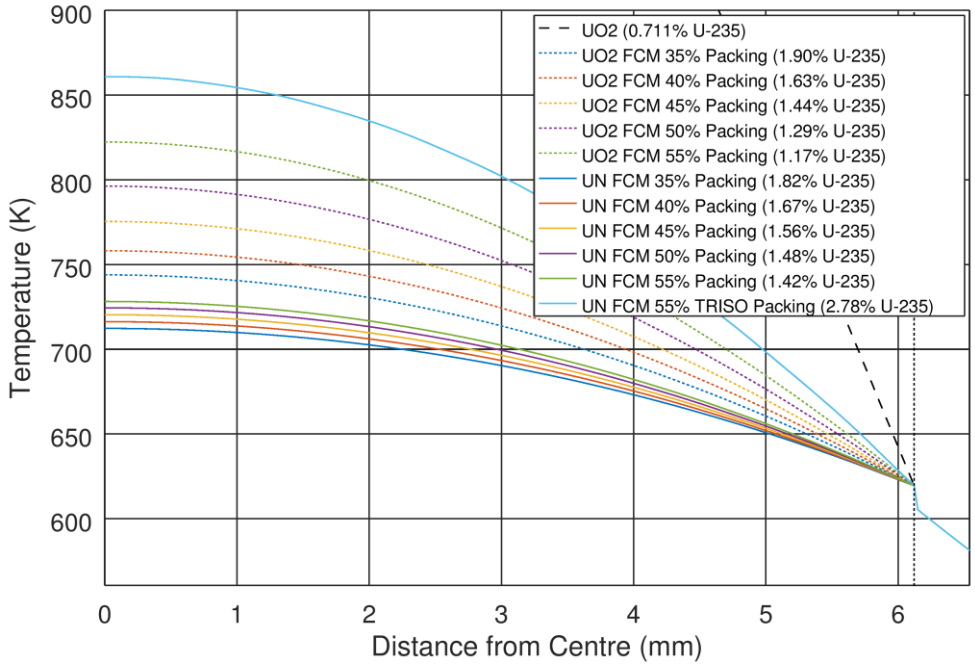

Figure 4.25: Average pin temperatures for FCM fuel (refuel rate same as UO_2)

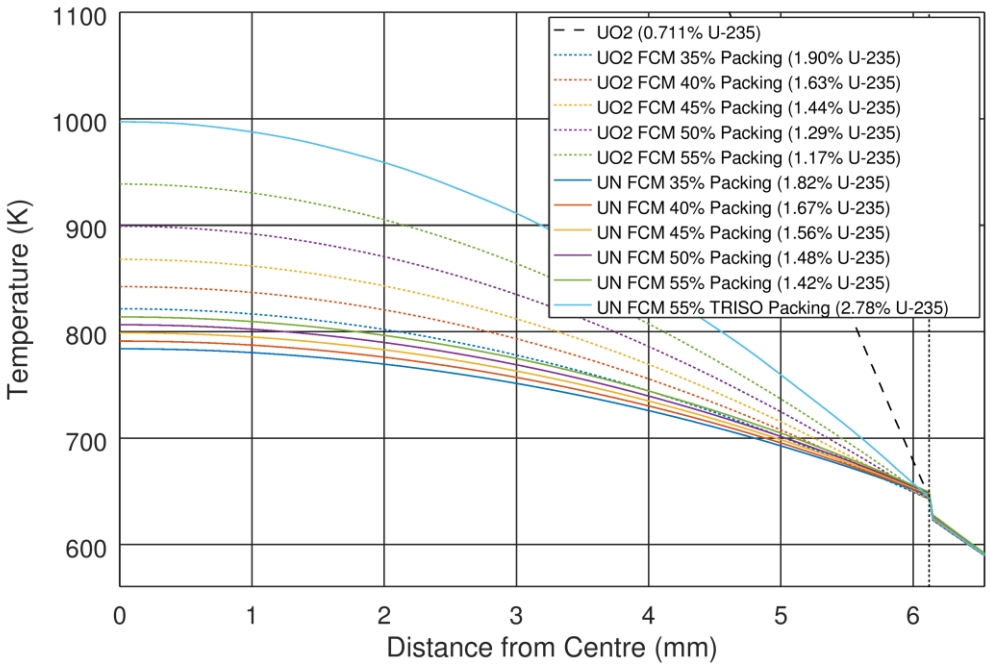

Figure 4.26: Hottest pin temperatures for FCM fuel (refuel rate same as UO_2)

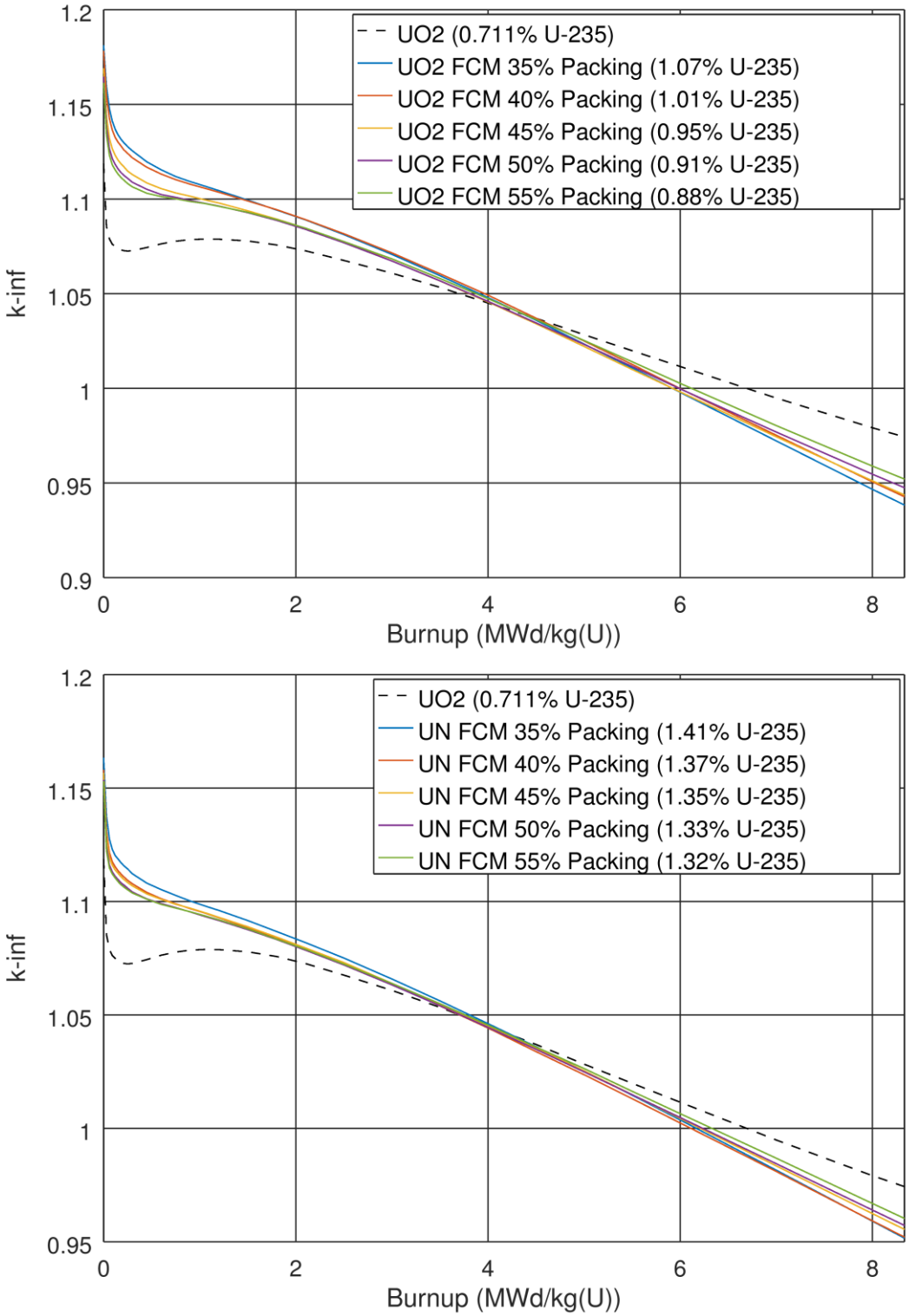

Figure 4.27: Reactivity of FCM fuel with burnup – calculated temperature

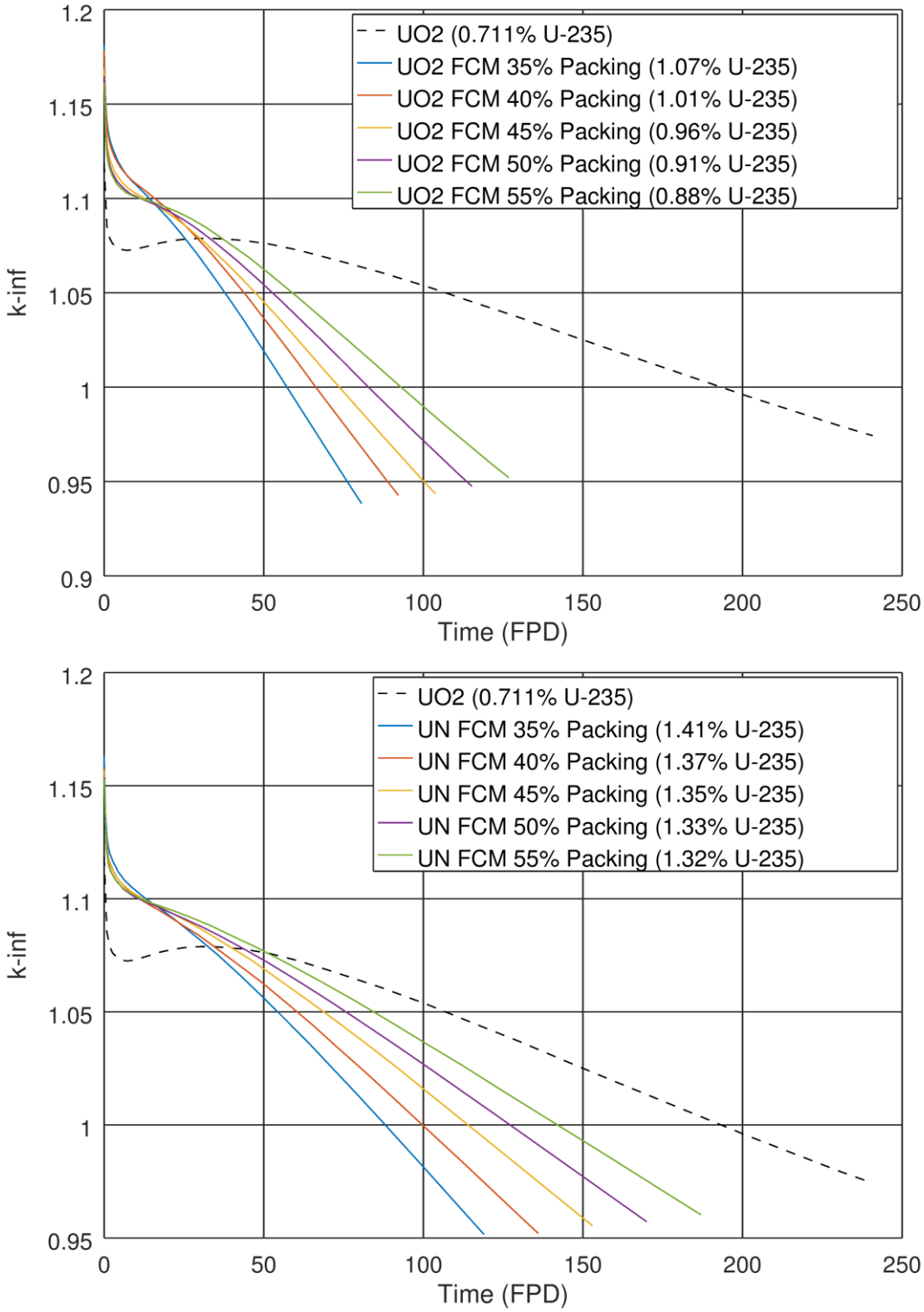

Figure 4.28: Reactivity of FCM fuel with time – calculated temperature

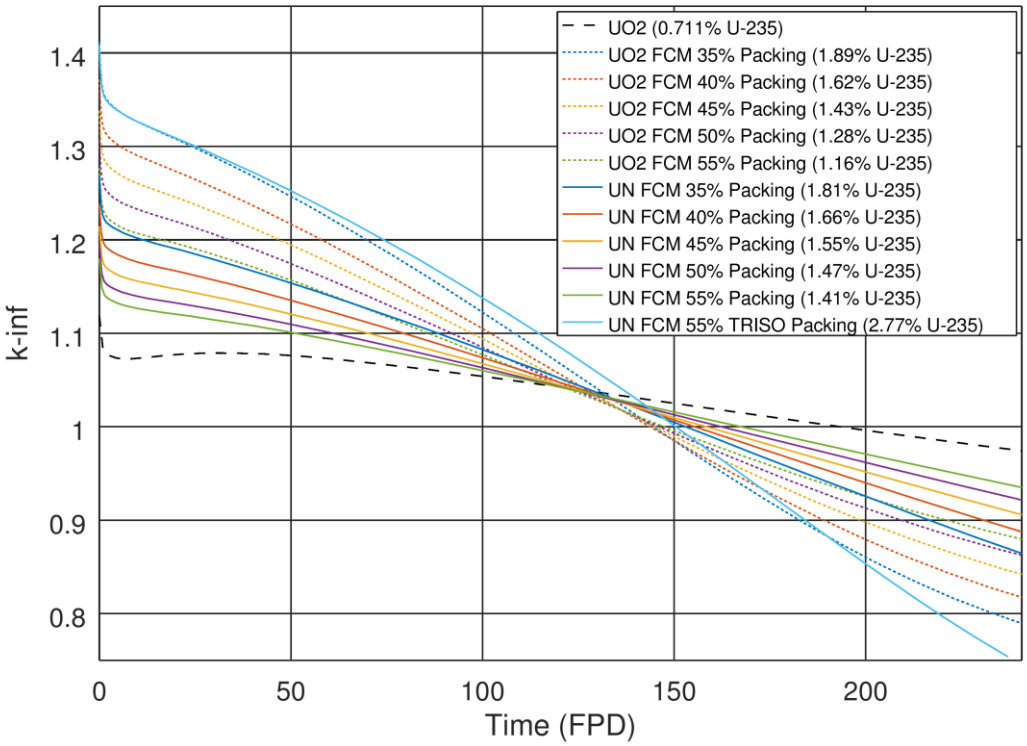

Figure 4.29: Reactivity of FCM fuel with fixed exit FPD – calculated temperature

Table 4.17: CVR and FTC calculations – UO_2 FCM

Description	Enrichment (wt% ^{235}U)	Burnup (MWd/kg(U))	Calculated T			T = 941.29 K	
			k_∞	CVR (mk)	FTC (pcm/K)	CVR (mk)	FTC (pcm/K)
UO_2 FCM in SiC 35% Packing Fraction 700 µm Diameter	1.070%	0	1.18147	12.05 ± 0.06	-1.75 ± 0.02	12.10 ± 0.06	-1.56 ± 0.02
		4	1.04807	10.39 ± 0.07	-0.48 ± 0.03	10.76 ± 0.07	-0.12 ± 0.03
	1.890%	0	1.41177	8.68 ± 0.05	-1.15 ± 0.02	8.80 ± 0.05	-1.03 ± 0.02
		4	1.27098	9.44 ± 0.05	-1.08 ± 0.02	9.52 ± 0.06	-0.84 ± 0.02
		12	1.07889	9.79 ± 0.07	-0.30 ± 0.03	10.10 ± 0.07	0.02 ± 0.03
UO_2 FCM in SiC 40% Packing Fraction 700 µm Diameter	0.711%	0	1.01866	15.95 ± 0.07	-2.20 ± 0.03	16.01 ± 0.07	-1.96 ± 0.03
		4	0.93745	8.89 ± 0.09	0.82 ± 0.03	9.69 ± 0.09	1.31 ± 0.03
	1.010%	0	1.17808	12.34 ± 0.06	-1.66 ± 0.02	12.53 ± 0.06	-1.53 ± 0.02
		4	1.04922	10.30 ± 0.07	-0.38 ± 0.03	10.79 ± 0.07	0.01 ± 0.03
	1.620%	0	1.37165	9.40 ± 0.05	-1.18 ± 0.02	9.40 ± 0.05	-1.09 ± 0.02
		4	1.22854	10.01 ± 0.06	-0.97 ± 0.02	10.15 ± 0.06	-0.76 ± 0.02
		11	1.05280	9.94 ± 0.07	-0.09 ± 0.03	10.40 ± 0.08	0.27 ± 0.03
	1.800%	0	1.41008	8.93 ± 0.05	-1.11 ± 0.02	8.97 ± 0.05	-1.02 ± 0.02
		4	1.26844	9.65 ± 0.06	-0.99 ± 0.02	9.69 ± 0.06	-0.82 ± 0.02
		12	1.07470	9.97 ± 0.07	-0.26 ± 0.03	10.50 ± 0.08	0.06 ± 0.03
UO_2 FCM in SiC 45% Packing Fraction 700 µm Diameter	0.950%	0	1.16881	12.89 ± 0.06	-1.65 ± 0.02	12.80 ± 0.06	-1.48 ± 0.02
		4	1.04558	10.62 ± 0.07	-0.25 ± 0.03	10.86 ± 0.08	0.04 ± 0.03
	1.430%	0	1.33787	10.11 ± 0.05	-1.24 ± 0.02	10.09 ± 0.05	-1.11 ± 0.02
		4	1.19501	10.35 ± 0.06	-0.90 ± 0.02	10.51 ± 0.06	-0.67 ± 0.02
		10	1.04268	10.17 ± 0.08	0.01 ± 0.03	10.74 ± 0.08	0.32 ± 0.03
UO_2 FCM in SiC 50% Packing Fraction 700 µm Diameter	0.910%	0	1.16434	13.14 ± 0.06	-1.57 ± 0.02	13.22 ± 0.06	-1.42 ± 0.02
		4	1.04593	10.81 ± 0.07	-0.20 ± 0.03	11.11 ± 0.08	0.07 ± 0.03
	1.280%	0	1.30639	10.69 ± 0.06	-1.28 ± 0.02	10.73 ± 0.06	-1.11 ± 0.02
		4	1.16553	10.70 ± 0.06	-0.78 ± 0.02	11.01 ± 0.07	-0.54 ± 0.02
		9	1.03934	10.62 ± 0.08	0.05 ± 0.03	11.09 ± 0.08	0.36 ± 0.03
UO_2 FCM in SiC 55% Packing Fraction 700 µm Diameter	0.880%	0	1.16149	13.39 ± 0.06	-1.53 ± 0.02	13.53 ± 0.06	-1.42 ± 0.02
		4	1.04748	10.94 ± 0.08	-0.17 ± 0.03	11.41 ± 0.08	0.12 ± 0.03
	1.160%	0	1.27726	11.28 ± 0.06	-1.28 ± 0.02	11.40 ± 0.06	-1.17 ± 0.02
		4	1.14028	11.01 ± 0.07	-0.64 ± 0.03	11.35 ± 0.07	-0.44 ± 0.03
		8	1.04127	10.81 ± 0.08	0.06 ± 0.03	11.30 ± 0.08	0.29 ± 0.03
UO_2 FCM in SiC 40% Packing Fraction 650 µm Diameter	1.010%	0	1.17804	12.43 ± 0.06	-1.70 ± 0.02	12.48 ± 0.06	-1.52 ± 0.02
		4	1.04914	10.50 ± 0.07	-0.37 ± 0.03	10.73 ± 0.07	0.01 ± 0.03
	1.620%	0	1.37161	9.32 ± 0.05	-1.21 ± 0.02	9.44 ± 0.05	-1.10 ± 0.02
		4	1.22858	9.97 ± 0.06	-0.97 ± 0.02	10.05 ± 0.06	-0.78 ± 0.02
		11	1.05276	9.95 ± 0.08	-0.12 ± 0.03	10.45 ± 0.08	0.25 ± 0.03
UO_2 FCM in SiC 40% Packing Fraction 750 µm Diameter	1.010%	0	1.17809	12.54 ± 0.06	-1.69 ± 0.02	12.47 ± 0.06	-1.51 ± 0.02
		4	1.04914	10.38 ± 0.07	-0.39 ± 0.03	10.69 ± 0.07	-0.03 ± 0.03
	1.620%	0	1.37170	9.34 ± 0.05	-1.20 ± 0.02	9.45 ± 0.05	-1.08 ± 0.02
		4	1.22867	9.87 ± 0.06	-0.96 ± 0.02	9.97 ± 0.06	-0.76 ± 0.02
		11	1.05272	9.84 ± 0.08	-0.10 ± 0.03	10.49 ± 0.08	0.27 ± 0.03

Table 4.18: CVR and FTC calculations – UN FCM

Description	Enrichment (wt% ^{235}U)	Burnup (MWd/kg(U))	Calculated T			T = 941.29 K	
			Fresh Fuel k_∞	CVR (mk)	FTC (pcm/K)	CVR (mk)	FTC (pcm/K)
UN FCM in SiC 35% Packing Fraction 700 µm Diameter	1.410%	0	1.16310	11.06 ± 0.06	-1.64 ± 0.02	11.26 ± 0.06	-1.42 ± 0.02
		4	1.04632	10.68 ± 0.07	-0.74 ± 0.03	10.95 ± 0.07	-0.34 ± 0.03
	1.810%	0	1.26720	9.51 ± 0.06	-1.37 ± 0.02	9.54 ± 0.06	-1.22 ± 0.02
		4	1.14431	10.08 ± 0.07	-1.00 ± 0.03	10.39 ± 0.07	-0.73 ± 0.03
		8	1.06089	10.55 ± 0.07	-0.56 ± 0.03	10.68 ± 0.08	-0.13 ± 0.03
UN FCM in SiC 40% Packing Fraction 700 µm Diameter	1.370%	0	1.15800	11.33 ± 0.06	-1.60 ± 0.02	11.37 ± 0.07	-1.40 ± 0.03
		4	1.04401	11.13 ± 0.08	-0.71 ± 0.03	11.22 ± 0.08	-0.30 ± 0.03
	1.660%	0	1.23832	9.94 ± 0.06	-1.43 ± 0.02	10.24 ± 0.06	-1.24 ± 0.02
		4	1.11739	10.74 ± 0.07	-0.94 ± 0.03	10.75 ± 0.07	-0.63 ± 0.03
		7	1.05536	10.91 ± 0.08	-0.54 ± 0.03	11.27 ± 0.08	-0.18 ± 0.03
UN FCM in SiC 45% Packing Fraction 700 µm Diameter	1.350%	0	1.15663	11.61 ± 0.07	-1.59 ± 0.02	11.57 ± 0.07	-1.49 ± 0.03
		4	1.04511	11.48 ± 0.08	-0.66 ± 0.03	11.58 ± 0.08	-0.27 ± 0.03
	1.550%	0	1.21411	10.79 ± 0.06	-1.45 ± 0.02	10.81 ± 0.06	-1.27 ± 0.02
		4	1.09661	11.04 ± 0.07	-0.85 ± 0.03	11.24 ± 0.07	-0.56 ± 0.03
		7	1.03485	11.52 ± 0.08	-0.41 ± 0.03	11.82 ± 0.08	-0.04 ± 0.03
UN FCM in SiC 50% Packing Fraction 700 µm Diameter	1.330%	0	1.15381	11.80 ± 0.07	-1.58 ± 0.03	11.89 ± 0.07	-1.36 ± 0.03
		4	1.04460	11.74 ± 0.08	-0.67 ± 0.03	12.11 ± 0.08	-0.30 ± 0.03
	1.470%	0	1.19528	11.14 ± 0.06	-1.45 ± 0.02	11.34 ± 0.07	-1.29 ± 0.03
		4	1.08081	11.56 ± 0.08	-0.79 ± 0.03	11.76 ± 0.08	-0.46 ± 0.03
		6	1.04091	11.87 ± 0.08	-0.51 ± 0.03	12.27 ± 0.09	-0.15 ± 0.03
UN FCM in SiC 55% Packing Fraction 700 µm Diameter	1.320%	0	1.15286	12.13 ± 0.07	-1.55 ± 0.03	12.46 ± 0.07	-1.35 ± 0.03
		4	1.04565	12.18 ± 0.08	-0.66 ± 0.03	12.54 ± 0.08	-0.32 ± 0.03
	1.410%	0	1.18009	11.62 ± 0.07	-1.45 ± 0.03	11.76 ± 0.07	-1.29 ± 0.03
		4	1.06902	11.96 ± 0.08	-0.74 ± 0.03	12.20 ± 0.08	-0.44 ± 0.03
		5.5	1.03953	12.26 ± 0.08	-0.55 ± 0.03	12.46 ± 0.09	-0.18 ± 0.03
UN FCM in SiC 55% TRISO Packing Fraction 700 µm Kernel Diameter	2.770%	0	1.40828	7.29 ± 0.05	-1.16 ± 0.02	7.44 ± 0.05	-1.09 ± 0.02
		4	1.28607	8.13 ± 0.05	-1.10 ± 0.02	8.16 ± 0.05	-0.96 ± 0.02
		15	1.07873	9.16 ± 0.07	-0.41 ± 0.03	9.55 ± 0.07	-0.15 ± 0.03

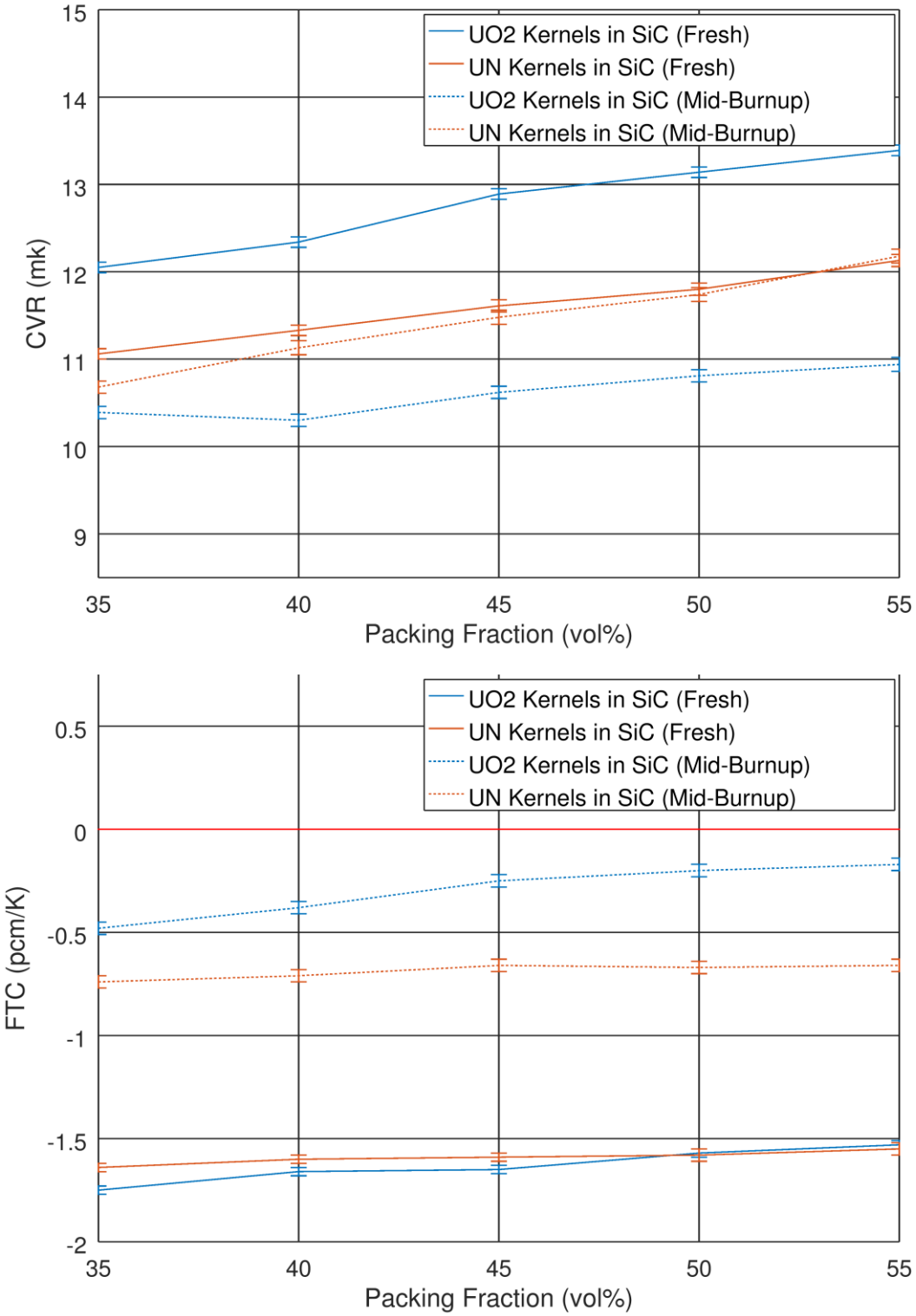

Figure 4.30: CVR and FTC for FCM fuel for 200 MWh/kg(U) exit burnup

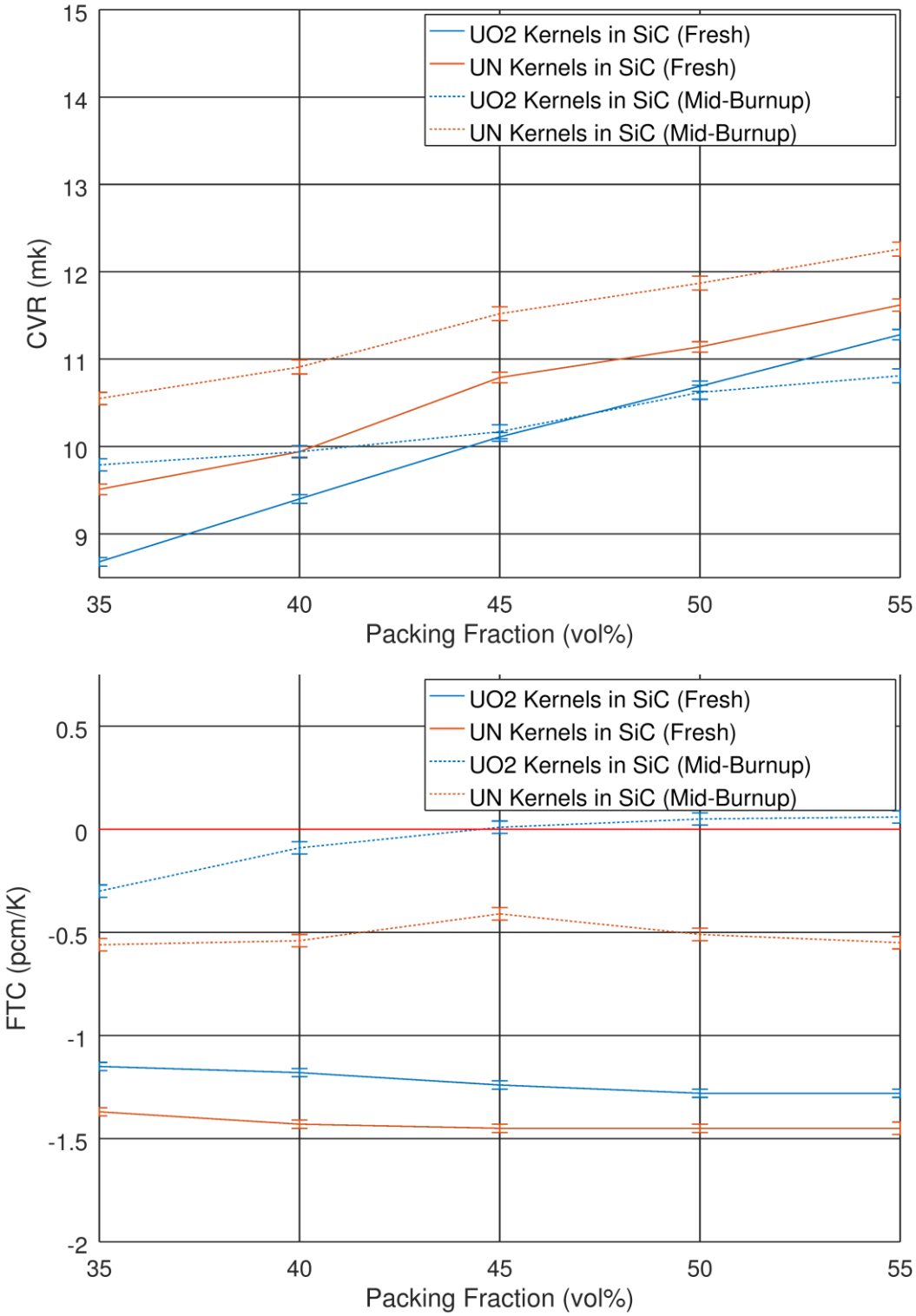

Figure 4.31: CVR and FTC for FCM fuel for fixed fuelling machine usage

In a transient, the power pulses are significantly smaller for FCM fuel than they are for UO_2 fuel, mainly due to the reduced CVR. In addition, the slightly greater heat capacity of SiC combined with a somewhat reduced spatial self-shielding effect (when using UO_2 kernels) results in a slightly slower temperature rise. For UO_2-kernel FCM, this can delay oxidation of zircaloy cladding by about a minute.

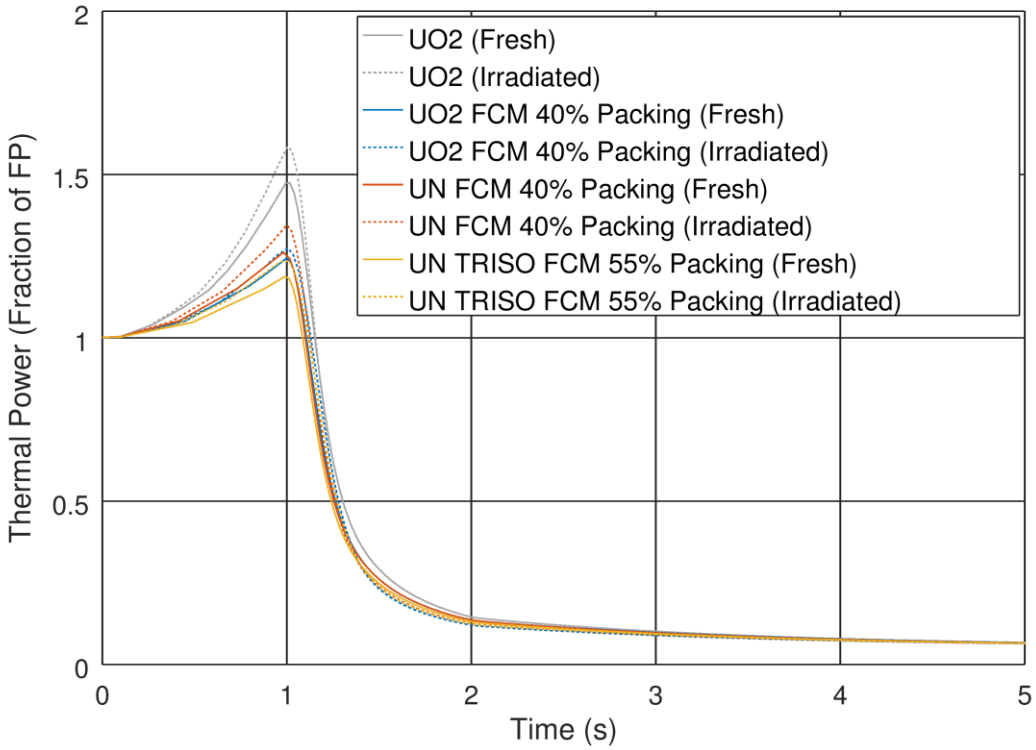

Figure 4.32: Reactor power transient for FCM fuel

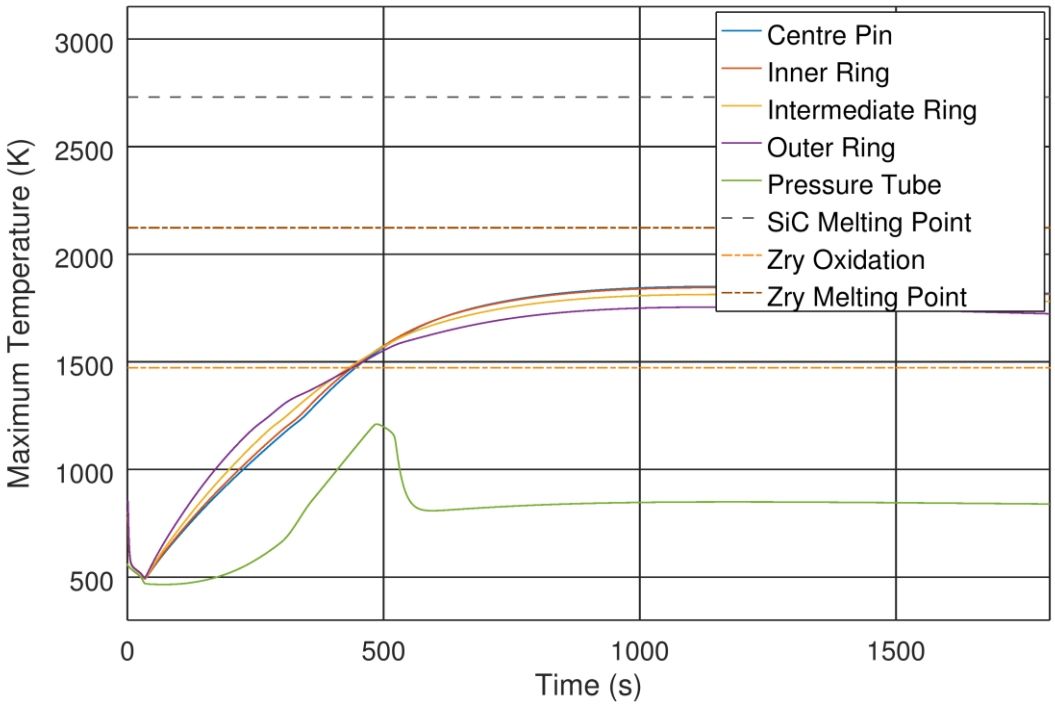

Figure 4.33: Fuel bundle temperature transient for fresh UO_2 FCM

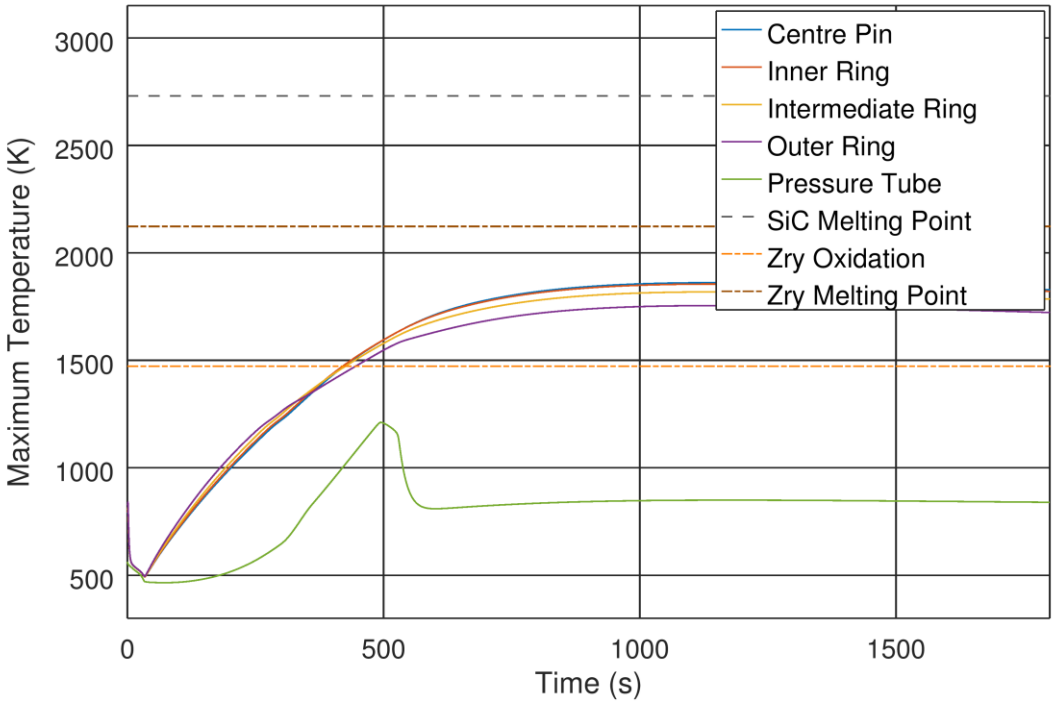

Figure 4.34: Fuel bundle temperature transient for irradiated UO_2 FCM

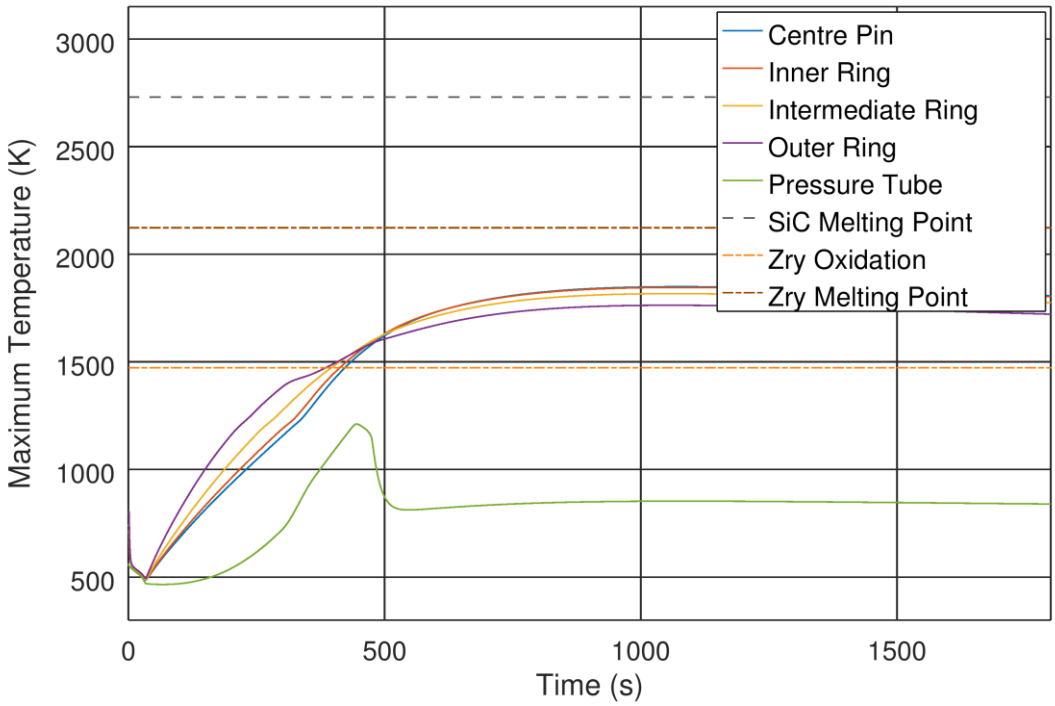

Figure 4.35: Fuel bundle temperature transient for fresh UN FCM

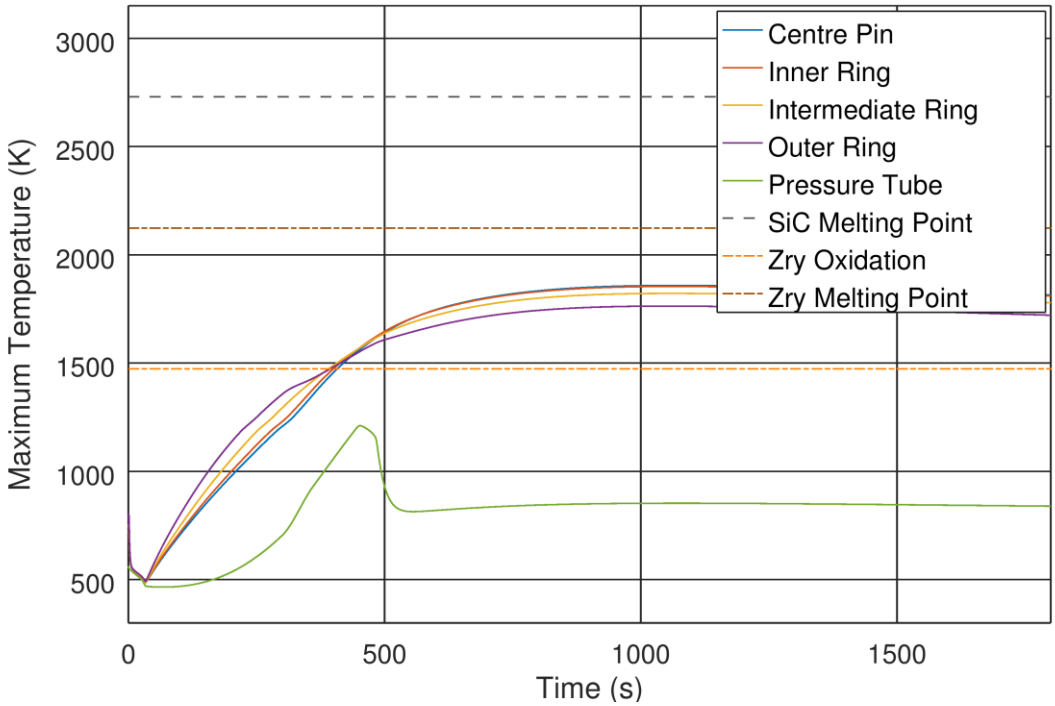

Figure 4.36: Fuel bundle temperature transient for irradiated UN FCM

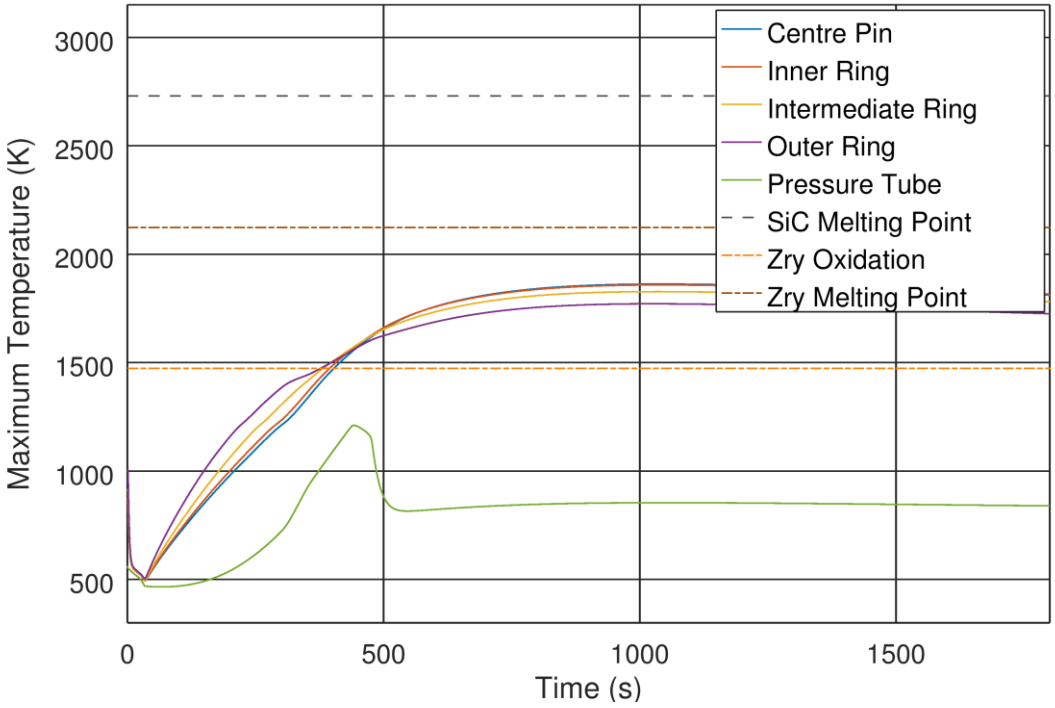

Figure 4.37: Fuel bundle temperature transient for fresh UN TRISO FCM

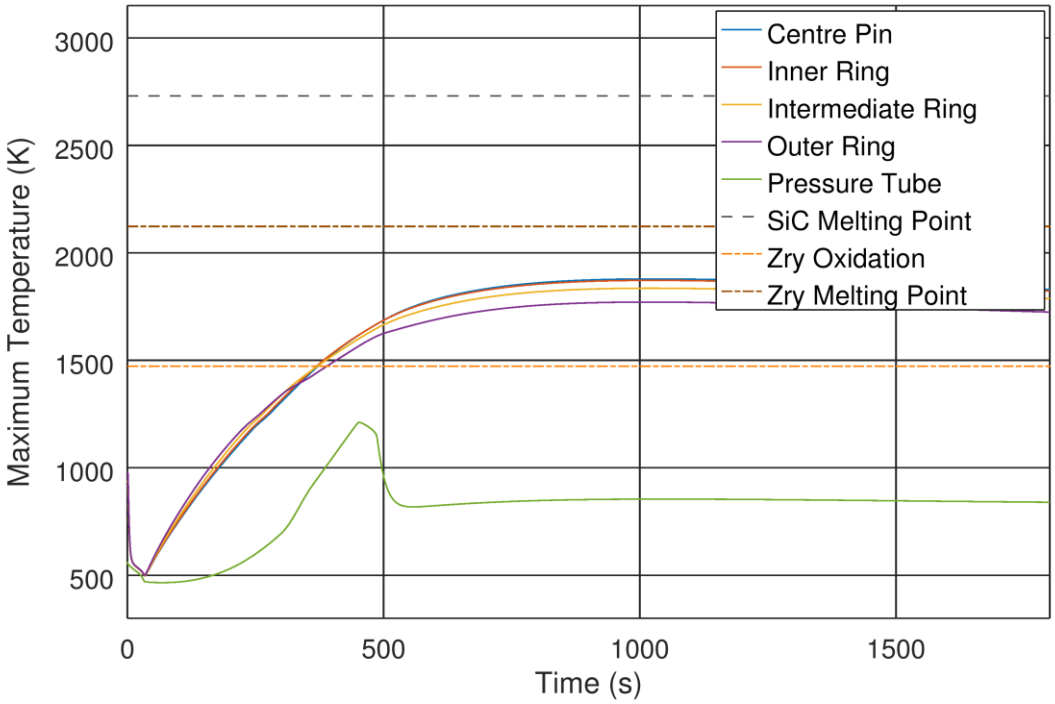

Figure 4.38: Fuel bundle temperature transient for irradiated UN TRISO FCM

4.5 Accident-Tolerant Cladding

In general, the primary effect on the neutronics due to cladding change is due to changes in neutron capture from the cladding. For each of the cases, the fuel is UO_2 with 3% SiC by volume. This requires a 0.72% enrichment when the cladding is zircaloy, but the enrichment can be kept at natural enrichment if the cladding is changed to SiC. Conversely, changing the cladding to a dual-layer zircaloy/FeCrAl cladding requires additional enrichment.

The use of a SiC cladding is expected to reduce fuel and cladding temperatures for a fresh bundle, as thermal conductivity values found for *fresh* SiC are greater than that found for zircaloy-4 in the range of the operating cladding temperature. The effect is more pronounced when the fuel is UO_2-based since a small reduction in temperature results in an increase the thermal conductivity of UO_2, further reducing the temperature.

However, for irradiated fuel, it is expected that the opposite will be the case, since the irradiation defects which accumulate in SiC result in a significant reduction in its thermal conductivity, resulting in higher temperatures than for metallic cladding. When irradiation of 4 MWd/kg(U) was factored in, the maximum centre-line temperature was 2121 K for zircaloy-4 cladding and 2159 K for SiC cladding.

There is some effect on the fuel's CVR, though not a substantial one, with up to roughly a 0.5 mk reduction in CVR depending on the cladding and burnup.

Table 4.19: Required Enrichment for ATF cladding

Cladding	Exit Burnup (MWh/kg(U))	Enrichment (wt% ^{235}U)	
		Fixed T	Calculated T
Zircaloy-4	200	0.72%	0.72%
SiC	200	0.711%	0.711%
Zircaloy-4 + FeCrAl	200	0.80%	0.79%

Table 4.20:

Average pin temperatures for ATF cladding

Cladding	Enrichment (wt% ^{235}U)	Fuel CL Temp. (K)	Fuel Avg. Temp. (K)	Clad Avg. Temp. (K)
Zircaloy-4	0.720%	1269.7	913.5	593.9
SiC	0.711%	1239.4	890.8	585.7
Zircaloy-4 + FeCrAl	0.800%	1269.0	913.0	596.2 (zirc4) 583.7 (FeCrAl)

Table 4.21: Maximum pin power for ATF cladding

Cladding	Enrichment (wt% ^{235}U)	Outer Ring Power Factor	Linear Element Rating (W/m^2)
Zircaloy-4	0.720%	1.13958	54722
SiC	0.711%	1.13918	54702
Zircaloy-4 + FeCrAl	0.800%	1.15219	55327

Table 4.22: Hottest pin temperatures for ATF cladding

Cladding	Enrichment (wt% ^{235}U)	Fuel CL Temp. (K)	Fuel Avg. Temp. (K)	Clad Avg. Temp. (K)
Zircaloy-4	0.720%	1760.3	1124.4	608.2
SiC	0.711%	1704.9	1087.0	596.6
Zircaloy-4 + FeCrAl	0.800%	1779.2	1132.1	611.9 (zirc4) 593.9 (FeCrAl)

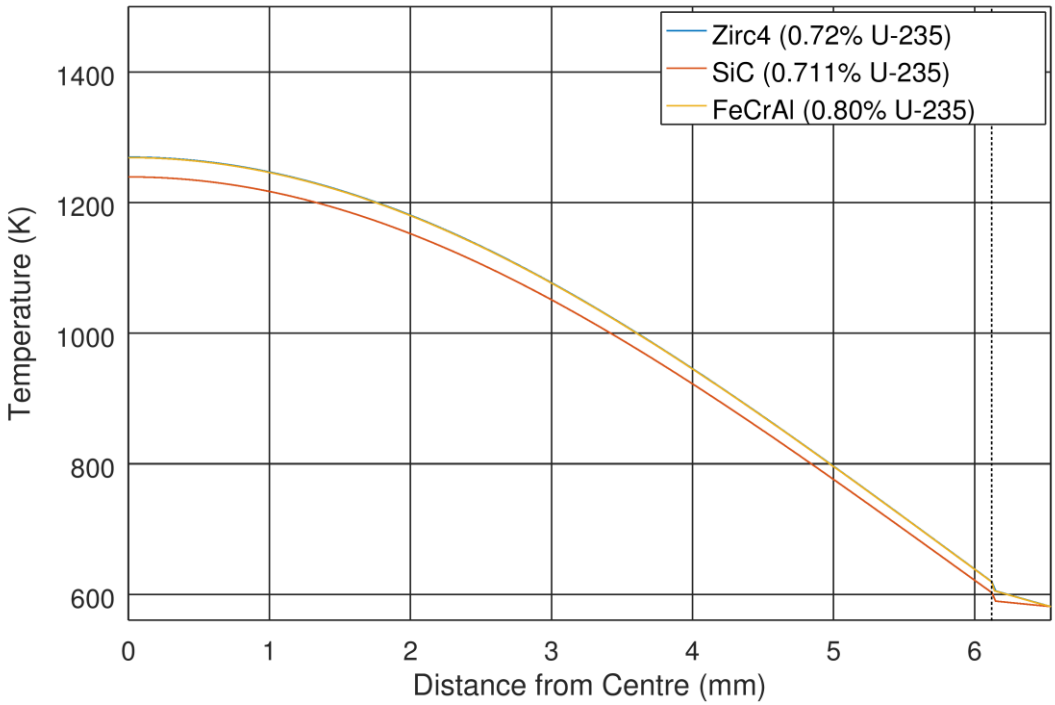

Figure 4.39: Average pin temperatures for ATF cladding

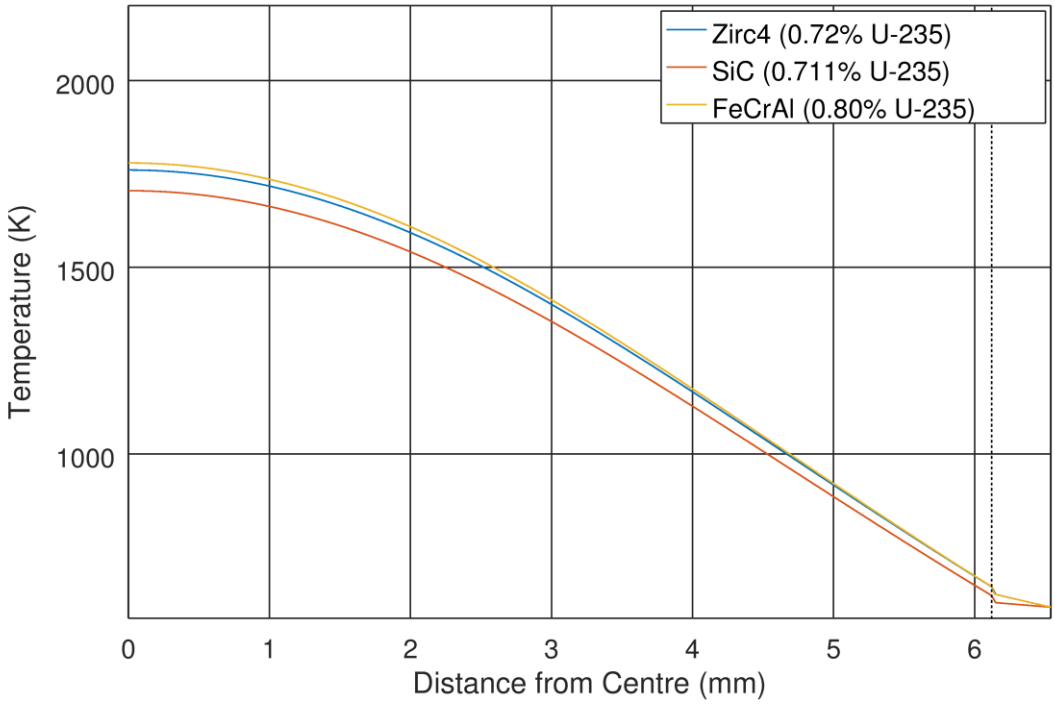

Figure 4.40: Hottest pin temperatures for ATF cladding

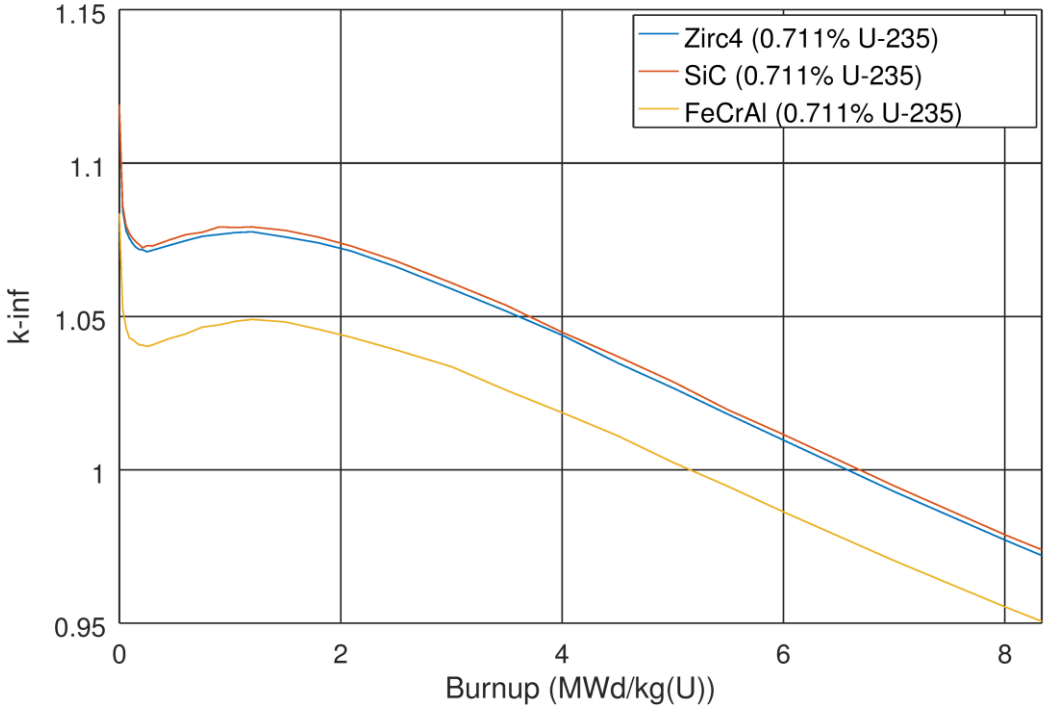

Figure 4.41: Reactivity of unenriched fuel with ATF cladding – fixed temperature

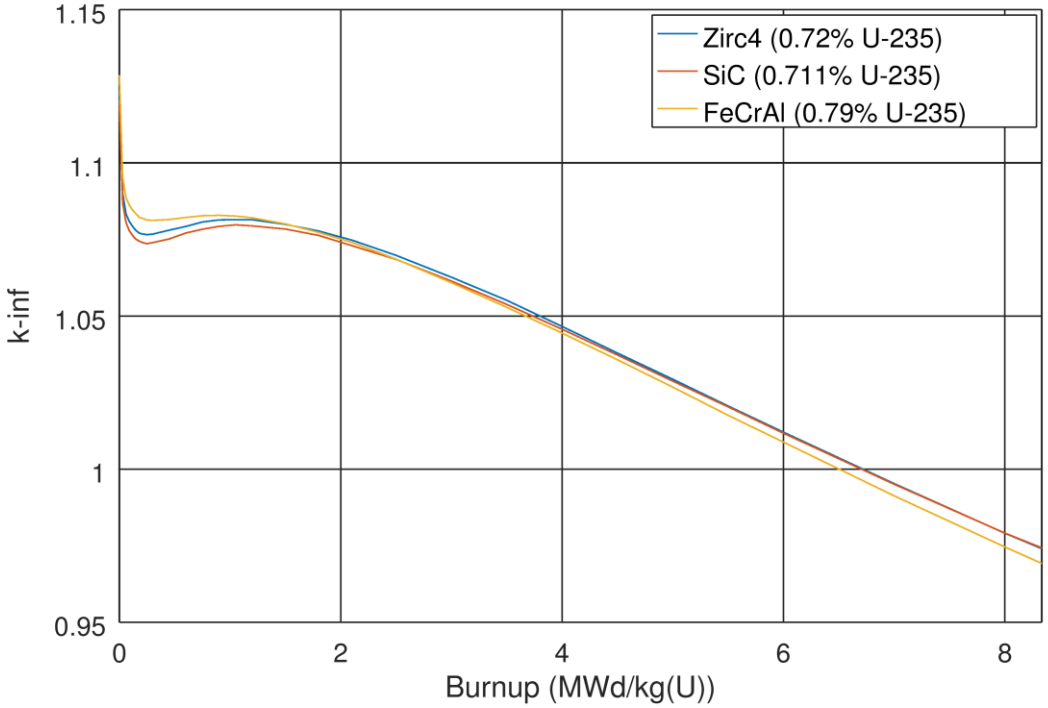

Figure 4.42: Reactivity of fuel with ATF cladding – calculated temperature

Table 4.23: CVR and FTC calculations for ATF cladding

Cladding	Enrichment (wt% ^{235}U)	Burnup (MWd/kg(U))	Calculated T			T = 941.29 K	
			k_∞	CVR (mk)	FTC (pcm/K)	CVR (mk)	FTC (pcm/K)
Zircaloy-4	0.720%	0	1.12319	16.49 ± 0.07	-1.24 ± 0.03	16.41 ± 0.07	-1.23 ± 0.03
		4	1.04638	14.37 ± 0.09	-0.18 ± 0.03	14.32 ± 0.09	-0.17 ± 0.03
SiC	0.711%	0	1.12010	16.10 ± 0.08	-1.27 ± 0.03	16.14 ± 0.07	-1.27 ± 0.03
		4	1.04563	13.84 ± 0.09	-0.22 ± 0.03	13.84 ± 0.09	-0.20 ± 0.03
Zircaloy-4 + FeCrAl	0.790%	0	1.12855	16.03 ± 0.08	-1.20 ± 0.03	15.82 ± 0.08	-1.19 ± 0.03
		4	1.04444	14.33 ± 0.09	-0.21 ± 0.03	14.27 ± 0.09	-0.23 ± 0.03

In a transient, the primary advantage for ATF cladding comes from the different properties of the cladding. Compared to zircaloy, both SiC and FeCrAl resist the oxidation by superheated steam. However, FeCrAl also has a lower melting point than zircaloy. Once this melting point is reached, the zircaloy layer underneath will be exposed to oxidation. However, the FeCrAl cladding can still delay this oxidation by several minutes.

On the other hand, SiC has a much higher melting point than zircaloy and FeCrAl, such that melting does not occur. In addition, the peak temperature is reduced from 1888 K (for zircaloy) to 1867 K (for SiC) due to the higher emissivity of SiC.

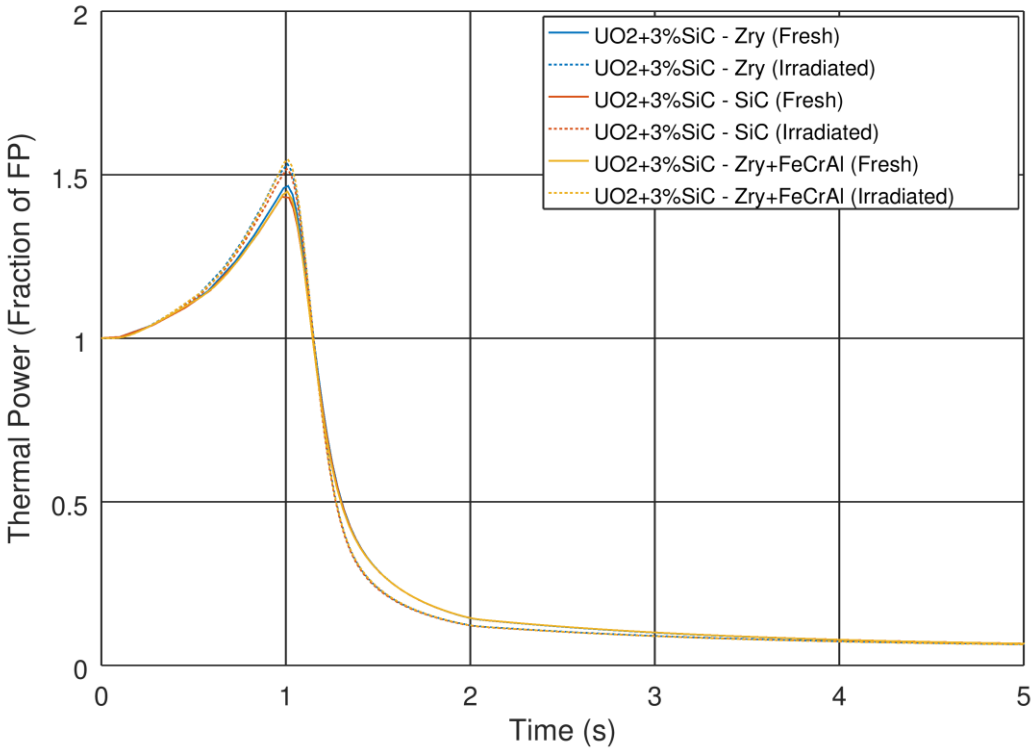

Figure 4.43: Reactor power transient for zircaloy and ATF cladding

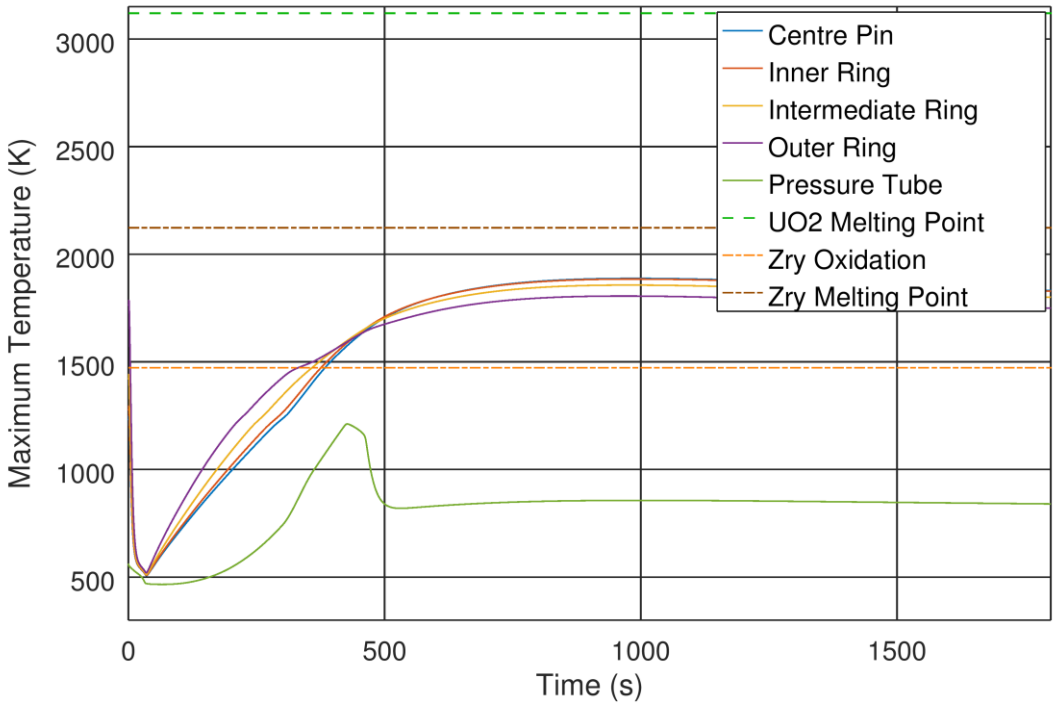

Figure 4.44: Fuel bundle temperature transient for fresh UO_2 + 3% SiC – Zirc4 clad

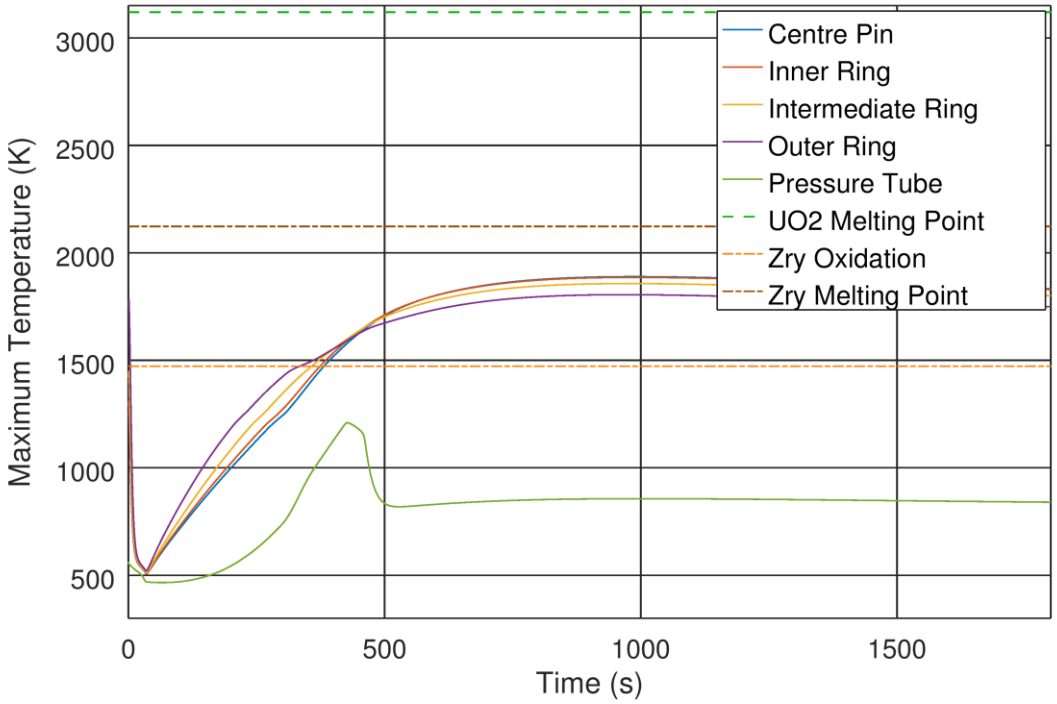

Figure 4.45: Fuel bundle temperature transient for irradiated UO_2 + 3% SiC – Zirc4 clad

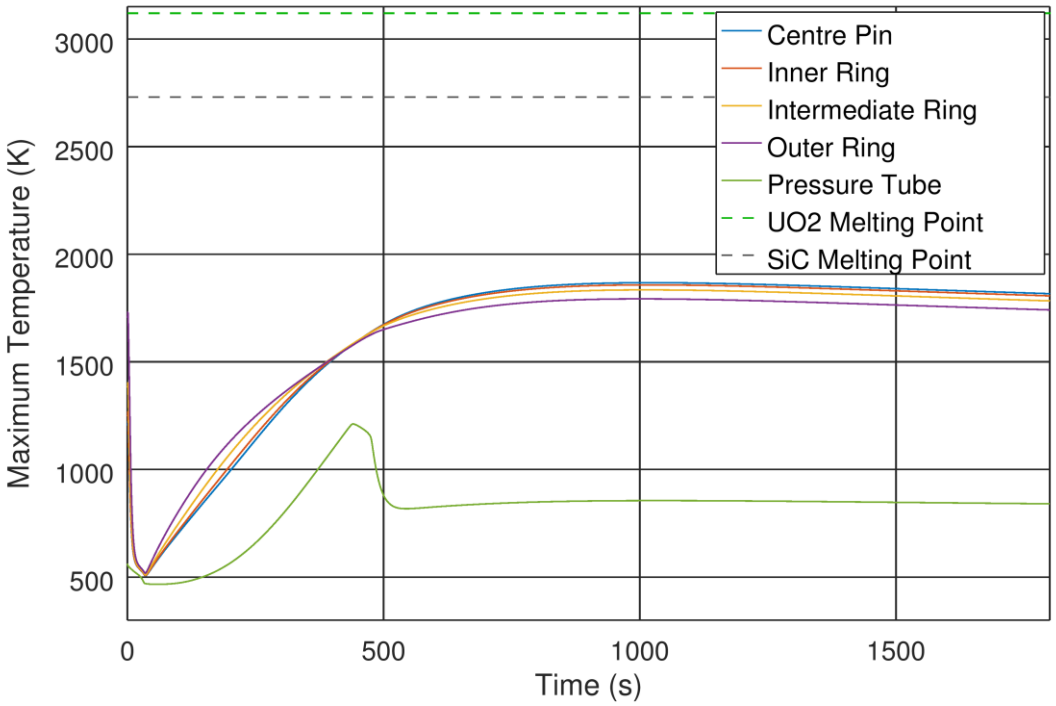

Figure 4.46: Fuel bundle temperature transient for fresh UO_2 + 3% SiC – SiC clad

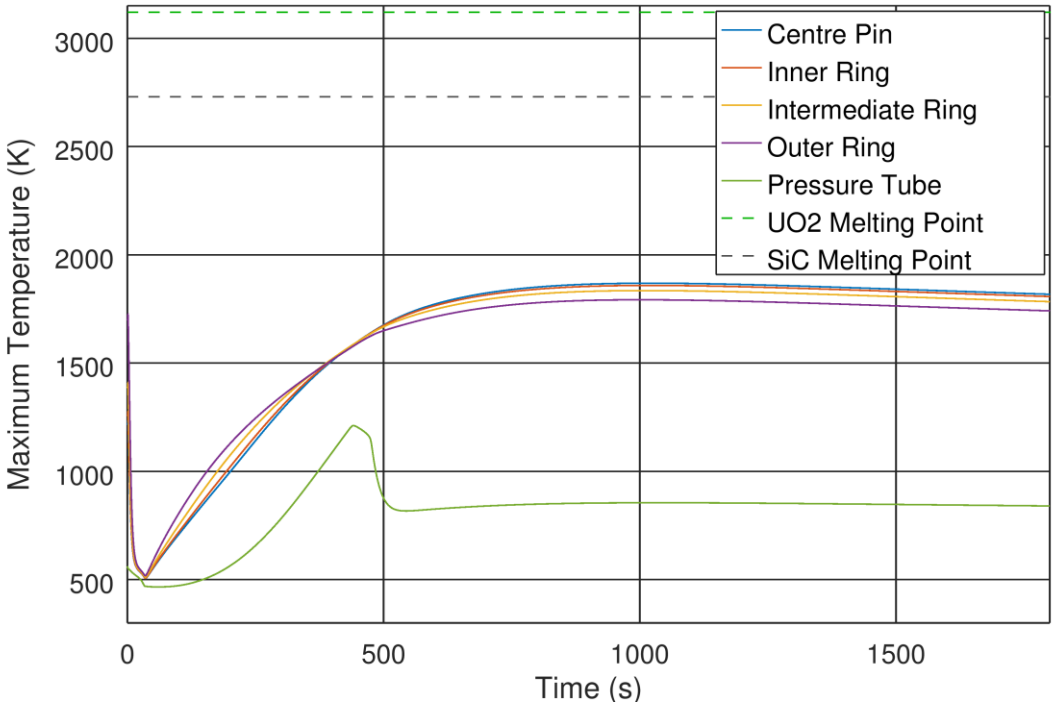

Figure 4.47: Fuel bundle temperature transient for irradiated UO_2 + 3% SiC – SiC clad

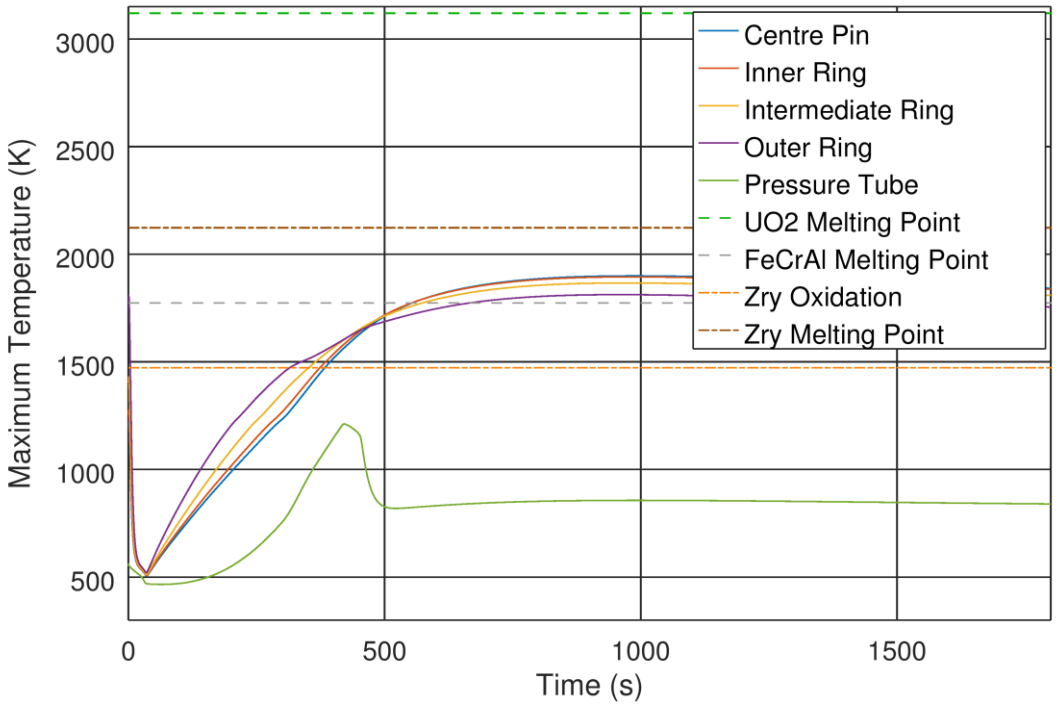

Figure 4.48: Fuel bundle temperature transient for fresh UO_2 + 3% SiC – Zirc4+FeCrAl clad

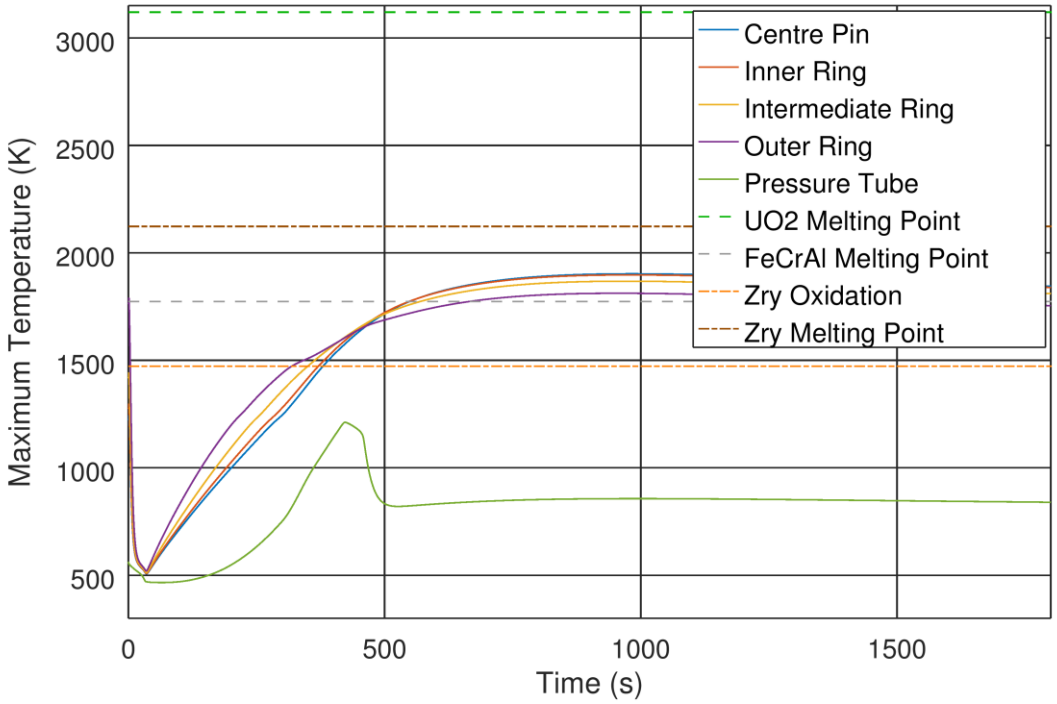

Figure 4.49: Fuel bundle temperature transient for irradiated UO_2 + 3% SiC – Zirc4+FeCrAl

4.6 Additional Figures – General Comparison of Results

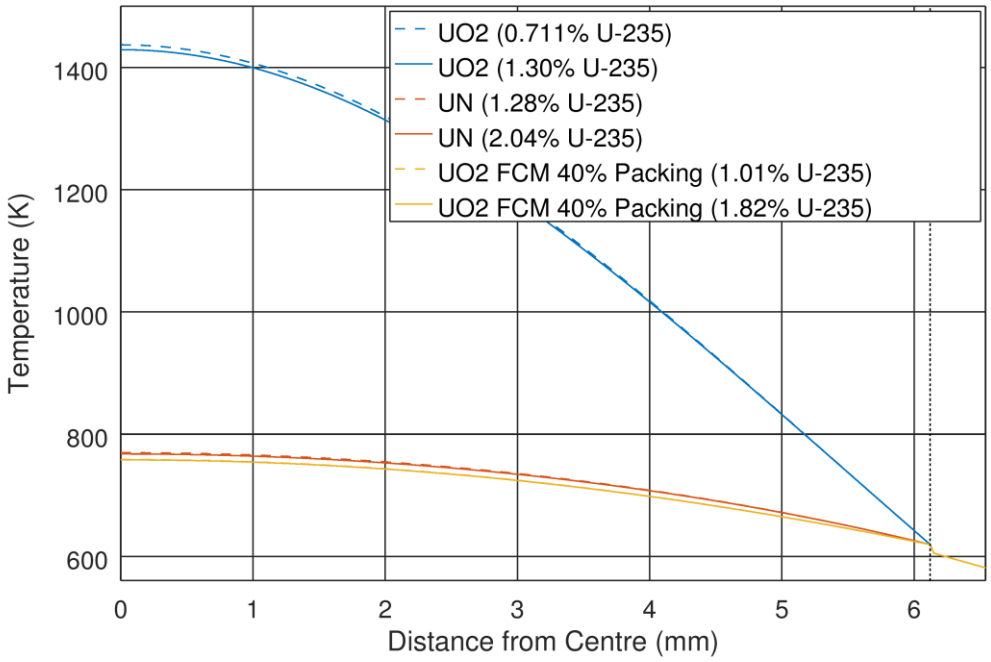

Figure 4.50: Average pin temperatures for high exit burnup fuel

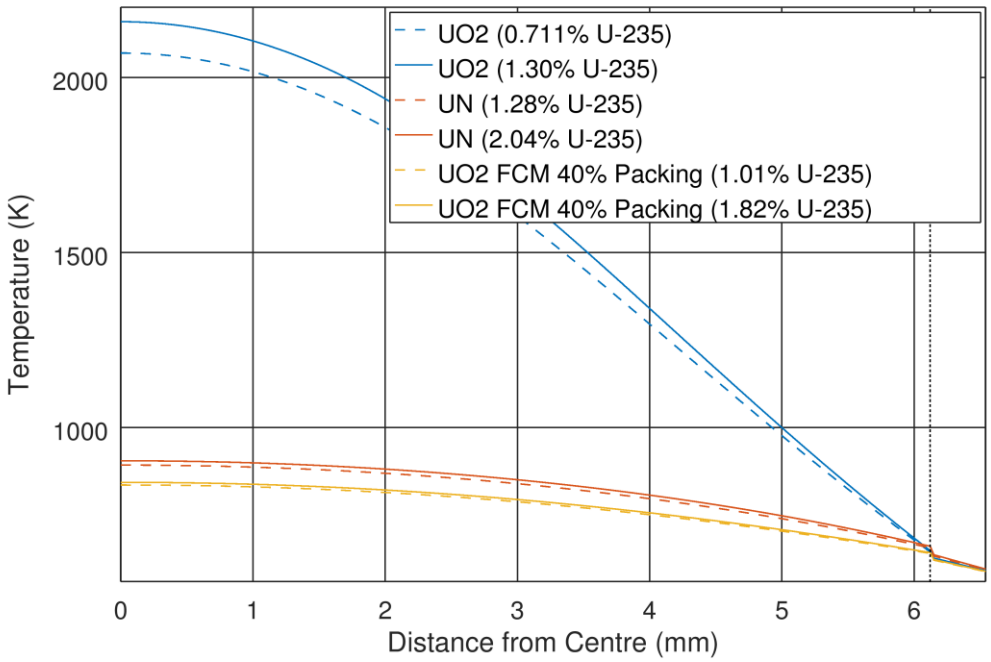

Figure 4.51: Hottest pin temperatures for high exit burnup fuel

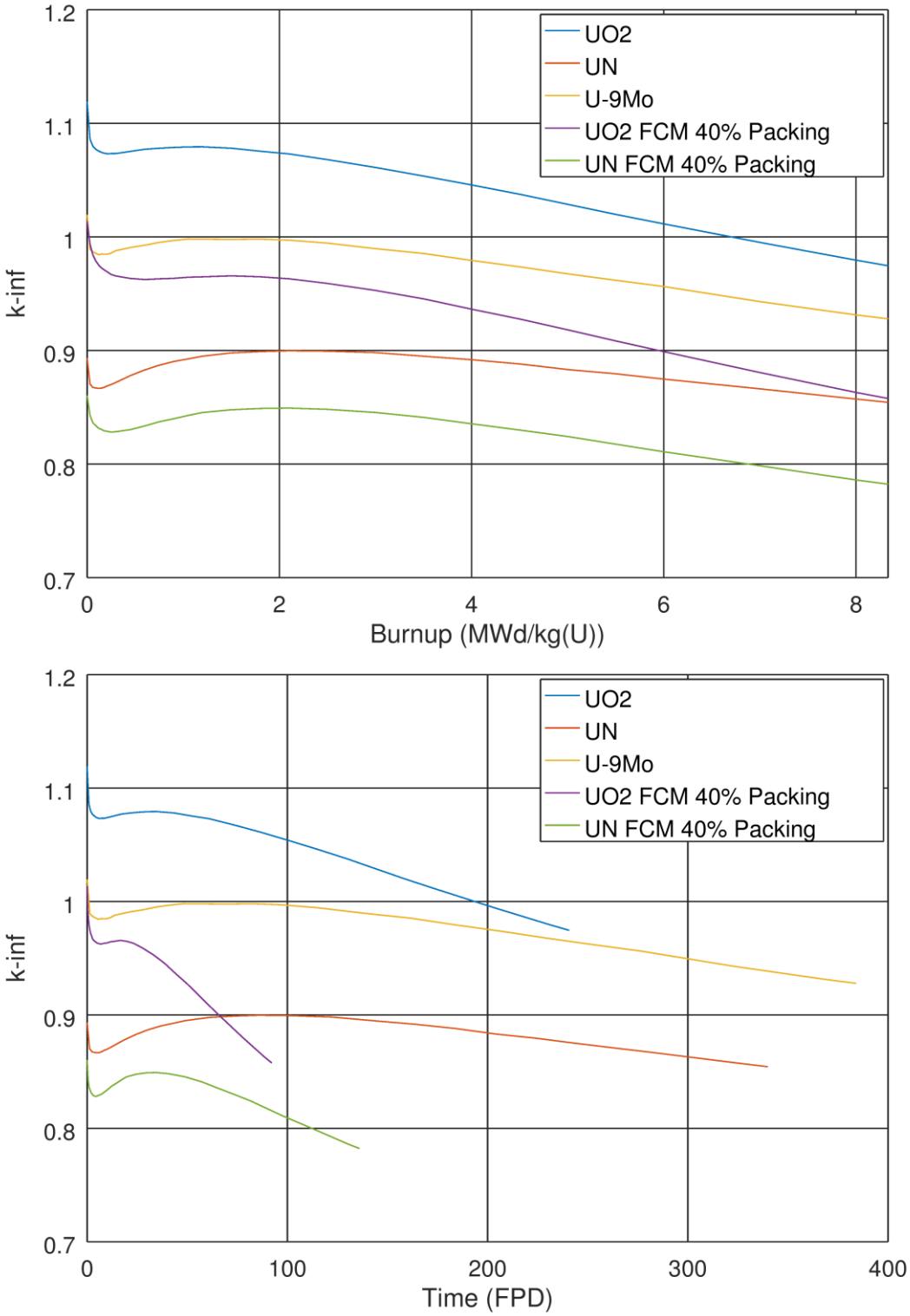

Figure 4.52: Reactivity of natural (unenriched) uranium fuels – fixed temperature

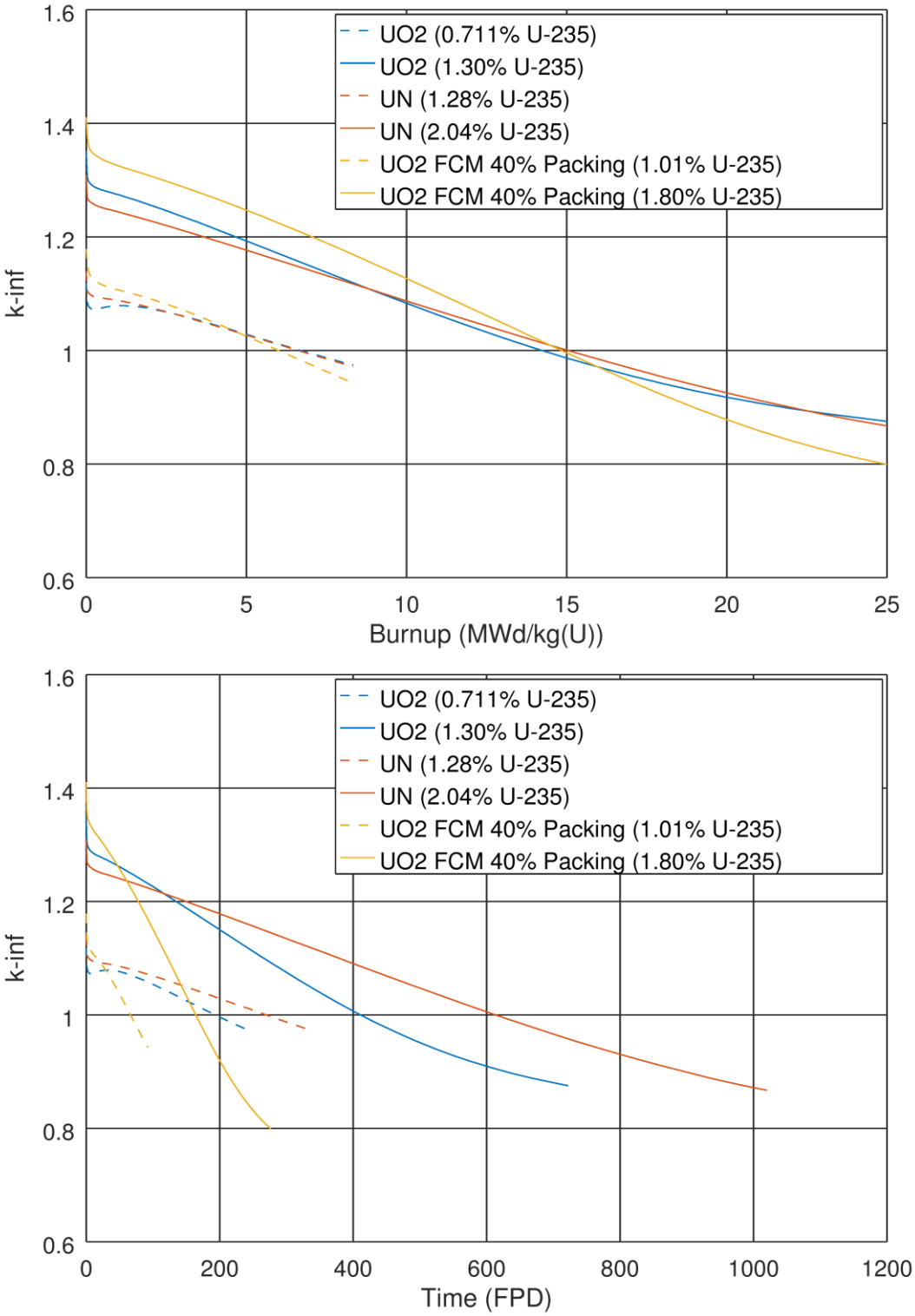

Figure 4.53: Reactivity of high exit burnup fuel – calculated temperature

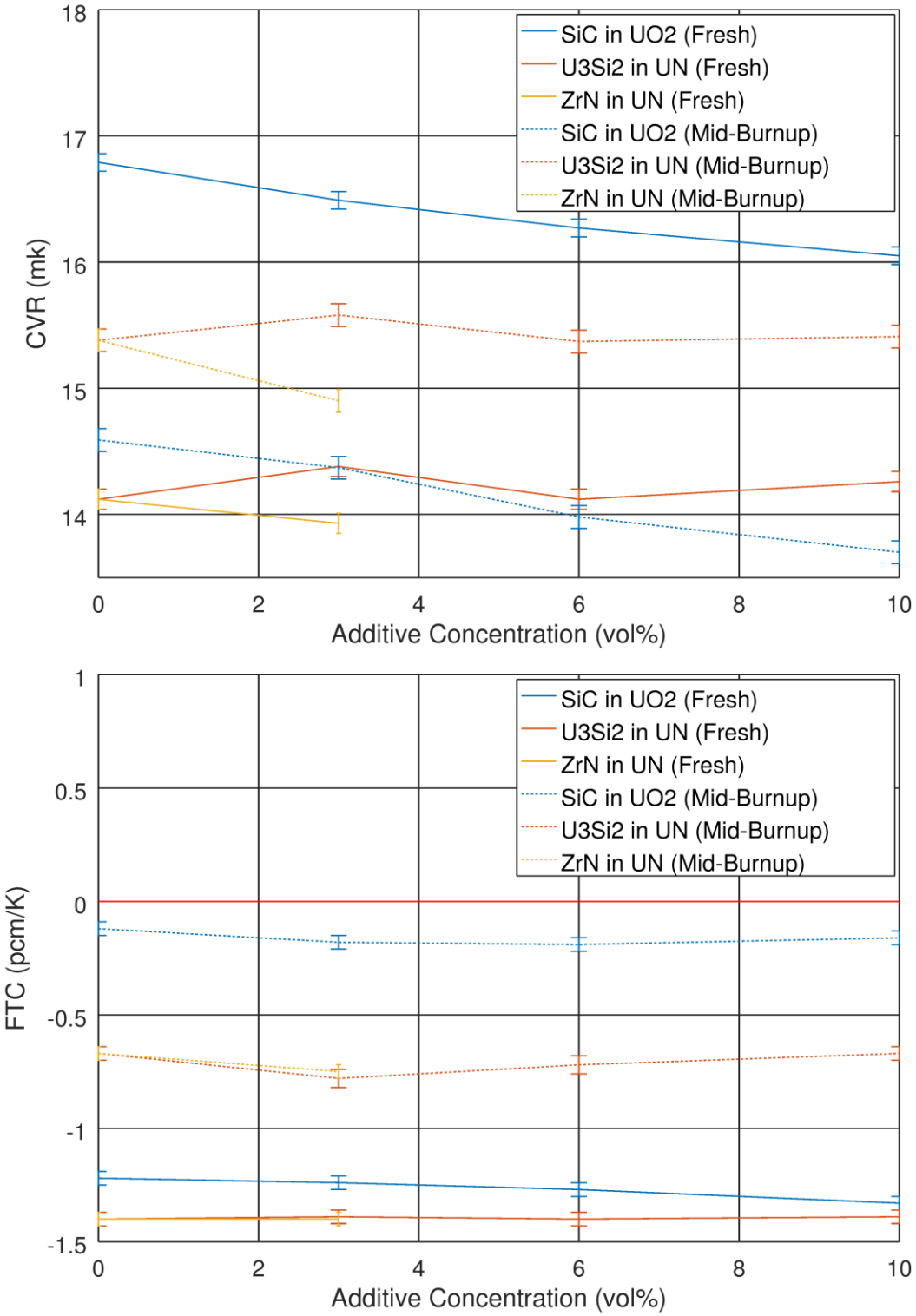

Figure 4.54: CVR and FTC for fuel with additives – calculated temperature

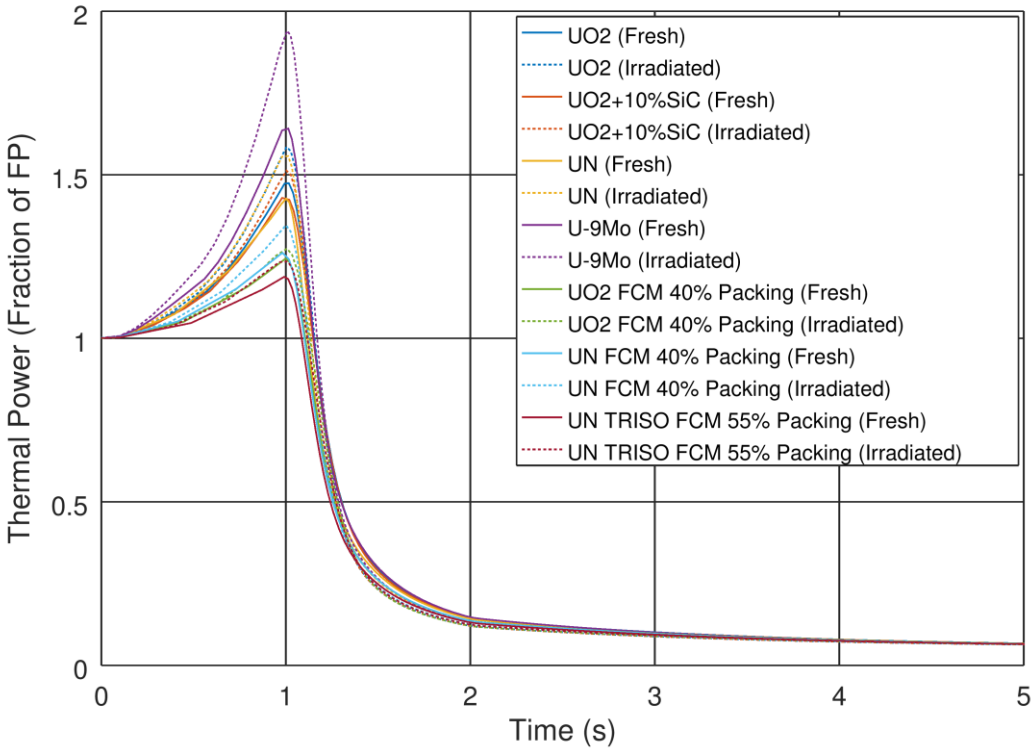

Figure 4.55: Reactor power transient for UO_2 and ATF fuel types

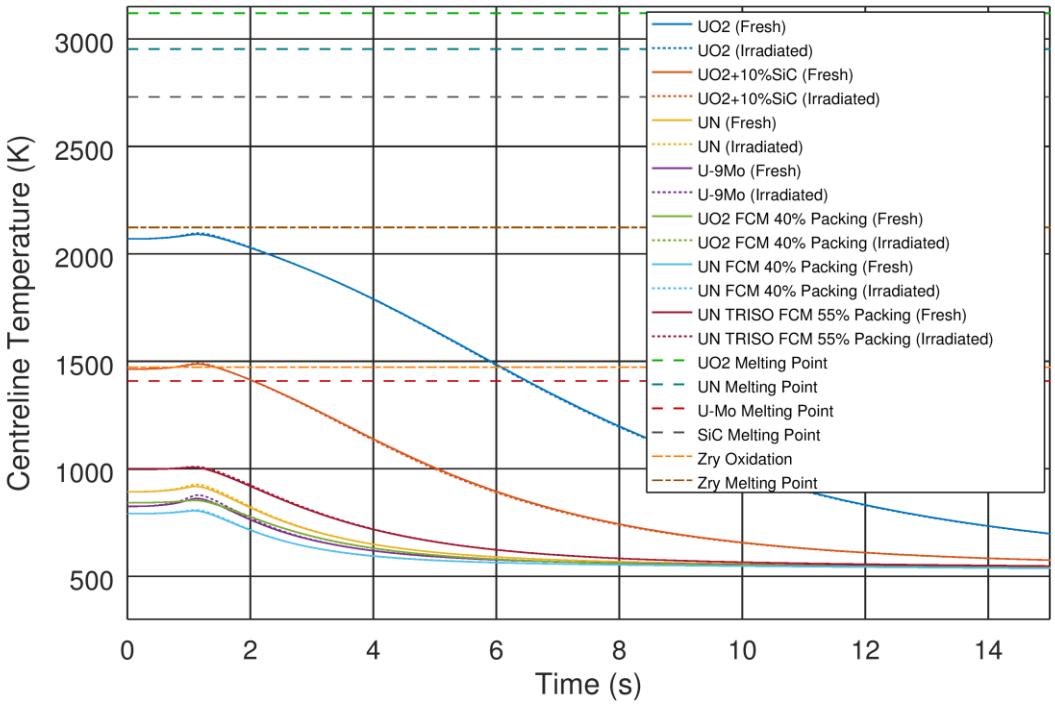

Figure 4.56: Initial fuel temperature transient for UO_2 and ATF fuel

5 Discussion

5.1 ATF Enrichment Requirements

One important observation is that nearly all ATF options, except for changing cladding to SiC, requires enrichment of the uranium to achieve a similar level of performance to standard UO_2 fuel. In terms of the four-factor formula $k_\infty = \eta f p \epsilon$, either the reproduction factor η or the thermal utilization factor f would be reduced compared to standard UO_2 fuel:

- Reducing the density of uranium in the fuel, either by mixing in an inert additive or forming FCM fuel, makes the fuel pellets less opaque to neutrons, thus less absorption in fuel can be expected relative to unchanged cladding, coolant, moderator, structural materials, and reactivity devices. This reduces f.
- Replacing the fuel material with one that has more parasitic absorption, such as UN or U-9Mo, reduces the reproduction factor η, as more of the neutrons captured in the fuel are actually being captured by lighter elements rather than uranium, so fewer can cause fission.
- Adding a material with stronger absorption to the cladding, such as FeCrAl, reduces f.

However, changing the fuel affects the burnup performance in an additional way. Fuels with low uranium density (particularly FCM fuel) contain less fissile material, and will thus lose their reactivity much more quickly as they are "burned". While the behaviours don't deviate substantially when plotting against burnup (energy produced per mass of uranium in the bundle), the difference is very notable when plotting against energy produced per bundle, as shown in Figure 4.52. Therefore, fuels with very low uranium density must have additional enrichment in order to achieve a similar refuelling rate as current CANDU fuel. The required enrichment can be estimated as the amount which maintains the same fissile mass (i.e. number of ^{235}U atoms), since the number of fissions in a bundle is roughly independent of the energy produced. However, due to other factors, such as changes in non-fission neutron reactions, and fission in bred nuclides such as ^{239}Pu, such an estimate is far from exact, and a better estimate of enrichment was made by actually simulating the burnup of different fuel designs at different enrichments.

Table 5.1: Comparison of theoretical enrichments by fissile mass to actual enrichments

Case	Estimated Enrichment	Actual Enrichment
UO_2	0.711%	0.711%
UO_2 FCM – 35% Packing	2.12%	1.89%
UO_2 FCM – 55% Packing	1.35%	1.16%
UN FCM – 35% Packing	1.44%	1.81%
UN FCM – 55% Packing	0.92%	1.41%
UN FCM – 55% TRISO Packing	2.51%	2.77%

For the UO_2 FCM cases, the actual enrichment is less than estimated based on fissile mass, thus for UO_2 FCM, the bundles contain fewer fissile atoms than a standard UO_2 bundle. This is likely achievable due to the significant reduction in the amount of ^{238}U which acts as an absorber. Not all the ^{235}U in a standard bundle is fissioned since eventually the bundle is not reactive enough and must be discharged from the core. While ^{239}Pu is bred from ^{238}U, this eventually saturates since the ^{239}Pu will be consumed by fission as well. Eventually, the amount of fissile material remaining, as a fraction of total heavy metal, drops to the point where the fuel must be discharged.

Since SiC is not a strong absorber of neutrons, this fraction is similar in UO_2 FCM as it is for homogeneous UO_2 fuel. However, the starting fraction is greater, since the fuel is enriched, thus a greater fraction of the initial ^{235}U can be fissioned. In addition, since the neutron economy is very high, the initial reactivity of the FCM fuel is significantly higher since there is substantially less absorption from ^{238}U. This means that the reactivity at discharge can be lower, since in a full core, the positive reactivity of fresher bundles and negative reactivity of old bundles cancels out so that the reactivity of the full core is zero. This is shown in Figure 4.29, where k_∞ is greater for FCM than UO_2 for freshly inserted bundles, while k_∞ is less for FCM than UO_2 for bundles nearing discharge.

For FCM with UN kernels, the extra absorption from ^{14}N substantially reduces the neutron economy of the fuel, outweighing the other effects and resulting in an enrichment higher than the prediction, i.e. that the bundle will initially contain *more* ^{235}U atoms than a standard UO_2 bundle. This is most substantial for the higher packing fractions, for which the other factors that would permit a lower enrichment are reduced.

Enriching the fuel results in an increase in η and f that brings reactivity back up to a level comparable to currently-used fuel. However, a transition from natural uranium fuel to SEU would either require construction of enrichment facilities, or import from other countries with enrichment facilities such as the United States. While SEU can improve economics over NU even for standard fuel, it becomes even more necessary for ATF, and absolutely necessary for most cases which cannot even go critical on NU, thus the

establishment of a supply of SEU would have to be considered. All the enrichments considered, however, are less than typical LWR enrichments, thus existing facilities that produce LEU for LWRs should be able to supply SEU for ATF CANDUs.

5.1.1 Performance of UO_2-SiC Composite Fuel

Adding SiC to UO_2 fuel would be the simplest ATF option to implement, as it would provide a significant benefit in reducing fuel temperatures while having only a modest impact on other properties.

For this fuel, without enrichment, the exit burnup would be decreased slightly (about 10%), along with the amount of uranium contained in the fuel (also about 10%), such that there would be a small, but still noticeable, decrease in bundle average residence time (about 20%), requiring about 25% more refuelling, which is significant and would put extra load on refuelling machines.

If enriched to match exit burnup, an enrichment of about 0.73% would be needed, but the bundle's average residence time would still be about 10% shorter than a normal bundle. Extrapolation suggests, then, that an enrichment of roughly 0.75% would achieve a similar refuelling rate to current fuel.

However, once enrichment is being performed, the advantage of not requiring any enrichment infrastructure to make the fuel is lost, thus there is little to discourage the selection of a higher level of enrichment, such as 0.9%, 1%, or even 1.2%, which would reduce the refuelling rate substantially, as long as a proper safety analysis is performed on that level of enrichment.

5.2 CVR and FTC

The positive coolant void reactivity of a CANDU reactor is a combination of several effects. The presence of coolant in the fuel channel can scatter fast neutrons into the resonance region where they can then re-enter the fuel and be captured. When the coolant is voided, this can only occur in the moderator region, which is further separated from the fuel and thus it is less likely for neutrons to re-enter the fuel before being fully thermalized. Therefore, this introduces a positive component to CVR [61]. Once the neutrons are thermalized in the moderator, they pass through the coolant before re-entering the fuel. Since the coolant is hotter than the moderator, the neutrons are "cold" and tend to be upscattered by the coolant. This makes it more likely that a few neutrons will be captured in low-lying resonances. Thus, with the coolant voided, the thermal spectrum becomes colder, so fewer neutrons are captured by uranium resonances, contributing positive reactivity [61]. However, as the fuel burns, plutonium builds up,

which has a low-lying *fission* resonance. A "colder" neutron spectrum reduces the number of neutrons absorbed in this resonance, contributing a negative component to the CVR. As a result, the equilibrium core has a smaller CVR than a fresh core [61].

Different fuel configurations have different behaviour in CVR since changing materials or enrichment introduces new neutron reactions or changes the weight of existing reactions, and these may be affected differently by coolant voiding. The most straightforward example is with silicon carbide, where fuel with much of the uranium-containing material displaced by silicon carbide exhibited a lower CVR in the calculations. The most likely reason for this is that silicon carbide also can act as a scatterer of neutrons. This lessens the impact of the loss of coolant to in-channel moderation, so that the effect of the coolant voiding on the in-channel neutron spectrum is reduced. This would in turn lessen the reactivity contributions of the previously discussed effects.

The fuel temperature coefficient is similarly influenced. As fuel temperature increases, resonances are broadened. This results in increased capture of neutrons in the resonance energy range due to reduced resonance self-shielding, which makes FTC negative [61]. However, as the fuel is burned, this particularly affects the low-lying plutonium fission resonance, with an energy of around 0.3 eV. As fuel temperature increases, this resonance broadens, capturing more of the thermal neutrons and giving a positive contribution to FTC [61]. Thus, for the equilibrium CANDU reactor, the FTC is close to zero.

A notable observation is that, for the FCM fuel, when tested at 941 K, the FTC tended to be worse than standard UO_2 fuel when irradiated. It is possible that this may be related to upscattering by SiC, which would put more neutrons closer to the plutonium fission resonance. However, this discounts the advantage of FCM fuel that the improved thermal conductivity leads to lower temperatures. The FTC is more negative at lower temperatures, since at higher temperatures, there is greater overlap between the thermal neutron spectrum and the broadened plutonium fission peak, so the effect of a change in temperature becomes more and more pronounced as the temperature is increased. Conversely, lowering the temperature reduces the overlap and thus reduces this positive contribution to FTC, lowering the FTC overall. Overall, FCM enriched for a similar lifetime as standard UO_2 fuel has a similar FTC to the corresponding non-FCM fuel.

When comparing the different options, uranium nitride has a similar CVR to standard UO_2 fuel while substantially improving FTC. U-9Mo improves the FTC by making it less dependent on burnup, but has a significantly worse CVR. FCM fuel has similar FTC to UO_2 or UN fuel, depending on the kernel material, but improves the CVR.

5.3 Fuel Temperature

In terms of temperature performance, all ATF options improve over standard UO_2 fuel by reducing fuel average and centre-line temperatures. This would, in turn, reduce the rate of volatile fission product diffusion, thus reducing internal pin pressure, as well as reducing the amount of fission products that would be released in the case of a cladding failure. The most modest change is to add up to 10% silicon carbide by volume to the UO_2 pellets. This does not substantially change the fuel behaviour but lowers the centre-line temperature of the hottest pins from over 2000 K to under 1500 K, or roughly a 30% temperature decrease.

The other ATF options require more enrichment but provide substantially greater benefit in terms of temperature reduction. However, their properties are also significantly more different from UO_2, so more thorough safety analysis would be needed. In addition, the weight of a bundle would change significantly. UN and U-9Mo bundles would be significantly heavier than UO_2 bundles, making them more difficult to handle and putting additional load on fuelling machines, fuel channels, etc. Conversely, FCM bundles would be very light compared to UO_2 bundles, which again affects the mechanical loads so that fuel handling systems would need to be re-evaluated.

5.4 Severe Accident Evaluation

In terms of a severe accident, certain behaviours may change compared to UO_2 fuel. The size of a LOCA-induced power transient varies between fuel types. When compared to UO_2, UN performs similarly, U-9Mo performs worse, and FCM performs better. The rate of heat-up is largely similar for most ATF options compared to UO_2.

As pointed out in the literature review, radiation becomes an important heat transport mechanism in a severe accident [9]. As the pins heat up, they radiate heat at a rate proportional to the fourth power of their temperature. This heats up the pressure tube, which is weakened and will either expand or sag until contact is made with the calandria tube, at which point heat can be conducted to the moderator, which acts as a large heat sink. The fuel can then remain sufficiently cool through radiation of decay heat, for as long as heat can be transferred to the moderator, which is typically until the moderator starts to boil away.

In general, the inner pins would become hotter as they would be insulated by the outer pins. The primary concern would be if the decay heat were enough that the fuel in these pins could melt, or the cladding fail, releasing fission products into the HTS. For example, a study gives the following curve for CANDU fuel with a blowdown period of roughly 40 seconds before heatup begins. Maximum temperatures approach 2100 K,

which is enough to melt the cladding. The bundle would be expected to "slump", i.e. fall apart.

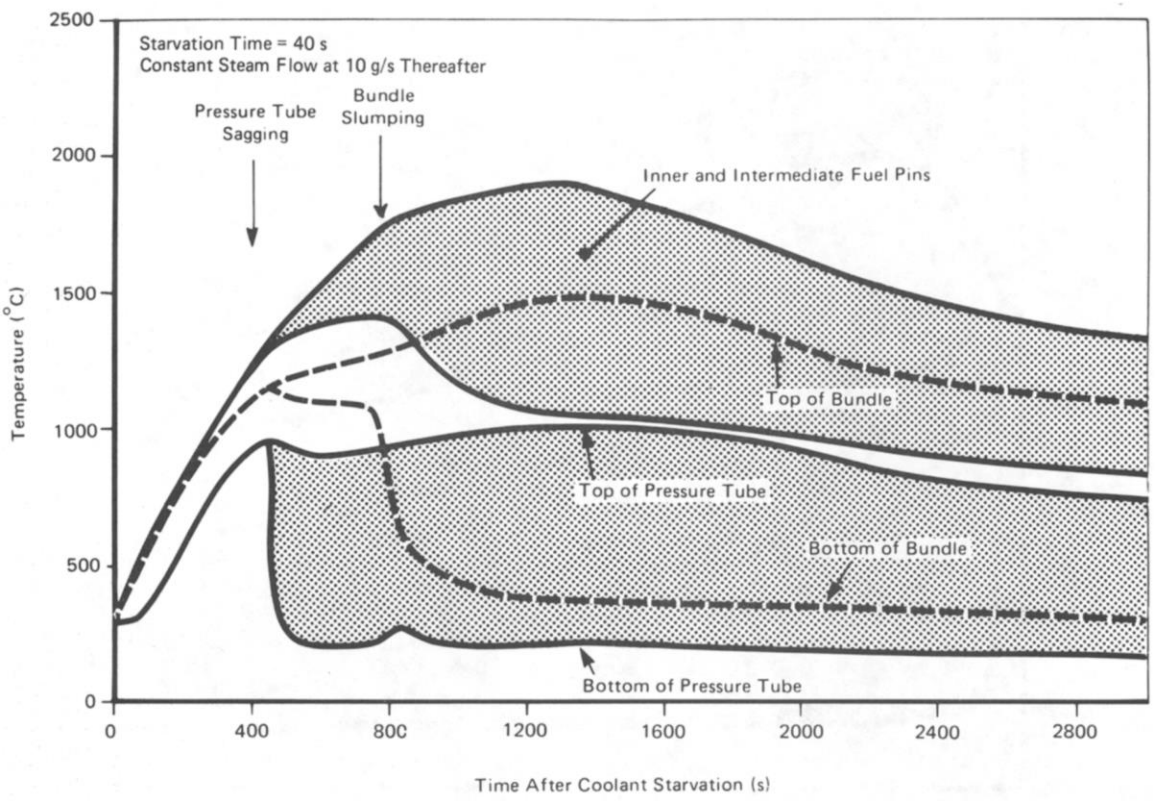

Figure 5.1: Fuel heatup in CANDU severe accident [26]

The FlexPDE model with radiation was developed to produce a simplified version of the result shown in the figure above. Pressure tube sagging was factored in only by its effect on the pressure tube temperature, while the bundle slumping effect was ignored. Additionally, the pressure tube was modelled by a single temperature, while each ring of pins was modelled by one pin. However, what the simple model shows is that changing to ATF fuel would only have a small effect on the peak temperatures, by perhaps 100 K or so.

However, the main concern is when the melting points of ATF materials are compared to the results. For standard UO_2 fuel, significant zircaloy oxidation can be expected, which may generate some additional heat, but the zircaloy wouldn't melt unless this additional heat allowed the melting point to be exceeded. In addition, the oxidation of zirconium increases its melting point, providing an additional margin. The fuel itself would remain well below its melting point.

Changing the fuel to UN or to FCM would not present any major concerns as far as this model goes, since their melting points are still well above the predicted maximum temperatures. However, changing the fuel to U-9Mo presents a concern in terms of accident tolerance since the fuel's melting point would be exceeded. Thus, fuel could potentially melt in such a bundle, resulting in greater fission product release and an adverse outcome compared to UO_2 fuel for this particular scenario.

Changing the cladding would reduce the amount of oxidation that occurs. However, the two-layer cladding with a FeCrAl surface coating would exceed the melting temperature of FeCrAl, so melting of this layer and exposure of the zircaloy below to oxidation would occur. SiC cladding does not have this disadvantage, and also radiates its heat somewhat more efficiently to the pressure tube.

It should be noted that the analysis was done on a high-power bundle, and the decay heat was assumed to be independent of the bundle's burnup. Thus, the "fresh fuel" cases are not as realistic as less decay heat would be expected than was modelled. Meanwhile, since mid-burnup bundles have less fissile material than fresh bundles, it would be expected that such a bundle would operate at a lower power and thus not have as much decay heat as was modelled. Finally, bundles near the channel edges would be operating at significantly less power and would thus produce significantly less decay heat. However, since heat transport by radiation is proportional to the fourth power of temperature, the effect on peak fuel temperature in the transient can be expected to be small.

For U-9Mo fuel, for example, the high-power pins in most channels would be expected to melt, since there is only a roughly 200 K temperature difference between the temperature for the pressure tube to sag and the fuel to melt, which is significantly exceeded in the high-power case. Bundles near the channel edges may survive since they would be at a lower temperature when the heatsink to moderator is established and the pressure tube temperature can decrease. However, this is overall still a negative for U-9Mo as ATF, since other ATF materials and even UO_2 would not be expected to melt.

This also affects other severe accidents where cooling is lost. In an SBO, once the steam generators dry up, natural convection of coolant will fail and bundles will heat up, particularly once channels start to dry up. The pressure tube must heat up and deform to transfer heat to the moderator. While the decay heat is significantly less at this point, it can still be expected that U-9Mo would melt before it could radiate enough heat to the pressure tube to cause it to deform rapidly, particularly if the loss of cooling occurs within the first day or so of a shutdown.

Not modelling the degradation of thermal conductivity of materials from irradiation limits the accuracy of the initial part of the transient, which includes the steady-state

temperature, which would be higher than what using "fresh" thermal conductivity values predicts. However, the "late" part, where the fuel heats up from decay heat due to a loss of cooling, is not significantly affected by this omission, since the temperature distribution in the pin becomes mostly uniform when the fuel's thermal conductivity is no longer the main limiting factor for heat transfer.

5.5 Additional Discussion

There are several additional changes that could have been made which were not considered in the analysis. The most obvious would be changes to the fuel geometry. The 37-element bundle is a compromise between neutron economy and heat transfer. Another possible bundle design is the CANFLEX bundle, which uses larger pins for the two centre rings, where the thermal flux is less and thus heat transfer requirements are reduced compared to the outer rings of pins. Increasing the size of the inner pins increases the amount of heat in the inner pins relative to the outer pins, which can potentially reduce the maximum operating temperature of the fuel. Since the spatial self-shielding effect is even stronger for UN and U-9Mo fuel, the potential to design a bundle with more significant pin size differences for these fuel types exists, and may even be required to maintain a sufficiently high DNBR.

Since ATF fuel has a lower operating temperature due to the improved thermal conductivity, another option is to consider bundles that have fewer, but larger, pins overall, as fuel centre-line temperatures would still remain below that for current UO_2 fuel. Such a geometry change would tend to increase the volume of fuel in the bundle, which is especially beneficial to FCM. However, maximum channel and bundle powers are generally limited by critical heat flux. If the pin size is increased and the number of pins reduced, the total surface area for convection into coolant is reduced, reducing the DNBR since a larger heat flux would be required for the same bundle power. Therefore, it is unlikely that the number of pins in a CANDU bundle could be reduced substantially regardless of the fuel material, and the best that could be done is an adjustment of pin sizes for each ring based on the spatial self-shielding effect. Similarly, a significant power uprate would be unlikely since changing the fuel material does little to improve the DNBR.

Another possibility is, since fuel is being enriched, that different rings can be loaded with different enrichments, with higher enrichment for the inner pins, to compensate for the spatial self-shielding effect. However, this presents an additional manufacturing challenge to ensure pellets of the correct enrichments are loaded in the correct pins and that the pins are correctly assembled by enrichment into the bundle.

In terms of cladding, changes to the cladding thickness were not considered. Typical CANDU cladding is designed to "collapse" onto the fuel pellets when subject to operating conditions. SiC is much more brittle than metallic cladding, though, and may not be able to be designed as collapsible, which would require a significantly thicker cladding, which would reduce the fuel volume and thus increase enrichment requirements and/or increase refuelling rates.

6 Conclusions & Further Research

The various ATF options were compared to UO_2 in various metrics. The following summarizes the results:

Table 6.1: Comparison of ATF options[1]

Metric	UO_2 +SiC	UN	UN+ U_3Si_2	UN+ ZrN	U-9Mo	UO_2 FCM	UN FCM	UN TRISO FCM	SiC Clad	FeCrAl Clad
Neutron Economy		- -	- -	- -	-	-	- -	- -	+	-
Uranium Density	-	+	+	+	+ +	- -	- -	- - -		
Enrichment	-	- -	- -	- -	-	- -	- -	- - -		-
CVR					- -	+	+	+ +		
FTC		+	+	+	+ +	-	+	+		
Fuel Temperature	+	+ +	+ +	+ +	+ +	+ +	+ +	+ +		
Fuel Melting Point		-	- -	-	- - -	-	-	-		
Fuel Stability[2]		- -								
FP Containment[3]						+	+	+ +		
Clad Oxidation									+ +	+ +
Clad Ductility									- -	

Overall, all ATF fuel options reduce the fuel temperature, generally at the expense of neutron economy. FCM additionally adds additional barriers to fission product release, but at the expense of uranium density. ATF cladding options serve primarily to resist oxidation in high-temperature steam environments when compared to zirconium alloys.

Mixing in a small amount of SiC into UO_2 provides significant fuel temperature reductions under operating conditions without substantially altering the fuel's other properties, unlike with other fuel options, although the 10% reduction in uranium density would increase fuelling requirements by roughly 25% more bundles per day, unless the fuel were changed from NU to SEU to get a higher exit burnup.

[1] - - - Drastically worse
- - Significantly worse
- Somewhat worse
(blank) Similar (to UO_2) or undetermined
+ Somewhat better
++ Significantly better

[2] Chemical stability, e.g. reactivity to water

[3] Independent of temperature change

Table 6.2: Advantages and disadvantages of various ATF options

ATF Option	Advantages	Disadvantages
UO_2 with added SiC	Significant reduction in fuel centre-line temperature Minimal change to fuel behaviour Minimal enrichment requirements Neutron economy similar to UO_2	Higher fuel temperature than other ATF options
UN	Low fuel temperatures More negative FTC than UO_2 Increased uranium density	Significantly reduced neutron economy due to ^{14}N Requires significant enrichment UN reactive with water
UN with added U_3Si_2	Low fuel temperatures Slightly better neutron economy than pure UN Higher uranium density than UO_2 U_3Si_2 can protect UN from water	Less uranium density than pure UN Neutron economy is still significantly worse than UO_2 U_3Si_2 has lower melting point
UN with added ZrN	Low fuel temperatures – less than for UN	Less uranium density than pure UN Higher enrichment than UN
U-9Mo	Very low fuel temperatures More negative FTC than UO_2 when irradiated Highest uranium density	Reduced neutron economy versus UO_2 (better than UN) Higher CVR than UO_2 Very low melting point Fuel melting in severe accident scenarios
UO_2 FCM	Very low fuel temperatures Lower CVR than UO_2	Less negative FTC than UO_2 Very low uranium density reduces neutron economy Significant enrichment required to compensate for uranium density
UN FCM	Very low fuel temperatures Lower CVR than UO_2 More negative FTC than UO_2	Low uranium density Low neutron economy Significant enrichment required to compensate for uranium density
UN TRISO FCM	Low fuel temperatures Lower CVR than UO_2 More negative FTC than UO_2	Extremely low uranium density Low neutron economy Significant enrichment required to compensate for uranium density
SiC Cladding	Slightly better neutron economy than zirconium alloys Oxidation resistant Higher melting point than zirconium alloys	More brittle than metals
Zirc4+FeCrAl Cladding	Oxidation resistant	Reduces neutron economy Lower melting point than zirconium alloy – can melt in severe accident

Table 6.3: Comparison of UO_2 and ATF for a LOCA

Fuel[4]	Margin to M.P. LOCA Power Pulse	Margin to M.P. LOECC Transient	Potential Impact to Core Disassembly Time
UO_2	1030	1230	
UO_2 with added SiC	1240	850	Insignificant change
UN	2030	1120	Insignificant change
UN with added U_3Si_2[5]	1000	100	Insignificant change
U-9Mo	550	-420	N/A (fuel melted)
UO_2 FCM	1880	880	Insignificant change
UN FCM	1930	880	Insignificant change
UN TRISO FCM	1720	870	Insignificant change

However, overall, for scenarios evaluated in this study, none of the accident-tolerant fuels evaluated in this study are demonstrated to be substantially more accident-tolerant than the standard UO_2 bundles currently used in CANDU reactors. For the case of a LOCA with LOECC, UO_2 fuel is already "accident-tolerant" in that substantial radiation release does not occur. Cladding oxidation would occur, though the fuel would not melt. Cladding oxidation would produce hydrogen gas, and release small amounts of radionuclides (mainly noble gases) in the case that the cladding cracks. Both of these are manageable, particularly if the HTS remains intact. Only in the case where operator intervention is delayed for so long that the moderator and shield tank water become ineffective as a heatsink and enough moderator boils away to expose fuel channels would a meltdown be expected.

Comparatively, for the initial power pulse, the margin for melting is large for all cases. For the LOECC transient, the peak temperature is similar between all cases, so that the margin depends primarily on the melting point of the fuel. While the margin is large for most fuel, the margin is small for U_3Si_2, thus a more detailed analysis would be warranted if this material were being considered. For U-9Mo, on the other hand, the margin is *negative*, thus this fuel, despite being proposed as accident-tolerant fuel, would actually be "accident-*intolerant*" as CANDU fuel, as fuel melting would be expected roughly five minutes into this type of accident. Therefore, further evaluation of U-Mo alloys as CANDU fuel is not recommended, particularly under the notion of being "accident-tolerant", as the consequences of certain accidents is substantially greater for U-Mo alloys than for UO_2.

[4] For composite fuel, the lowest melting point of the fuel's components is used.

[5] Approximate values (uses temperature data from UN case and melting point of U_3Si_2).

Generally, the point at which this would progress into a severe accident is when, in the case that moderator cooling is not available, moderator begins to boil and expose fuel channels, in which case the fuel can melt and/or the fuel channels disassemble [9]. While not evaluated in this study, it is expected that the time for the heat-up of the fuel after loss of the moderator as a heatsink would be insubstantial compared to the time it takes to heat the large volume of moderator to its boiling point, and boil enough of it to expose fuel channels. The time needed to boil the moderator is independent on the fuel type, as the decay heat is identical in all cases. Thus, the duration from the start of the accident to when core disassembly is expected would not be affected significantly by changing from UO_2 to a different fuel material.

Overall, accident-tolerant fuel and cladding would only have a minor impact on the progression of this scenario. Accident-tolerant fuel meat, particularly FCM fuel, could reduce the amount of radionuclides possibly released in the case of fuel damage, though since releases even for UO_2 can be considered relatively minor, the benefit is not substantial. Accident-tolerant cladding could potentially reduce the amount of hydrogen generated, which can lower the risk of a hydrogen explosion if the current level of risk is deemed to be too high.

6.1 Paths for Future Research

There are a number of paths for further research. Within neutronics, additional properties of the different fuel types could be determined. Such properties include moderator boron and gadolinium poison reactivity worth, xenon reactivity (equilibrium and peak), and reactivity device worths (liquid zone controllers, adjuster rods, mechanical control absorbers, and shutdown rods).

In particular, determining the worths of reactivity devices is important from both a control and a safety perspective. The liquid zone controllers are used for day-to-day balancing of core power and to account for the variation of core reactivity between daily refuellings. If their worth is reduced, it would become more difficult to control the reactor under normal conditions. The control absorbers and shutdown rods are needed to reduce reactor power during abnormal conditions. If their worth is reduced, then the control absorbers may not insert negative reactivity quickly enough, or insert enough negative reactivity, to bring reactor power down quickly enough in a stepback. The shutdown rods may not insert negative reactivity quickly enough to counteract rapid reactivity insertions such as from a LOCA. Additionally, the shutdown depth may be impaired and not ensure a guaranteed shutdown state from SDS1.

Serpent has the capability to perform full core calculations without the simplifying assumptions that are required by diffusion codes. Any relevant details in the core, including fuel bundles, fuel channels, reactivity devices, and structural materials, can be modelled in three dimensions. This permits an accurate determination of core reactivity and flux distribution, but requires several orders of magnitude more computational time than running a diffusion code.

Therefore, an ideal methodology for a full-core Serpent calculation would be to start with lattice calculations, including normal cells, edge cells, and supercells which contain reactivity devices, both in "inserted" and "withdrawn" states. Serpent is well-suited to modelling CANDU cells with reactivity devices due to the 3d modelling capabilities, thus not requiring approximations that are needed with 2d deterministic codes. The few-group constants would be calculated for all these cells, which can then be plugged into any diffusion code. The diffusion code would then be used to perform full-core calculations on the CANDU core for the purpose of obtaining a reasonable "equilibrium core" configuration, by performing a core follow. Performing the core follow in Serpent would be infeasible. Once an equilibrium core configuration is obtained, properties such as reactivity device worths can be determined more accurately through a full core Serpent calculation. This can be done on several different equilibrium cores to account for variations in fuel distribution.

Theoretically, a core follow in Serpent would be the most accurate method, especially if coupled to thermal-hydraulics code to determine fuel and coolant temperatures throughout the core. A script could shift fuel properties in the input file to represent refuelling, and also determine proper liquid zone levels. Nuclide concentrations would be calculated on individual bundles as opposed to being looked up as a function of burnup only. However, since a full-core Serpent calculation can take hours or days, as opposed to seconds for a diffusion calculation, performing a core follow to a satisfactory equilibrium state would take an unreasonably long time without an extremely large amount of computational resources. In addition, the Monte Carlo nature of Serpent means that the precision of burnups in such a calculation would be affected by statistical uncertainty. To reduce the uncertainty, sufficient neutron histories per pin is required, which further increases computation time.

In addition to reactivity device worths, a full core Serpent calculation would be ideal for determining the following properties:

- Actual equilibrium values for CVR and FTC. Potential effects on neutron leakage are not captured by measuring CVR and FTC on a lattice cell. In addition, since fuel in an equilibrium core consists of a range of burnups, rather than a single burnup,

values for fuel at a specific burnup, such as mid-burnup, are not exactly representative of the actual CVR and FTC for an equilibrium core, which are the values which determine how the actual reactor would behave.

- Accurate core-wide values for properties such as coolant temperature coefficient, moderator temperature coefficient, and soluble poison reactivity coefficients.
- Distribution of core power – maximum channel and bundle powers, with and without adjusters.

It is hypothesized that significant changes to the fuel can potentially affect reactivity device worths. Consider the one-group criticality equation [62]:

$$k = \frac{\nu\Sigma_f}{\Sigma_a + DB^2} \tag{6.1}$$

The absorption term Σ_a can be split into components for fuel, moderator, structural materials, and reactivity devices:

$$k = \frac{\nu\Sigma_f}{\Sigma_{aF} + \Sigma_{aM} + \Sigma_{aS} + \Sigma_{aR} + DB^2} \tag{6.2}$$

Under equilibrium conditions, $k = 1$. The reactivity worth from a fixed amount of additional absorption is:

$$\frac{dk}{d\Sigma_{aR}} \approx -\frac{1}{\Sigma_{aF} + \Sigma_{aM} + \Sigma_{aS} + \Sigma_{aR} + DB^2} \tag{6.3}$$

Effectively, the more absorption (or leakage) already present in the core, the less negative reactivity is contributed by a fixed amount of additional absorption, such as from inserting a reactivity device. Thus, for ATF with stronger absorption, such as UN and U-9Mo, it is possible that reactivity device worths may be reduced. For FCM with UO_2 kernels, which are less strongly absorbing, it is possible that reactivity device worths may be increased. Switching a reactor to ATF may require changing the amount of absorbing material in rods, or adding neutron poison to the zone controller water.

Another possibility for future research is to test the behaviour with other bundle geometries, such as CANFLEX, or combine with other concepts related to improved safety or economics, such as increasing the enrichment to reduce uranium requirements, or adding neutron poison to certain pins to obtain a negative CVR. These would be straightforward to test using Serpent for lattice calculations.

In particular, considering increasing enrichment to get a higher exit burnup and fuel lifetime, in order to potentially reduce uranium consumption, becomes significantly more attractive if ATF were to be used in CANDU reactors. Even with UO_2, enrichments between

0.9% and 1.2% have been considered to reduce fuel-cycle costs [63]. Alternatively, the outer channels in such a core could be refuelled more frequently to improve power flattening and uprate the core power [63].

With ATF, increasing enrichment becomes even more attractive. Lower fuel temperatures result in less fission gas release, permitting higher exit burnups. In addition, unenriched ATF performs poorly compared to unenriched UO_2 in terms of economics. For UO_2 with 10% added SiC, the amount of energy that can be extracted per bundle is reduced by 20% if no enrichment is performed. For UN, U-9Mo, and FCM, the fuel must be enriched or the core cannot become critical. Therefore, enrichment is highly desirable for ATF fuel, and if enrichment is being performed, a level of enrichment that maximizes economic and safety benefits can be chosen. The combination of switching to a bundle geometry such as CANFLEX, changing fuel and/or cladding material to ATF, and increasing enrichment to get a high exit burnup, can potentially provide a combination of economic and safety benefits over standard natural UO_2 fuel.

Another significant extension would be to perform a true multi-physics analysis on ATF fuel. This dissertation primary focused on reactor physics aspects, with only minimal thermal analysis, primarily meant as a comparative study on ATF rather than a detailed analysis on exact behaviour. The most significant addition would be to couple the reactor physics calculations to a thermal-hydraulic code such as CATHENA, to get a more accurate picture on heat transport than the simple correlations used in the FlexPDE models. For example, in the transient analysis, the correlation for the heat transfer coefficient to the coolant as pressure decreased had no physical backing, while the voiding transient is based very roughly on existing data and thus the rate of reactivity insertion is likely to be inaccurate. Therefore, the results may only be used to compare the different ATF options to UO_2 fuel, not to make any definitive conclusions on the individual behaviour of a specific ATF option. Therefore, there would be significant value in replacing the very simple FlexPDE model with a more comprehensive thermal-hydraulic model, such as by using CATHENA, for which not only more accurate values for normal operating conditions could be calculated, but accidents such as large and small LOCAs and SBOs could be more accurately modelled for ATF. Coupling to Serpent would permit replacing point kinetics with spatial kinetics. Other codes could be used to better simulate other phenomena of severe accidents, such as pressure tube creep and bundle deformation. Fuel performance codes could potentially be used to calculate the actual amount of fission gas release and compare the performance to UO_2.

7 References

[1] International Atomic Energy Agency, Thermophysical Properties Database of Materials for Light Water Reactors and Heavy Water Reactors, Vienna: International Atomic Energy Agency, 2006.

[2] A. Labib and M. Harris, "Learning how to learn from failures: The Fukushima nuclear disaster," *Engineering Failure Analysis,* vol. 47, pp. 117-128, 2015.

[3] S. Zinkle, K. Terrani, J. Gehin, L. Ott and L. Snead, "Accident tolerant fuels for LWRs: A perspective," *Journal of Nuclear Materials,* vol. 448, pp. 374-379, 2014.

[4] J. Powers, W. Lee, F. Venneri, L. Snead, C. Jo, D. Hwang, J. Chun, Y. Kim and K. Terrani, "Fully Ceramic Microencapsulated (FCM) Replacement Fuel for LWRs," 2013.

[5] E. Lahoda, L. Hallstadius, F. Boylan and S. Ray, "What Should be the Objective of Accident Tolerant Fuel?," *Transactions of the American Nuclear Society,* vol. 110, pp. 733-736, 2014.

[6] L. J. Ott, K. Robb and D. Wang, "Preliminary assessment of accident-tolerant fuels on LWR performance during normal operation and under DB and BDB accident conditions," *Journal of Nuclear Materials,* vol. 448, pp. 520-533, 2014.

[7] J. Creasy, "Thermal Properties of Uranium-Molybdenum Alloys: Phase Decomposition Effects of Heat Treatments," 2011.

[8] L. Haacke, "Principles of Nuclear Safety, Course 4.3, Module 03 - Defence in Depth," CANTEACH, 1996.

[9] J. C. Luxat, "Thermal-Hydraulic Aspects of Progression to Severe Accidents in CANDU Reactors," *Nuclear Technology,* vol. 167, pp. 187-210, 2009.

[10] D. Permar, A. Cartas and H. Wang, "Innovative Accident Tolerant UO2 Composite Fuel For Use in LWRs," *Transactions of the American Nuclear Society,* vol. 109, pp. 185-186, 2013.

[11] D. Permar, Z. Chen and J. Tulenko, "Enhanced Accident Tolerant UO2-Diamond Composite Fuel Pellets Prepared by SPS," *Transactions of the American Nuclear Society,* vol. 109, pp. 267-269, 2013.

[12] K. Spencer, L. Sudderth, R. Brito, J. Evans, C. Hart, A. Hu, A. Jati, K. Stern and S. McDeavitt, "Sensitivity study for accident tolerant fuels: Property comparisons and behavior simulations in a simplified PWR to enable ATF development and design," *Nuclear Engineering and Design,* vol. 309, pp. 197-212, 2016.

[13] L. Ortega, J. Evans and S. McDeavitt, "Development of a High Density Uranium Nitride-Uranium Silicide Composite Accident Tolerant Fuel," *Transactions of the American Nuclear Society,* vol. 110, pp. 999-1000, 2014.

[14] H. G. Kim, J. H. Yang, W. J. Kim and Y. H. Koo, "Development Status of Accident-tolerant Fuel for Light Water Reactors in Korea," *Nuclear Engineering and Technology,* vol. 48, pp. 1-15, 2016.

[15] S. Bragg-Sitton, M. Todosow, R. Montgomery, C. Stanek, R. Montgomery and W. Carmack, "Metrics for the Technical Performance Evaluation of Light Water Reactor Accident-Tolerant Fuel," *Nuclear Technology,* vol. 195, pp. 111-123, 2016.

[16] J. Harp, P. Lessing and R. Hoggan, "Uranium silicide pellet fabrication by powder metallurgy for accident tolerant fuel evaluation and irradiation," *Journal of Nuclear Materials,* vol. 466, pp. 728-738, 2015.

[17] K. Johnson, A. Raftery, D. Lopes and J. Wallenius, "Fabrication and microstructural analysis of UN-U3Si2 composites for accident tolerant fuel applications," *Journal of Nuclear Materials,* vol. 477, pp. 18-23, 2016.

[18] D. Burkes, G. Mickum and D. Wachs, "Thermophysical Properties of U-10Mo Alloy," 2010.

[19] T. Besmann, D. Shin and S. Voit, "Development and Properties of Uranium Nitride Fuels: Oxide Conversion and Thermochemistry," *Transactions of the American Nuclear Society,* vol. 106, pp. 1117-1118, 2012.

[20] P. Malkki, "The manufacturing of uranium nitride for possible use in light water reactors," 2015.

[21] L. Ortega, B. Blamer, J. Evans and S. McDeavitt, "Development of an accident-tolerant fuel composite from uranium mononitride (UN) and uranium sesquisilicide (U3Si2) with increased uranium loading," *Journal of Nuclear Materials,* vol. 471, pp. 116-121, 2016.

[22] B. Jaques, J. Watkins, J. Croteau, G. Alanko, B. Tyburska-Püschel, M. Meyer, P. Xu, E. Lahoda and D. Butt, "Synthesis and sintering of UN-UO2 fuel composites," *Journal of Nuclear Materials,* vol. 466, pp. 745-754, 2015.

[23] G. Youinou and R. Sen, "Impact of Accident-Tolerant Fuels and Claddings on the Overall Fuel Cycle: A Preliminary Systems Analysis," *Nuclear Technology,* vol. 188, pp. 123-138, 2014.

[24] J. Harp, P. Lessing and R. Hoggan, "Uranium Silicide Fabrication for use in LWR Accident Tolerant Fuel," *Transactions of the American Nuclear Society,* vol. 110, pp. 990-993, 2014.

[25] A. Lotts, *Review of Information on U-Mo Alloys and U-Mo-UO2 Dispersion Fuels,* 1960.

[26] R. A. Brown, C. Blahnik and A. P. Muzumdar, "Degraded Cooling in a CANDU Reactor," *Nuclear Science and Engineering,* vol. 88, pp. 425-435, 1984.

[27] Y.-H. Lee and T. Byun, "A comparative study on the wear behaviors of cladding candidates for accident-tolerant fuel," *Journal of Nuclear Materials,* vol. 465, pp. 857-865, 2015.

[28] N. Brown, A. Wysocki, K. Terrani, K. Xu and D. Wachs, "The potential impact of enhanced accident tolerant cladding materials on reactivity initiated accidents in light water reactors," *Annals of Nuclear Energy,* vol. 99, pp. 353-365, 2017.

[29] B. Cheng, Y. J. Kim and P. Chou, "Improving Accident Tolerance of Nuclear Fuel with Coated Mo-alloy Cladding," *Nuclear Engineering and Technology,* vol. 48, pp. 16-25, 2016.

[30] M. Gussev, T. Byun, Y. Yamamoto, S. Maloy and K. Terrani, "In-situ tube burst testing and high-temperature deformation behavior of candidate materials for accident tolerant fuel cladding," *Journal of Nuclear Materials,* vol. 466, pp. 417-425, 2015.

[31] A. Magyar, J. Sabella, M. Loff, D. Frazer, M. Szwabowski, R. Meyer and D. Moon, "Accident Tolerant Refractory Metal Based Cladding for Light Water Reactors," *Transactions of the American Nuclear Society,* vol. 109, pp. 179-181, 2013.

[32] X. Wu, W. Li, Y. Wang, Y. Zhang, W. Tian, G. Su, S. Qiu, T. Liu, Y. Deng and H. Huang, "Preliminary safety analysis of the PWR with accident-tolerant fuels during severe accident conditions," *Annals of Nuclear Energy,* vol. 80, pp. 1-13, 2015.

[33] C. Deck, G. Jacobsen, J. Sheeder, O. Gutierrez, J. Zhang, J. Stone, H. Khalifa and C. Back, "Characterization of SiC--SiC composites for accident tolerant fuel cladding," *Journal of Nuclear Materials,* vol. 466, pp. 667-681, 2015.

[34] J. Stone, R. Schleicher, C. Deck, G. Jacobsen, H. Khalifa and C. Back, "Stress analysis and probabilistic assessment of multi-layer SiC-based accident tolerant nuclear fuel cladding," *Journal of Nuclear Materials,* vol. 466, pp. 682-697, 2015.

[35] H. Matsumiya, K. Yoshioka, T. Kikuchi, T. Sugita, S. Higuchi and N. Yoshida, "Reactivity measurements of SiC for accident-tolerant fuel," *Progress in Nuclear Energy,* vol. 82, pp. 16-21, 2015.

[36] E. Herderick, K. Cooper and N. Ames, "New Approach to Join SiC for Accident-Tolerant Nuclear Fuel Cladding," *Advanced Materials & Processes,* vol. 170, pp. 24-27, 2012.

[37] J. H. Park, H. G. Kim, J. Y. Park, Y. I. Jung, D. J. Park and Y. H. Koo, "High temperature steam-oxidation behavior of arc ion plated Cr coatings for accident tolerant fuel claddings," *Surface & Coatings Technology,* vol. 280, pp. 256-259, 2015.

[38] J. H. Chun, S. W. Lim, B. D. Chung and W. J. Lee, "Safety evaluation of accident-tolerant FCM fueled core with SiC-coated zircalloy cladding for design-basis-accidents and beyond DBAs," *Nuclear Engineering and Design,* vol. 289, pp. 287-295, 2015.

[39] J. Carr, G. Vasudevamurthy, L. Snead, B. Hinderliter and C. Massey, "Investigations of Aluminum-Doped Self-Healing Zircaloy Surfaces in Context of Accident-Tolerant Fuel Cladding Research," *Journal of Materials Engineering and Performance,* vol. 25, pp. 2347-2355, 2016.

[40] B. Garcia-Diaz, L. Olson, C. Verst, R. Sindelar, E. Hoffman, B. Hauch, B. Maier and K. Sridharan, "MAX Phase Coatings for Accident Tolerant Nuclear Fuel," *Transactions of the American Nuclear Society,* vol. 110, pp. 994-996, 2014.

[41] R. Shapiro, I. Younker and M. Fratoni, "Neutronic performance of accident tolerant fuels," *Transactions of the American Nuclear Society,* vol. 109, pp. 1351-1353, 2013.

[42] I. Younker and M. Fratoni, "Neutronic evaluation of coating and cladding materials for accident tolerant fuels," *Progress in Nuclear Energy,* vol. 88, pp. 10-18, 2016.

[43] *Private Communication from Nihan Onder,* CNL, 2016.

[44] J. Leppänen, "PSG2 / Serpent – a Continuous-energy Monte Carlo Reactor Physics Burnup Calculation Code," VTT Technical Research Centre of Finland, 2009.

[45] J. Leppänen, M. Pusa, T. Viitanen, V. Valtavirta and T. Kaltiaisenaho, "The Serpent Monte Carlo code: Status, development and applications in 2013," *Ann. Nucl. Energy,* vol. 82, pp. 142-150, 2015.

[46] X-5 Monte Carlo Team, "MCNP — A General Monte Carlo N-Particle Transport Code, Version 5," Los Alamos National Laboratory, 2003.

[47] J. Leppänen, "Performance of Woodcock delta-tracking in lattice physics applications using the Serpent Monte Carlo reactor physics burnup calculation code," VTT Technical Research Centre of Finland, Espoo, 2010.

[48] PDE Solutions Inc., FlexPDE 6 Version 6.40, PDE Solutions Inc., 2016.

[49] Atomic Energy Control Board, Fundamentals of Power Reactors Module One Science & Engineering Fundamentals, Atomic Energy Control Board, 1993.

[50] T. Rucker and C. Johnson, "Calculation of Uranium Isotopic Activity Composition Based on Data from Various Assay Methods," in *43rd Annual Conference on Bioassay, Analytical, and Environmental Radiochemistry*, Charleston, 1997.

[51] M. A. B. Da Silva, R. Narain and W. E. de Vasconcelos, "A Quantitative Estimate on the Heat Transfer in Cylindrical Fuel Rods to Account for Flux Depression Inside Fuel," in *2011 International Nuclear Atlantic Conference*, Belo Horizonte, 2011.

[52] S. C. Cheng and R. I. Vachon, The Prediction of the Thermal Conductivity of Two and Three Phase Solid Heterogeneous Mixtures, Auburn: Auburn University, 1968.

[53] Thermalloys AB, "FeCrAl alloys," 2012. [Online]. Available: http://www.thermalloys.com/index.php/en/alloys/fecralalloys.html. [Accessed 2016].

[54] F. J. Doria, "CANDU Safety #16: Large Loss-of-Coolant Accident with Coincident Loss of Emergency Core Cooling," Atomic Energy of Canada Limited, 2001.

[55] "Wolfram|Alpha curated data," 2016.

[56] E. W. Lemmon, M. L. Huber and M. O. McLinden, "NIST Standard Reference Database 23: Reference Fluid Thermodynamic and Transport Properties-REFPROP, Version 9.1," National Institute of Standards and Technology, Standard Reference Data Program, Gaithersburg, 2013.

[57] S. Glasstone and A. Sesonske, Nuclear Reactor Engineering, Van Nostrand Reinhold, 1967.

[58] P. M. Mathew and I. M. George, "Total Emissivity of Zircaloy-4 at High Temperatures," AECL Whiteshell Laboratories, Pinawa, 1996.

[59] Omega, "Emissivity of Common Materials," [Online]. Available: http://www.omega.ca/literature/transactions/volume1/emissivityb.html. [Accessed 2016].

[60] M. A. Jessee and M. D. DeHart, "TRITON: A multipurpose transport, depletion, and sensitivity and uncertainty analysis module," Oak Ridge National Laboratory, Oak Ridge, 2011.

[61] B. Rouben, "Reactivity Coefficients," McMaster University, 2015.

[62] J. R. Lamarsh and A. J. Baratta, Introduction to Nuclear Engineering, 3rd ed., Upper Saddle River: Prentice-Hall, Inc., 2001.

[63] X. Zhonsheng and P. G. Boczar, "CANDU Fuel-Cycle Vision," CANTEACH, 2014.

[64] J. W. Eaton, D. Bateman, S. Hauberg and R. Wehbring, "GNU Octave version 4.2.0 manual: a high-level interactive language for numerical computations," 2016. [Online]. Available: http://www.gnu.org/software/octave/doc/interpreter.

Appendix A: Heat Transfer Coefficients for Fuel and Cladding Materials

Table A.1: Thermal conductivities for UO_2-SiC mixtures

Base	UO_2	UO_2	UO_2	UO_2
Additive		SiC	SiC	SiC
Additive vol. %	0%	3%	6%	10%
Density (g/cm^3)	10.63	10.39	10.15	9.83
Temperature	k (W/m · K)	k (W/m · K)	k (W/m · K)	k (W/m · K)
298.15	8.0359	8.8881	9.5382	10.3467
300	8.0119	8.8618	9.5101	10.3165
400	6.9382	7.6611	8.2150	8.9041
500	6.0865	6.7172	7.2012	7.8036
600	5.4067	5.9752	6.4102	6.9517
700	4.8408	5.3655	5.7645	6.2609
800	4.3730	4.8648	5.2359	5.6973
900	3.9731	4.4382	4.7859	5.2181
1000	3.6292	4.0721	4.4002	4.8078
1100	3.3333	3.7564	4.0670	4.4527
1200	3.0813	3.4870	3.7820	4.1482
1300	2.8594	3.2490	3.5299	3.8786
1400	2.6675	3.0426	3.3109	3.6441
1500	2.5095	2.8721	3.1295	3.4492
1600	2.3815	2.7336	2.9821	3.2907
1700	2.2736	2.6165	2.8574	3.1566
1800	2.1996	2.5361	2.7715	3.0640
1900	2.1556	2.4884	2.7207	3.0094
2000	2.1316	2.4626	2.6935	2.9803
2100	2.1377	2.4698	2.7016	2.9897
2200	2.1577	2.4921	2.7257	3.0160
2300	2.2037	2.5432	2.7809	3.0765
2400	2.2677	2.6134	2.8561	3.1578
2500	2.3477	2.7012	2.9504	3.2602
2600	2.4377	2.7997	3.0560	3.3747
2700	2.5437	2.9157	3.1804	3.5096
2800	2.6577	3.0395	3.3124	3.6520
2900	2.7777	3.1697	3.4514	3.8019
3000	2.9037	3.3062	3.5971	3.9592
3100	3.0337	3.4464	3.7463	4.1196
3120	3.0577	3.4720	3.7732	4.1482

Table A.2: Thermal conductivities for UN mixtures

Base	UN	UN	UN	UN	UN
Additive		U_3Si_2	U_3Si_2	U_3Si_2	ZrN
Additive vol. %	0%	3%	6%	10%	3%
Density (g/cm^3)	14.01	13.95	13.90	13.82	13.57
Temperature	k (W/m · K)	k (W/m · K)	k (W/m · K)	k (W/m · K)	k (W/m · K)
298.15					
373.15	15.6404	15.4184	15.1875	14.8740	14.6317
473.15	17.0402	16.8049	16.5606	16.2290	15.9048
573.15	18.2614	18.0232	17.7763	17.4417	17.3050
673.15	19.3530	19.1182	18.8755	18.5469	18.5165
773.15	20.3452	20.1234	19.8949	19.5861	19.5881
873.15	21.2585	21.0584	20.8531	20.5762	20.5731
973.15	22.1071	21.9339	21.7570	21.5189	
1073.15	22.9017	22.7607	22.6173	22.4247	23.1048
1173.15	23.6502	23.5525	23.4537	23.3213	23.8496
1273.15	24.3591	24.3116	24.2639	24.2002	24.5831
1373.15	25.0331				

Table A.3: Thermal conductivities for ATF with UO_2 Kernels

Particle	UO_2	UO_2	UO_2	UO_2	UO_2
Matrix	SiC	SiC	SiC	SiC	SiC
Packing Fraction	35%	40%	45%	50%	55%
Temperature	k (W/m · K)	k (W/m · K)	k (W/m · K)	k (W/m · K)	k (W/m · K)
298.15	39.4261	35.6313	31.9297	28.3171	24.7817
300	39.3154	35.5321	31.8416	28.2400	24.7153
400	33.1794	30.0170	26.9328	23.9239	20.9810
500	28.8676	26.1269	23.4541	20.8470	18.2975
600	26.1615	23.6625	21.2252	18.8472	16.5210
700	24.4417	22.0764	19.7689	17.5165	15.3114
800	23.3177	21.0238	18.7851	16.5983	14.4553
900	22.5552	20.2948	18.0878	15.9304	13.8134
1000	22.0377	19.7905	17.5952	15.4476	13.3376
1100	21.6700	19.4218	17.2245	15.0732	12.9565
1200	21.4095	19.1528	16.9460	14.7835	12.6529
1300	21.2242	18.9544	16.7337	14.5559	12.4073
1400	21.0956	18.8107	16.5743	14.3795	12.2113
1500	21.0089	18.7082	16.4554	14.2430	12.0549
1600	20.9589	18.6432	16.3749	14.1461	11.9396
1700	20.9334	18.6032	16.3202	14.0758	11.8519
1800	20.9325	18.5896	16.2936	14.0356	11.7969
1900	20.9563	18.6034	16.2972	14.0287	11.7787
2000	20.9965	18.6352	16.3207	14.0437	11.7849
2100	21.0583	18.6917	16.3721	14.0902	11.8267
2200	21.1245	18.7531	16.4289	14.1428	11.8753
2300	21.2135	18.8411	16.5163	14.2301	11.9636
2400	21.3028	18.9296	16.6043	14.3183	12.0529
2500	21.4073	19.0360	16.7131	14.4302	12.1696
2600	21.5173	19.1490	16.8297	14.5513	12.2966
2700	21.6419	19.2794	16.9664	14.6954	12.4501
2800	21.7591	19.4016	17.0941	14.8295	12.5923
2900	21.8842	19.5333	17.2329	14.9765	12.7492
3000	22.0169	19.6742	17.3826	15.1359	12.9204
3100	22.1450	19.8101	17.5269	15.2895	13.0850
3120	22.1637	19.8293	17.5467	15.3100	13.1064

Table A.4: Thermal conductivities for ATF with UN Kernels

Particle	UN	UN	UN	UN	UN	UN TRISO
Matrix	SiC	SiC	SiC	SiC	SiC	SiC
Packing Fraction	35%	40%	45%	50%	55%	55%
Temperature	k (W/m · K)	k (W/m · K)	k (W/m · K)	k (W/m · K)	k (W/m · K)	k (W/m · K)
298.15	43.7814	40.6243	37.5538	34.5729	31.6813	19.2421
300	43.6970	40.5550	37.4992	34.5325	31.6549	19.1947
400	38.8814	36.5390	34.2597	32.0464	29.9004	16.5747
500	35.5742	33.7858	32.0428	30.3477	28.7019	14.7516
600	33.6889	32.2510	30.8469	29.4786	28.1474	13.6438
700	32.6764	31.4673	30.2846	29.1297	28.0037	12.9730
800	32.1802	31.1282	30.0975	29.0892	28.1042	12.5621
900	31.9927	31.0541	30.1330	29.2306	28.3475	12.3090
1000	31.9929	31.1398	30.3015	29.4791	28.6732	12.1539
1100	32.1083	31.3224	30.5493	29.7899	29.0449	12.0616
1200	32.2948	31.5635	30.8436	30.1357	29.4403	12.0100
1300	32.5245	31.8392	31.1640	30.4993	29.8458	11.9853
1400	32.7798	32.1342	31.4975	30.8703	30.2531	11.9787
1500	33.0492	32.4386	31.8360	31.2419	30.6567	11.9841
1600	33.3253	32.7461	32.1741	31.6099	31.0537	11.9977
1700	33.6030	33.0526	32.5086	31.9717	31.4420	12.0167
1800	33.8793	33.3554	32.8374	32.3257	31.8206	12.0392
1900	34.1519	33.6528	33.1591	32.6711	32.1891	12.0639
2000	34.4195	33.9438	33.4730	33.0074	32.5473	12.0899
2100	34.6812	34.2278	33.7788	33.3346	32.8953	12.1165
2200	34.9366	34.5045	34.0763	33.6525	33.2332	12.1433
2300	35.1854	34.7737	34.3656	33.9615	33.5614	12.1700
2400	35.4276	35.0356	34.6469	34.2617	33.8802	12.1963
2500	35.6632	35.2902	34.9203	34.5535	34.1900	12.2221
2600	35.8923	35.5378	35.1860	34.8371	34.4913	12.2473
2700	36.1150	35.7785	35.4445	35.1130	34.7843	12.2718
2800	36.3316	36.0127	35.6959	35.3815	35.0695	12.2955
2900	36.5423	36.2405	35.9406	35.6428	35.3472	12.3185
3000	36.7473	36.4622	36.1788	35.8973	35.6178	12.3408
3100	36.9468	36.6781	36.4109	36.1454	35.8816	12.3623
3120	36.9860	36.7205	36.4566	36.1942	35.9336	12.3665

Appendix B: Ring Power Factors

Table B.1: Ring power factors for non-FCM fuel

Fuel	Cladding	Enrichment (wt% ^{235}U)	Ring Power Factor			
			Centre	Inner	Intermediate	Outer
UO_2	Zirc4	0.711	0.75856	0.79603	0.90857	1.14236
		1.30	0.67472	0.72556	0.87034	1.19599
UO_2 + 3% SiC	Zirc4	0.72	0.76187	0.79940	0.91077	1.13958
	SiC	0.711	0.76537	0.80179	0.90989	1.13918
	Zirc4 + FeCrAl	0.80	0.74085	0.78356	0.90154	1.15219
UO_2 + 6% SiC	Zirc4	0.72	0.76506	0.80407	0.91290	1.13643
UO_2 + 10% SiC	Zirc4	0.73	0.76944	0.80919	0.91528	1.13289
UN	Zirc4	0.711	0.61520	0.66711	0.83895	1.23971
		1.28	0.53001	0.59069	0.78996	1.30258
		2.04	0.44946	0.51344	0.73674	1.36828
UN + 3% U_3Si_2	Zirc4	1.27	0.53502	0.59449	0.79360	1.29860
UN + 6% U_3Si_2	Zirc4	1.25	0.54263	0.59924	0.79757	1.29395
UN + 10% U_3Si_2	Zirc4	1.23	0.54680	0.60680	0.80084	1.28902
UN + 3% ZrN	Zirc4	1.30	0.53803	0.59734	0.79614	1.29579
U-9Mo	Zirc4	0.94	0.61658	0.67372	0.84234	1.23517

Table B.2: Ring power factors for FCM fuel

Particle	Packing %	Enrichment (wt% ^{235}U)	Ring Power Factor			
			Centre	Inner	Intermediate	Outer
UO_2	35%	1.08	0.85201	0.87760	0.94673	1.08453
		1.90	0.80759	0.83666	0.92758	1.11342
	40%	0.711	0.86595	0.88895	0.95221	1.07632
		1.01	0.84551	0.87246	0.94414	1.08833
		1.63	0.80687	0.83790	0.92697	1.11345
		1.82	0.79361	0.82908	0.92343	1.11948
	45%	0.96	0.83916	0.86565	0.94166	1.09262
		1.44	0.80195	0.83562	0.92727	1.11428
	50%	0.92	0.83225	0.86021	0.93812	1.09717
		1.29	0.80084	0.83482	0.92611	1.11539
	55%	0.88	0.82584	0.85418	0.93574	1.10113
		1.17	0.79634	0.83128	0.92547	1.11724
UN	35%	1.42	0.75554	0.79063	0.90528	1.14652
		1.82	0.71996	0.76568	0.89259	1.16527
	40%	1.38	0.73376	0.77415	0.89646	1.15910
		1.67	0.71157	0.75285	0.88658	1.17402
	45%	1.36	0.71115	0.75565	0.88695	1.17286
		1.56	0.69291	0.74075	0.87881	1.18427
	50%	1.34	0.69206	0.73852	0.87786	1.18570
		1.48	0.67938	0.72763	0.87199	1.19394
	55%	1.32	0.67266	0.72134	0.86944	1.19811
		1.42	0.66155	0.71440	0.86436	1.20443
UN TRISO	55%	2.78	0.76750	0.80259	0.91079	1.13819

Table B.3: Ring power factors for irradiated fuel (mid-burnup)

Fuel	Cladding	Enrichment (wt% ^{235}U)	Ring Power Factor			
			Centre	Inner	Intermediate	Outer
UO_2	Zirc4	0.711	0.76495	0.80533	0.91046	1.13764
UO_2 + 3% SiC	Zirc4	0.72	0.77287	0.80929	0.91369	1.13373
	SiC	0.711	0.77420	0.80914	0.91348	1.13384
	Zirc4 + FeCrAl	0.80	0.75644	0.79915	0.90957	1.14077
UO_2 + 10% SiC	Zirc4	0.73	0.78440	0.82172	0.91935	1.12517
UN	Zirc4	1.28	0.55643	0.61521	0.81849	1.27391
U-9Mo	Zirc4	0.94	0.63371	0.68815	0.85677	1.21979
UO_2 FCM 40% Packing	Zirc4	1.01	0.87626	0.89682	0.95417	1.07182
		1.63	0.90937	0.92745	0.96720	1.05109
UN FCM 40% Packing	Zirc4	1.38	0.77108	0.80860	0.91648	1.13219
		1.67	0.78698	0.82404	0.92584	1.11993
UN TRISO FCM 55% Packing	Zirc4	2.78	0.90792	0.92436	0.97098	1.04968

Appendix C: Point Kinetics Parameters for Transient

Table C.1: Point kinetics parameters for UO_2 and ATF fuel

Fuel	Clad	Enrichment (wt% ^{235}U)	Burnup (MWd/kg(U))	Prompt	Delayed Group		Feedback	
				Λ (ms) ±0.1%	β (mk) ±1.5%	λ (s^{-1}) ±3.0%	CVR (mk) ±1%	FTC (pcm/K) ±0.03
UO_2	Zirc4	0.711	0	0.820	6.65	0.79	16.79	-1.22
			4	0.774	4.62	0.76	14.59	-0.12
UO_2 +3% SiC	Zirc4	0.72	0	0.826	6.64	0.81	16.49	-1.24
			4	0.785	4.77	0.73	14.37	-0.18
	SiC	0.711	0	0.833	6.68	0.79	16.10	-1.27
			4	0.788	4.74	0.74	13.84	-0.22
	Zirc4 +FeCrAl	0.79	0	0.784	6.75	0.80	16.03	-1.20
			4	0.764	4.85	0.77	14.33	-0.21
UO_2 +10% SiC	Zirc4	0.73	0	0.853	6.63	0.79	16.05	-1.33
			4	0.816	4.69	0.76	13.70	-0.16
UN	Zirc4	1.28	0	0.546	6.80	0.81	14.12	-1.40
			4	0.565	5.68	0.77	15.38	-0.67
U-9Mo	Zirc4	0.93	0	0.568	6.70	0.83	19.15	-1.01
			4	0.571	5.05	0.79	20.02	-1.05
UO_2 FCM 40% Packing	Zirc4	1.01	0	1.168	6.68	0.76	12.34	-1.66
			4	1.260	5.10	0.71	10.30	-0.38
		1.62	0	0.820	6.47	0.74	9.40	-1.18
			11	1.150	4.85	0.70	9.94	-0.09
UN FCM 40% Packing	Zirc4	1.37	0	0.784	6.72	0.81	11.33	-1.60
			4	0.842	5.62	0.75	11.13	-0.71
		1.66	0	0.689	6.56	0.77	9.94	-1.43
			7	0.805	5.40	0.76	10.91	-0.54
UN TRISO FCM 55% Packing	Zirc4	2.77	0	0.718	6.35	0.77	7.29	-1.16
			15	1.061	5.32	0.72	9.16	-0.41

Appendix D: Description of Monte Carlo View Factor Calculation

To determine view factor coefficients for modelling radiation heat transfer in a CANDU channel, a Monte Carlo method was utilized to approximate the coefficients. Rays were randomly sampled from each pin, as well as from the inner surface of the pressure tube. The point at which to start the ray is determined by choosing a random angle between 0 and 2π. The direction is chosen by generating a random angle α between $-\pi/2$ and $\pi/2$ from the surface normal. The ray is given a weight of $\cos\alpha$.

The ray is then traced to determine if its path will interest the surface of another pin. If it does, it is determined which pin is closest. If it does not, it means the ray will interest the inner surface of the pressure tube. A random number uniformly distributed from 0 to 1 is then sampled; if it is less than the surface emissivity for the interested surface, then the ray is absorbed and the result is tallied according to the weight of the ray. Otherwise, a reflection occurs.

When a reflection occurs, the intersection point is sampled, along with the angle of the surface normal. If the reflection is shiny (for non-oxidized metals), then the angle of reflection is calculated accordingly, so that the angle between the incident ray and surface normal is the same as the angle between the reflected ray and surface normal. Otherwise, if the reflection is diffuse, the reflected angle is equal to the angle of the surface normal plus a random angle $\alpha = \sin^{-1} A$ where A is a random number uniformly distributed between -1 and 1. The reflected ray, with the same weight as the incident ray, is then traced in the same manner. This continues recursively until an absorption is sampled.

When tallying the results, the pins are binned by rings, such that the centre pin has a value of 1 and the rings are numbered up to 4 from inside to outside. The pressure tube is assigned a value of 0. This results in 25 view factors v_{ab} where a is the emitting surface and b is the absorbing surface, and $0 \leq a, b \leq 4$.

For each value of a, five tallies t_{ab} are zero-initialized. Rays are then sampled from all emitting surfaces which are a part of bin a, with an equal number of samples from each pin in a given ring. For each sampled ray, once the absorbing surface is determined, the corresponding bin b is determined, and t_{ab} is incremented by the weight of the ray. Once this is done, the view factors for that emitter are calculated by normalizing the tallies:

$$v_{ab} = \frac{t_{ab}}{\sum_{i=0}^{4} t_{ai}}$$

Once the view factors are calculated for each emitter, the view factor matrix can be fed into FlexPDE to be used in the boundary condition for each pin.